THE MAGNETIC BEHAVIOUR OF THE {111}-ORIENTED IRON WHISKER

by

Scott Douglas Hanham
B.Sc., University of Toronto, 1973
M.Sc., University of Toronto, 1975

A THESIS SUBMITTED IN PARTIAL FULFILLMENT
OF THE REQUIREMENTS FOR THE DEGREE OF
DOCTOR OF PHILOSOPHY
in the Department
of
Physics

SIMON FRASER UNIVERSITY
November 1980

APPROVAL

Name: Scott Douglas Hanham

Degree: Doctor of Philosophy

Title of Thesis: The Magnetic Behaviour of the [111]-oriented Iron Whisker

Examining Committee:

Chairman: Leslie E. Ballentine

Anthony S. Arrott
Senior Supervisor

John F. Cochran

Michael Plischke

Suso Gygax

Earl R. Callen
External Examiner
Professor, Department of Physics
American University, Washington, D.C.

Date Approved: 15 Dec. 1980

PARTIAL COPYRIGHT LICENSE

I hereby grant to Simon Fraser University the right to lend my thesis, project or extended essay (the title of which is shown below) to users of the Simon Fraser University Library, and to make partial or single copies only for such users or in response to a request from the library of any other university, or other educational institution, on its own behalf or for one of its users. I further agree that permission for multiple copying of this work for scholarly purposes may be granted by me or the Dean of Graduate Studies. It is understood that copying or publication of this work for financial gain shall not be allowed without my written permission.

Title of Thesis/Project/Extended Essay

The Magnetic Behaviour of the [111]-Oriented Iron Whisker

Author: _____
(signature)

Scott Douglas Hanham
(name)

Dec 19/80
(date)

ABSTRACT

The magnetic behaviour of [111]-oriented iron whiskers is studied as a function of magnetic field applied along the whisker length and as a function of temperature. Based on ac susceptibility measurements and observed Bitter patterns in low applied fields, a domain structure is proposed for this orientation of whisker. This is compared with observations made on [100] and the rare [110]-oriented iron whiskers.

The technique of growing iron whiskers is described. Theories of whisker growth are discussed. The role of carbon in iron whisker growth and its detection in small concentrations is considered.

The approach to saturation in the [111] direction for an iron whisker with its long axis in that direction is studied by ac susceptibility measurements. The data at room temperature is analyzed to give the magnetization, intrinsic susceptibility, and demagnetizing field at each of 15 cross-sections along the length for applied fields from 10 to ~ 1000 oe. It is concluded that mean field anisotropy theory does not account for the results. The approach to saturation in the [111] direction may represent the behaviour of the 3-state Potts model.

The magnetic response of a [111]-oriented iron whisker is measured up to and through the Curie temperature. The anisotropy constant is found from the response in the range of fields between that necessary to bring the magnetization in the central cross section of the whisker to $M_s/\sqrt{3}$ and that to reach M_s. We extract an anisotropy field H_k proportional to K_1/M_s and analyze its dependence on M_s and on temperature. The results indicate that $K_1/M_s \sim M_s^n$ with $n = 3.11 \pm 0.05$ for the temperature range $0.0005 <$

$(T_c - T)/T_c < 0.002$ with n increasing at lower temperatures. To our knowledge this is the first observation of the power law behaviour of the anisotropy in a cubic ferromagnet just below the Curie temperature.

At lower temperatures the analysis is complicated by the field dependence of the demagnetizing field. The anisotropy field H_k is extracted from the critical applied field which just saturates the centre of a [111] whisker at each temperature. This is accomplished by calculating the demagnetizing field using a method of modelling the sources of the demagnetizing field on the surface of a cylinder. The sensitivity of the method permits extraction of K_1 values over five orders of magnitude. The results are compared with those of others from torque curve and FMR measurements.

For the purposes of the above analysis, the temperature dependence of the spontaneous magnetization M_s is measured from room temperature to the Curie temperature. This is derived from the departure field which just saturates the centre of a [100] iron whisker. Minor corrections for the anisotropy are made. The results agree well with the measurements of others. A fit function to the data is given which can be used as the calibration curve of an iron whisker magnetic thermometer.

ACKNOWLEDGEMENTS

It has been a great honour and privilege for me to have been supervised by Professor Anthony S. Arrott during the course of this research. His enthusiasm for physics and confidence for success are only two of the things he has taught me which I hope never to forget. His guidance in this work was invaluable.

I wish to thank Bret Heinrich for many long hours of experimental help and advice. His presence in the laboratory made for many enjoyable times of doing physics.

I wish to thank Calvin Winter, Andrew Kurn, and Terry Templeton for hours spent in computer assistance. The technical and secretarial staffs of the Physics Department and of the Faculty of Science were a tremendous help to me on many occasions. In particular I wish to thank Valerie Drostle for all her work in preparing the final manuscript.

I wish to express appreciation to Simon Fraser University for its good level of financial support in the form of scholarships and teaching assistantships.

Finally, last but not least, I want to thank my wife and fellow scientist, Ann, for her support, encouragement and patience throughout this work.

TABLE OF CONTENTS

LIST OF TABLES

LIST OF FIGURES

I. INTRODUCTION: THE ROLE OF MAGNETIC ANISOTROPY IN FERROMAGNETIC CRYSTALS

Many properties of a material, such as strength and elasticity, are dependent on crystallographic direction in a lattice. The internal energy of a ferromagnet is dependent also on the orientation of the spontaneous magnetization in a crystal. Magnetic anisotropy is well known from the measurement of B-H curves with the field H applied in various directions with respect to a crystal sample. Fig. (1) shows the B-H curves for iron at room temperature for three directions of the applied field. These curves show that there are "easy" and "hard" directions for magnetization. For iron the easy and hard directions are the [100] and [111] respectively at all temperatures.

Ferromagnets are strongly interacting systems of magnetic moments which, like any system, want to achieve their lowest energy state. The strongest interaction is called exchange which tries to align each moment with its neighbours. This results in a spontaneous magnetization M_s (magnetic moments/unit volume), the property which is synonymous with ferromagnetism. Exchange is a Coulomb interaction mediated by the Pauli exclusion principle, which forbids electrons with the same spin from being in the same place at the same time, but not electrons with different spins. Thus the electrostatic energy of a system depends on the relative orientation of its spins. The exchange energy of two atoms with spins S_i, S_j is $U_{ij} = -2JS_i \cdot S_j$ where J is the exchange integral which is related to the overlap of charge distributions of the two atoms. This is called the Heisenberg model. From mean field theory and the observed Curie temperature of 1043 K (the temperature where a ferromagnet changes into a paramagnet), one can calculate

a value of J = 11.9 meV. If exchange were the only interaction in a ferromagnet, then all of the moments would be aligned in a single domain. Such single domain particles exist, but are fine particles of very small sizes. Careful calculations of critical radii for single domain behaviour are given by Brown (1969). He finds that spheres of iron and nickel are stable as single domains below radii of 16.7 and 38.2 nm respectively.

However ferromagnets are not so simple, even if they are fine particles. First of all there are magnetic dipole-dipole interactions. Divergences in the magnetization (charge) are avoided in the bulk, but magnetic charge on the surface of a fine particle results. This charge is the source of a demagnetizing field which opposes the magnetization. Since a particle is usually not spherical, the magnetization will align in a particular direction, and the charge will distribute on the surface of the particle in a particular way, in order to minimize the total magnetic energy. This is a simple example of magnetic anisotropy, called shape anisotropy, resulting from dipole-dipole interactions.

A second kind of anisotropy is called magnetocrystalline anisotropy and is the main subject matter of this thesis. It is the result of spin-orbit interactions which are aware of the crystal symmetry. The spin angular momentum vector of each magnetic moment interacts with the orbital angular momentum of electrons which see the internal electric potential, which in turn possesses the symmetry of the lattice. As a result the magnetic moments prefer to align along certain crystallographic directions or axes.

The simplest type of magnetocrystalline anisotropy is uniaxial anisotropy as found in cobalt. Below 400°C, the most stable crystal structure for cobalt is hexagonal. At low temperatures the magnetization

lies along the c-axis. With increased temperature the angle between the easy direction and the c-axis varies almost linearly with temperature from zero at 220°C to $\pi/2$ at 320°C at which temperature and above the easy direction lies in the basal plane along the $[1\bar{1}00]$ direction. Above 400°C and up to the Curie point, cobalt is most stable in a fcc crystal structure. Nickel has a fcc structure and iron a bcc structure from 0° K to their respective Curie points. Thus these three 3-d transition ferromagnetic metals all have cubic symmetry and consequently display cubic anisotropy. As will be explained below, cubic anisotropy can result in [100] type directions as being easy directions while [111] type directions are the hard directions. This is the case in iron. Vice versa is possible as well, which is the case in cobalt. Finally, because magnetocrystalline anisotropy is strongly temperature dependent, these directions can change with temperature. Below approximately 200°C, nickel has [111] type easy directions while above this temperature it has [100] easy directions.

The subject of magnetocrystalline anisotropy in ferromagnets and related experimental results have been extensively reviewed by Darby and Issac (1974).

Ferromagnets with dimensions larger than the exchange length can minimize their total energy by forming regions of aligned magnetic moments called domains. In each domain, the magnetization is equal to the spontaneous magnetization M_s which would be found in the fine particle. The magnetization in each domain tries to align as closely as possible to an easy direction to minimize its anisotropy energy. In zero field, the ferromagnet can be in a demagnetized state or at least a state of net magnetization less than the value M_s. This depends on the arrangement of

domains within the ferromagnet.

Separating the domains are narrow regions called walls. In traversing a wall, the direction of magnetization rotates smoothly from being in one easy direction to being in another easy direction in an adjacent domain. When the rotation takes place in the plane of the wall, it is called a Bloch wall. Discontinuity in the component of magnetization normal to a wall is avoided, otherwise a charged wall would result at a cost of magnetostatic energy. The formation of a wall requires a cost of both exchange energy E_e and anisotropy energy E_k in a one to one ratio. The thickness of a wall is $\sim(E_e/E_K)^{1/2}$.

Domain walls are classified as 180 degree walls or 90 degree walls depending on the relative angle of the magnetization in each of the adjacent domains. In a thin layer of bubble material such as rare-earth iron garnets, there are serpentine or stripe domains separated by 180 degree walls. A strong uniaxial anisotropy exists aligning the moments either parallel or antiparallel to the normal to the layer. A bias field when applied causes the antiparallel domains to shrink down into cylindrically shaped domains called bubbles.

In iron, both 180 degree and 90 degree domain walls exist. The classic domain structure for a bar of iron is called the Landau structure (see fig. 2). It is characterized by 4 domains, 2 major domains running the length of the bar and separated by a 180 degree wall, and 2 minor domains at the ends. The end domains or closure domains are separated from the long domains by 90 degree walls. Note that all walls and surfaces are charge free, except possibly where the walls intersect the surfaces.

The walls we have described so far are Bloch walls. Another type of

wall can exist in which the magnetization rotates in a plane perpendicular to the wall. This is called a Néel wall and if it occurred in the bulk of a ferromagnet, would be very costly in terms of magnetostatic energy due to charge on such a wall. However, returning again to the Landau structure, if the Bloch walls gradually became "Néel-like" at the side surfaces, a saving of magnetostatic energy would be achieved. The net result of this is the existence of two essential point singularities in the magnetization, one on each of the side surfaces, which is dictated by the topology (Arrott et al. 1979).

In the case of nickel with [111] easy directions, the walls, even though they are commonly called 90 degree walls, are not true 90 degree walls. Actually they are approximately either 70.53 degree walls or 109.47 degree walls; the angles are those of a tetrahedron.

It is interesting to note that a 180 degree wall can be thought of as a pair of 90 degree walls. Therefore what makes a 180 degree wall a stable entity? Kittel (1949) answered this question by pointing out the effect of magnetostriction. When a ferromagnet expands or contracts anisotropically depending on the direction of the spontaneous magnetization M_s, this is called magnetostriction. Similarly, an applied tensile or compressional stress can induce an effective magnetostrictive field which in turn results in a torque on M_s. This magnetoelastic property further complicates the story of the magnetostatics of ferromagnets. Two parallel domains separated by a 180 degree wall expand identically (magnetostriction is axial, not directional), stablizing the wall. Returning once again to the Landau structure, the thicker the bar of iron is, the larger the closure domains become. In iron, which has a positive magnetostriction, the total magnetic

energy in thicker bars can be reduced by having two or more parallel 180 degree walls. This allows more, but smaller closure domains. The cost in additional wall energy is more than made up by the saving in strain energy.

Domain structures are easily observed on the side surfaces of bars by means of the Bitter technique. A colloid suspension of ferrite particles is applied to the bar. The particles congregate at the walls making them visible with a light microscope. A discussion of the Bitter patterns observed on our samples will be given below. An alternative is to exploit the Kerr effect by which the plane of polarized light reflected from a magnetic surface is rotated depending on the state of magnetization at the surface. With the use of crossed polarizers, domains and walls become clearly visible. On transmission, the analogous principle is called the Faraday effect. This is commonly used to study bubble domains since thin layers of bubble material such as orthoferrites and garnets transmit light in the visible region.

Finally we can mention the case of ferromagnetic material with little or no magnetocrystalline anisotropy. Such ferromagnets are called soft or ideally soft, although these terms assume low defect densities as well. With no such anisotropy the formation of domains of rigidly aligned moments separated by narrow walls is not energetically necessary. Rather, more favourable conditions are achieved by a "curling pattern", an arrangement in which the moments locally remain as nearly aligned as possible, but, on the scale of the specimen, curls back on itself to achieve a demagnetized state.

Such a condition is observed in iron itself. As the temperature is increased, narrow walls begin to broaden out as the magnetocrystalline anisotropy rapidly decreases. Eventually wall thicknesses reach the same

size as sample thicknesses a few millidegrees below the Curie point. For a study of the magnetization processes in ideally soft materials, see the paper by Heinrich and Arrott (1975).

We have outlined the extensive role that magnetocrystalline anisotropy plays in ferromagnetism. The rest of this thesis reports a study of this in iron. The samples used are single crystals called whiskers. A study of their domain structures and ac susceptibilities is reviewed. A detailed measurement of the approach to saturation of an iron whisker as it is magnetized in the [111] direction is examined as well. The results are compared with mean field theory and the Potts model. Finally, measurements of the spontaneous magnetization M_s and the anisotropy field H_k as a function of temperature from room temperature to the Curie point are reported and discussed. In particular the temperature dependence and the magnetization dependence of the anisotropy of a cubic ferromagnet just below the Curie point is measured for the first time.

II. THE SAMPLES: IRON WHISKERS

All of the magnetic measurements described in this work are conducted on single crystals of iron called whiskers. The samples are grown, selected, and characterized for the measurements we wished to make. In this section we describe our technique for the growth of iron whiskers as well as the apparatus used. The theory of whisker growth is discussed. A report is made of the various attempts to measure and control the purity of the whiskers grown, particularly in terms of the magnetic disaccommodation or after-effect. In the next section a comparison is made between the three different orientations of whiskers in terms of domain structure, ac response, magnetization curves and observed Bitter patterns.

1. The Growth of Iron Whiskers

Iron whiskers are long thin fiber-like crystals. They are grown using a technique in which ferrous chloride is reduced in a hydrogen gas flow at approximately 710^{o}C. Whiskers of many of the transition metals, as well as of silicon, have been grown. The technique that we describe below is very similar to the technique first used by Brenner (1956,1963). Many researchers have adapted his technique to produce iron whiskers for their studies (see for example, Isin and Coleman 1965, Heinrich and Arrott 1972, Bloomberg 1973, Lonzarich 1973, Lowrey 1976, Berger 1978, and Hanham et al. 1979). Iron whiskers have been used for the investigation of micromagnetic and magnetostatic behaviour, domain structure, critical phenomena, exchange-

splitting, galvanomagnetic properties, and transport properties. Much of the current interest in whiskers is concerned with the production of refractory whiskers, e.g. aluminum oxide, boron carbide and silicon carbide. These materials offer an exceptional combination of high strength, high stiffness and low density as reinforcements in advanced composite materials.

A schematic drawing of our growth apparatus is shown in fig. (3). An iron boat is centrally located in a 50 mm x approx. 2 m quartz furnace tube in a Linberg furnace which is approximately 1 m long. The furnace has 3 zone control so that some variation of the temperature gradient along the furnace tube can be made. At the ends of the furnace, asbestos ribbon is wrapped around the furnace tube to insulate the furnace. The temperature of the centre of the furnace is measured with a chromel-alumel thermocouple and a voltmeter. At the inlet end of the furnace tube, a regulated flow of dry "hydrogen zero" gas (< 5 ppm hydrocarbons) is delivered from a cylinder through a Matheson hydrogen-purifier filter and two liquid nitrogen cold traps. The second cold trap can be by-passed through a water bubbler. This array of bubbler, cold traps and valves is made of pyrex. The valves are pyrex with teflon and viton parts and seals. No grease is used anywhere in the system. This array is connected to the hydrogen cylinder and to the furnace tube flange with tygon tubing. The furnace tube flange is a stainless steel quick-lock coupling with a viton o-ring. The coupling is heli-arc welded to a Kovar seal on the end of the furnace tube. The I.D. of the coupling is large enough to take an iron boat. The exit end of the furnace tube is closed except for a small 8 mm glass tube. This tube is connected with tygon tubing to a water bubbler which in turn is connected to some system for venting the exhaust gas. The depth of water in the bubbler

is kept close to 2 inches and determines the pressure in the furnace tube relative to the ambient pressure. The exit end of the furnace tube is fitted with a window so that the growth process can be watched with a telescope as it takes place.

We now wish to describe the growth technique. We first describe what we wish to achieve, that is, what we consider a good growth or run, and what we do to achieve this.

For the purposes of the kinds of measurements described in this thesis, a good run produces a boat with numerous whiskers with clean shiny surfaces. Although it is possible to achieve a tangled jungle of whiskers, our runs tend toward low yields, even to the extent of no whiskers at all. A coating of only small iron cubes and clusters in the bottom of the boat can occur. The whiskers we prefer are long thin crystals with regular crystal-plane surfaces. Ideally they should be untapered or have untapered sections which can be cut. Lengths and thicknesses hopefully lie in the 5 to 15 mm and .025 to .500 mm range respectively, although whiskers as long as 50-60 mm and with thicknesses from .005 to 1.000 mm have been grown.

These boats ideally should have a clean, shiny and glittery appearance. After they are removed from the furnace tube, they are stored in a glass tube with a rubber stopper containing calcium sulphate to absorb moisture, reducing the oxidation of the crystal surfaces.

How we achieve a good run cannot be stated in precise terms. We can only describe our technique and the kinds of things we are concerned about in order to produce a good run. There are no hard and fast rules that we know of for growing whiskers of the various orientations. We simply grow lots of whiskers and let statistics do the rest. Of the whiskers which we consider

useable, about 90% of them are [100] oriented i.e. they have a [100] oriented axis with four (100)-type side surfaces and a square cross section. The rest of the useable whiskers are [111] oriented with six (110)-type side surfaces and an hexagonal cross section. A very few rare whiskers are [110] oriented.

To make a boat, a piece of sheet iron (8" x 2.5" x 0.01", 99.99% Fe) is cut and cleaned with water and a scotchbrite pad. The sheet is bent into the shape of a shallow boat (about 0.5" deep) with pliers taking care not to put finger grease on the boat. It is important to make the sides of the boat just steep enough to contain the melted iron chloride, but no more than 45 degrees. Most of the whisker growth will occur on the sides of the boat provided they are not too steep. The ends of the boat are usually bent square to the bottom to enhance turbulent flow of the gas. A greater yield in the bottom of the boat was once produced by bending the bottom in a corrugated shape thus producing more side surfaces on which to grow. Scratching the various surfaces does not increase the yield nor does it provide preferred nucleation sites for whisker growth.

The empty boat is precleaned in the furnace tube with a rapid flow (about 20 ml/sec) of wet hydrogen. The temperature is maintained at 730°C for 2 hours. Wet hydrogen, produced by engaging the front water bubbler, is commonly known to be more effective in removing carbon from iron. The front bubbler does not contain sufficient water to bubble hydrogen through the water, but merely to pass the gas over this surface. The boat can be seen to be visibly cleaner after the process.

Into the clean cold boat is placed 40-50 gm of anhydrous ferrous chloride (supplier - ICN Pharmaceuticals Inc.), a beige-brown powder which is

photolytic. In a slow flow of dry hydrogen (about 2 ml/sec) the boat in the furnace tube is heated to the melting point of $FeCl_2$ (about 680°C) over a period of approximately 30 minutes. As the temperature continues to increase to the growth temperature, the front water bubbler is engaged for 30 minutes. Afterwards it is isolated with the valves and dry hydrogen is used for the remainder of the growth procedure. It is believed that the yield is increased by this initial introduction of water, that perhaps the water vapour aids in the nucleation of whiskers. In fact, in two runs where meticulous care was taken to clean the boat and the system, and where only dry hydrogen was used, boats with no whiskers were produced.

Whiskers have been successfully grown with the centre of the boat in the temperature range 690-730°C. At lower temperatures, the reaction is incomplete and whiskers too fine to be used (like a fine gauze pad) are produced. At higher temperatures the yield drops off and whisker as well as other iron growth occurs outside of the boat on the quartz furnace tube.

The distribution of whiskers in the boat and the yields are also affected by the flow rate and the temperature gradient. Too fast a flow reduces the yield. If the temperature profile is too flat, whisker growth is more likely outside of the boat.

Accompanying the growth of iron are two kinds of non-metallic by-products which are possibly hydrogen perchlorates. One is a fine white powder which appears as a beautiful snow storm in the ends of the furnace tube just outside of the furnace in the early stages of the growth process, particularly at the downstream end. The other is a growth of thin film-like wings which are beige-brown in colour and translucent. This appears in the zone between the end of the boat and the end of the furnace on each side of

the boat. The greatest growth of this kind occurs just inside the furnace at the downstream end at a temperature of about 150°C. The wings, if left to stand in air, decompose and are fairly corrosive. If the flow rate and temperature gradients are just right, a good separation of the three kinds of growth is achieved, and a clean uncontaminated boat is produced.

Whisker growth has been observed with the telescope mentioned above although this was difficult due to the white snow storm. There is a great deal of whisker formation in the first ten minutes after the growth temperature is reached. Possibly no further whisker formation takes place after this period of time. However the growth conditions of flow and temperature are maintained for another eight hours. This ensures that all of the ferrous chloride has been reduced.

Finally as the furnace is cooled (to room temperature in two hours), the hydrogen flow is increased and maintained at 20 ml/sec. Once cooled the boat can be examined and stored. Yields will vary from dozens of whiskers to none. Whiskers are picked from a boat with fine tweezers under a microscope. Undesirable ends are cleaved with a razor blade on a glass plate. Whiskers are easily handled with a magnetized needle and can be slid into a quartz capillary tube to be hermetically sealed or simply to be protected from being bent.

2. The Theory of Whisker Growth

Despite the amount of research that has been conducted on whiskers, both as a type of crystal growth to be understood as well as a source of materials

for research of their physical properties, a complete theory of whisker growth does not exist. In this section we briefly outline some of the proposed mechanisms of growth for whiskers and point out where each may or may not be applicable to the case of iron. More detailed descriptions of the various mechanisms can be found in the monographs by Wagner (1970) and Evans (1972).

Whiskers of a great number of elements and compounds have been found in nature or have been synthetically grown. The list includes examples of metals such as iron, zinc and tin, semiconductors such as silicon and germanium, refractory materials such as aluminum oxide, boron carbide, and silicon carbide, and naturally occurring fibers such as asbestos. The term whisker applies to a filamentary single crystal which is highly perfect in structure. It may not necessarily be chemically pure, a consequence of contamination during the growth process or subsequently during handling in an environment foreign to the growth environment. In fact such contamination may be a necessary requirement for the whisker growth to occur. Length to diameter ratios are commonly 100 - 1000 or more (at least 5). Diameters range from 0.02 to 1000 micrometres.

Rates of growth can vary over a range of seven orders of magnitude or more. Spontaneous growth can be as slow as 0.1 nm/sec while synthetic chemical growth under ideal conditions can be as fast as a few mm/sec.

Most whiskers can be grown with a uniform cross section which can be square, rectangular, hexagonal, triangular, circular, or even star-shaped. The axial growth direction and side faces usually have small Miller indices. Some species of whiskers such as nickel may be hollow. Unusual but regular shapes such as helices are also possible.

A high degree of structural perfection in terms of dislocation density and atomically smooth surfaces is possible in whiskers. A consequence of this perfection are properties of high mechanical strength, abnormally low vapour pressures compared to the bulk, large overvoltages necessary for electrodeposition or dissolution as well as properties which are specific to certain materials. Examples of this last category are the magnetic properties of iron whiskers and the ferroelectric properties of barium titanate whiskers.

All whisker growth involves four distinct steps:

i) initial nucleation on a substrate.

ii) a primary one-dimensional leader growth.

iii) a subsequent thickening of the primary growth.

iv) a final slowing-down of the rate of growth.

Step iii) may not occur. In our observations of the growth of iron whiskers, it never took place. Steps i) and ii) are the crucial stages of growth which need to be understood. How is nucleation in the initial stage of whisker growth brought about? What are the conditions and mechanism by which growth only occurs on the tip of the primary leader with no nucleation and growth on the side surfaces?

2.1 Nucleation of Whiskers and the Screw Dislocation

The classical picture of nucleation considers an atomically smooth crystal face in equilibrium with its vapour at a pressure P_e. Numerous atoms and small groups of atoms (or molecules) condense on the surface. They

are mobile and capable of diffusing long distances over the surface before evaporating. With increasing vapour pressure P, the number and size of condensed groups increase. Eventually a critical nucleation level $(P/P_e)_{crit}$ for two dimensional nucleation is reached where the surface nuclei are stable. This is the first step to crystal growth since a stable nucleus provides steps and ledges which are energetically favourable sites for atom deposition. Growth can therefore continue at supersaturation ratios well below $(P/P_e)_{crit}$ until an atomic layer is completed. Clearly the limiting factor in the growth of a perfect crystal is the nucleation problem, that is, starting new layers.

This simple picture predicts supersaturation values $(P/P_e)_{crit}$ in the range 5-10. However experimentally observed values are very close to unity. This discrepancy was first explained by Frank when he suggested that all real crystals contain screw dislocations which provide a source of steps for sustained crystal growth. [For a review of this field see, Neugebauer (1959) and Friedel (1964).] If a screw dislocation is present it is never necessary to nucleate a new layer. The crystal will grow in a spiral process at the exposed "edge" of the dislocation. Edge sizes h are usually only one or two atomic spaces since strain energy of a dislocation goes as h^2. It is likely that most crystal grown at low supersaturation will contain dislocations, otherwise the crystals would not exist.

The logical consequence of Frank's screw dislocation proposal is that whiskers contain one or more screw dislocations parallel to their axes. This offers a possible mechanism by which a whisker can grow below the critical supersaturation level at energetically favoured sites on its tip while maintaining smooth sides. Screw dislocations have been observed in whiskers

of some materials such as magnesium oxide and silicon by transmission electron microscopy, but not in all whiskers.

A study on the initial stage of the reduction growth of iron whiskers has been conducted by the Japanese researchers Tino and Mukoyama (1969). They used the Brenner technique of reducing $FeCl_2$ at 720°C with hydrogen to grow iron micro-crystals. They allowed the growth to occur for only ten minutes or less. The substrates on which they nucleated the micro-crystals were optically flat fused quartz plates. These plates had been etched with 2.5% HF which produced a regular succession of etch pits on the plate surfaces. The result was that almost all the micro-crystals of iron produced grew along the rows of etch pits. These micro-crystals were not randomly oriented on the quartz plates indicating the existence of some short range order in the quartz surfaces. Most of the micro-crystals grown had a square or rectangular (100) surface parallel to the surface of a plate, but some micro-crystals of other orientations were grown. The shorter the reaction time used, the larger the number of small-size crystals. Edge lengths ranged from 0.1 to 10's of micrometres, while heights were from one half to one times that of the edge length. The smallest micro-crystals grown appeared as small rounded points.

Upon etching these micro-crystals with 0.4% Picral, they found generally a few etch pits. These pits were located not only near the centre of a micro-crystal, but often near an edge or corner. Sub micro-crystals and sub whiskers were observed to grow near the corner of a micro-crystal. This seemed supportive of the view that the growth of an iron whisker can occur around a screw dislocation in the initial stage.

We generally find in the highest quality [100] iron whiskers which we

grow that three of the side surfaces are very smooth, while the fourth is blemished, often with a long rift valley running the length of the whisker. This imperfection is macroscopic on a 0.1 mm thick whisker, much larger than the edge pits observed on the micro-crystals in the early stages of growth by Tino and Mukoyama. This side imperfection is not observed in [111] oriented whiskers which we grow.

Tino and Mukoyama also observed the coalescence of several small micro-crystals into larger ones during re-growth experiments. Lattice misfits occurring during these coalescences may be eliminated by a thermally activated rearrangement of atoms towards more stable configurations. Conversely, such imperfections may provide favourable sites for crystal growth of the next upper layer. They also speculated "that the development of a micro-crystal or whisker may be carried through a number of births and deaths of active dislocations, but, nevertheless, the perfectness of the resultant crystal is still maintained, provided that the regular atomic arrangement in the basal part is established, the two-dimensional area of which is, however, limited to very small extent."

There are several reasons for not finding a screw dislocation in a whisker. There may be more than one screw dislocation of opposite sign present which could cancel the effect of a lattice twist. A screw dislocation may be moved out of a whisker by diffusion or by a thermally activated slip process during growth. Equally likely, another growth mechanism is the operative one, the most likely candidate being VLS (the vapour-liquid-solid mechanism).

2.2 Nucleation and the Vapour-Liquid-Solid (VLS) Mechanism

The VLS mechanism applies only to the growth of whiskers from the vapour. It was first proposed by Wagner and Ellis (1965) as a means by which whiskers can nucleate and grow at low temperatures without involving a screw dislocation. We briefly describe the growth mechanism in this section. For a review of the fundamental aspects of VLS growth of whiskers see the paper by Givargizov (1975).

The presence of a minute liquid alloy droplet on a substrate, which can act as a preferred site for whisker growth from the vapour, is the driving force for this mechanism to work. Molecules from the vapour can deposit in the liquid droplet at a much lower supersaturation ratios than $(P/P_e)_{crit}$ since the accommodation coefficient of a liquid is much higher than that of a solid. Liquids are "ideally rough" giving them large "sticking factors" for molecules striking their surfaces. In the presence of a vapour of whisker growth material, the droplet becomes supersaturated with these vapour molecules. Alternatively, a heterogeneous chemical reaction takes place between the molecules of the vapour phase as they hit the droplet surface resulting in a new phase of whisker growth material which supersaturates the droplet. Then at the liquid-solid substrate interface, precipitation occurs raising the droplet off the substrate. As long as the vapour is maintained, this process can continue. A whisker grows raising the alloy droplet at its tip.

There are several distinct steps that occur at the whisker tip. We list them in table (1) along with a suggested mechanism by which iron whiskers may grow via VLS and hydrogen reduction of ferrous chloride. Any one of these

steps can limit the growth rate.

The VLS mechanism, if it is to work, puts strong restrictions on the growth conditions. According to Evans (1972), the main requirements which must be simultaneously met for VLS growth are:

(1) The alloying agent or impurity must form a liquid solution with the whisker material at the growth temperature.

(2) The distribution coefficient for the impurity must be such that the impurity concentration is higher in the liquid than in the crystalline solid. If no further impurity is supplied through the vapour the value of the distribution coefficient determines the whisker length.

(3) The vapour pressure of the alloying agent must be low at the growth temperature. Loss of agent from solution does not necessarily change the alloy composition, but it does change the droplet volume and hence the whisker diameter.

(4) The alloy must not be susceptible to chemical side reactions or react with the substrate if that differs chemically from the whisker.

(5) The various V-S, V-L and L-S interfacial energies are crucial, since it is important to achieve the correct wetting angle for whisker formation.

(6) The temperature of the system must remain constant. Small fluctuations may cause large diameter variations.

The sensitivity of the diameter of a whisker to temperature may explain why many iron whiskers are grown with a uniform taper. If the whisker is formed by a VLS process as the temperature drifts, the size of the droplet,

the contact angle between the droplet and the whisker, and the supersaturation level can change.

The classic illustration of the VLS mechanism at work was accomplished when a researcher spelled out the letters "VLS" in tiny gold droplets on a silicon substrate. Subsequently under controlled growth conditions, a single silicon whisker was grown at each gold droplet location (see Wagner (1970) p.80).

3. The Role of Impurities in Whisker Formation

It is well known from extensive research into whisker growth that the presence of an impurity may be necessary for the formation of whiskers. In a study where silicon doped with arsenic was the growth material, it was found that the addition of small amounts of nickel iodide was essential for whisker growth (Greiner et al. 1961). In a process described by Wagner (1970) to grow silicon whiskers from high-purity silicon and iodine, only nodules and films were produced. However with the introduction of a trace amount of gold, a lush growth of whiskers was created. The ratio of filament to nodule deposit increased with the amount of gold added. Successful whisker growth was also achieved with Ni, Pd, Cu, Cd, Mg, and Os as impurities, while only nodules were produced with Zn, C, Mn, Sn, or Ce.

As mentioned above in the section on the growth of iron whiskers, no whiskers are produced when great care is taken to clean our growth system and to avoid the introduction of impurities such as water. We find that the introduction of water in the initial stages of growth increases the yield of

iron whiskers.

As is well known, iron has a high affinity for the interstitial and substitutional incorporation of carbon. In fact one of the best known phase diagrams for a binary alloy system is that of carbon in iron (Hansen 1958).

4. Carbon in Iron

In this work we are concerned with α-iron with very low concentrations of interstititial carbon. This phase is bcc and exists up to approximately 910°C. Therefore our growth of iron whiskers and our magnetic measurements from room temperature up to the Curie point (770°C) can be done all in the α-phase. At 910°C there is a first order phase change into the fcc γ-phase. Whenever we have heated a whisker through this transition temperature and then cooled through the Curie point, it has resulted in irreversible damage to the initially near-perfect crystal structure.

Several tests have been carried out either by us, or for us, to determine the carbon content of the iron whiskers which we are studying. The most conclusive of these was conducted by D.E. Hanham, Chief Chemist, International Nickel Company of Canada Ltd. in Port Colborne, Ontario. The analysis was performed on six samples, each consisting of one gram of iron whiskers. These whiskers were taken from a boat supplied to us by C.G. Lonzarich, Physics Department, UBC, Vancouver, BC. We consider these whiskers to be typical of our whiskers since a very similar technique was used to grow them. The only difference is Lonzarich's much greater yield of whisker growth which we attribute to the larger boat, larger furnace tube and

much larger amount of $FeCl_2$ used. It was his goal to produce great amounts of large size whiskers which he admirably achieved. We used Lonzarich's whiskers for this test because of the large sample size required.

The carbon concentration was determined by measuring the infrared absorption of the CO_2 produced in a complete combustion of a one gram sample of whiskers. The measurement was made using a device called the IR12, made by Leco.

The results of the six measurements in % carbon by weight are:

0.0022

0.0043

0.0020

0.0049

0.0230

0.0032

We reject the fifth measurement since we believe the sample was contaminated by a piece of tissue paper packed with the sample. Averaging the other five measurements produces a figure 0.0033(13) % carbon by weight = 150 ppm atomic ratio C/Fe. This establishes an upper limit for the total carbon content of our whiskers since greater care is taken to eliminate sources of carbon in our growth procedure.

The obvious questions at this point are what is the source of carbon, and, at what point is carbon taken into a whisker. As yet both of these questions remain unanswered. There is still sufficient doubt about the actual mechanism of iron whisker growth that the possible necessity for carbon in a VLS process cannot be ruled out. On the other hand, carbon may not be a catalyst for whisker production, being only an incidental impurity

in the growth environment. We cannot be absolutely sure that there is no source of carbon within our growth procedure.

The other and very reasonable possibility is that carbon is incorporated in iron whiskers subsequent to their growth when they are removed from the furnace tube. Kishi and Roberts (1975) show, using x-ray and vacuum ultraviolet [He(II)] photoelectron spectroscopy, that carbon monoxide readily dissociates on clean iron films at room temperature. At lower temperatures only molecular CO is adsorbed. However at 295 K both adsorbed molecular and dissociated CO is observed, and at 350 K only dissociated carbon and oxygen can be detected. When a film is pre-adsorbed with sulphur by exposure to H_2S, the dissociation of CO is suppressed and consequently adsorption entirely in the molecular state occurs. Finally they also find, when an iron film with adsorbed CO is exposed to H_2S, that the chemisorbed oxygen is removed and desorbed as H_2O by hydrogen generated from the H_2S dissociation. This leaves carbidic carbon on the surface.

A study of the equilibrium surface segregation of carbon on iron (100) faces has been reported by Grabke and coworkers (1975). They dissolved 0-120 wt. ppm C in iron single crystals with specially prepared (100) surfaces by carborizing them in a flow of CH_4-H_2 mixtures at 800°C. They then studied the composition and structure of carbon chemisorbed on the (100) surfaces using Auger electron spectroscopy (AES) and low energy electron diffraction (LEED) in a vacuum system at a pressure of less than 10^{-9} torr. This study was possible because the rate of desorption of carbon from a surface was sufficiently slow and the solubilities were sufficiently high that an equilibrium between carbon atoms adsorbed on the surface and carbon atoms dissolved in the bulk could be established quickly without depleting

the adsorbate. The driving force for this surface segregation is the release of elastic energy minus the decreased binding energy accompanying the relocation of a carbon atom from the bulk to the surface.

Using LEED they detected the deposit of graphite on the surface which dissolved once a sample was heated above the graphite solubility curve. This dissolving process was monitored by AES as well which showed the formation of fine structure associated with carbon atoms, and the disappearance of fine structure attributed to graphite. The adsorption of carbon was measured as the ratio of peak heights for carbon and for iron versus temperature. At low temperature this ratio approached the value 0.6, which probably corresponds to the formation of a surface structure in a saturated limit. With calibration against known alloys this limiting value was determined to be C/Fe = 0.2 on the surface, vastly different from the ppm levels of the bulk samples. This ratio corresponds to a surface structure p(2x2). However the LEED pattern indicated a c(2x2) structure.

AES analyses have also been conducted on some of our iron whiskers by Physical Electronics Inc. of Minneapolis, Minnesota. The bulk interstitial carbon content had been determined by us, using a magnetic technique described below, to be approximately 10 ppm. Physical Electronics found the carbon content of the surface to be C/Fe = 0.2 in agreement with the AES work of Grabke and co-workers.

Another possible method of determining the carbon content of a whisker is to measure its electrical resistivity. Swartz and Cuddy (1971) have made resistivity measurements on high purity iron wires (resistivity ratio = 180) from 4 to 1300 K. These wires had been charged with known amounts of carbon and nitrogen using several different gas mixture treatments. They reported

$(\rho_{Fe + C} - \rho_{Fe})_T$ values as a function of carbon concentration and temperature. As well they determined a value for the depression of the Curie temperature $dT_c/dX = -1.5 \pm 0.7^{o}$/atm% at 155 $\pm$ 10 ppm carbon. Measurements of the resistivity of our whiskers indicated carbon concentrations on the 10-100 ppm level which were consistent with a measurement by a magnetic technique. However accurate measurements of the resistivity of a whisker were not possible because of the small size of a whisker. Such a measurement also does not discriminate between increased resistivity due to carbon and that due to nitrogen.

However high resistivity ratios have been measured in the 900-4000 range for several of our whiskers. R.V. Coleman claims the highest resistivity ratio measured on an iron whisker in his laboratory is 10,000.

Finally we turn to a magnetic technique which we use for detecting mobile interstitial carbon in an iron whisker near room temperature. This technique exploits a phenomenon called the magnetic after-effect.

5. The Magnetic After-Effect

It has been known for a long time that a small amount of interstitial carbon or nitrogen in α-iron gives rise to the magnetic after-effect or disaccommodation effect. The mechanism of this effect has been theoretically explained by Néel (1952, 1959) and has been experimentally studied by many researchers (see Hejnal (1977) and references therein). The interstitial atoms redistribute themselves among interstitial sites giving rise to a directional order. Through a magnetocrystalline coupling, this results in a

stabilization of domain walls. To describe this phenomenon, Néel adds to the usual terms of magnetic anisotropy, an energy called the stabilization energy, which can attain values of the order of 100 erg/cm^3. Néel derives a general expression for the pressure of a 90 or 180 degree wall at a given time, which causes the diffusion of the foreign atoms, knowing the earlier position of the wall which has been moved.

We mention the magnetic after-effect here as another possible method of detecting interstitial carbon in iron. This can be done by observing the drop in measured ac susceptibility for a [100] iron whisker. This can be thought of as a wall of interstitial carbon gas collecting at the position of a Landau wall. When the wall is rapidly moved to a new position, the effective ac susceptibility increases to the level which would be if there were no interstitial carbon. Then with a time constant of approximately one second at room temperature, the measured ac susceptibility decreases. The size of the drop depends on the dimensions of the sample, the amplitude and frequency of ac drive, and on the amount of interstitial carbon.

The time constant of diffusion is strongly dependent on temperature according to Arrhenius diffusion theory. This is useful for distinguishing between interstitial carbon and interstitial nitrogen since their time constants are quite different at room temperature (about 0.1 sec for N).

This effect can be used as a convenient non-destructive measure of the amount of mobile interstitial carbon and nitrogen in an iron whisker. This can be studied as a function of temperature and as a function of various treatments of the whisker, either to decrease or increase the amount of interstitial gas.

III. THE THREE TYPES OF WHISKERS

There are three species of iron whiskers, each with its own orientation, namely the [100], [111], and [110]. In this section we compare these whiskers in terms of their domain structures. The information about the domain structures is obtained from, or inferred from, Bitter patterns and ac susceptibility measurements. We first describe these two techniques, and then follow with a comparison of the three whiskers.

1. The Bitter Technique

This technique is a method of making direct observation of domain wall patterns on the side surfaces of a magnetic crystal. A colloidal suspension of fine ferrite particles is placed on a smooth crystal face. The particles tend to congregate wherever a domain wall intersects the crystal surface. This makes the pattern of walls clearly visible with an optical microscope. By applying a dc magnetic field to the crystal, domains can be observed to grow at the expense of others by means of wall motions. Both translational motion of long straight walls and wall bowing can be seen. With a careful study of these wall motions and of the relative angles of the walls on the crystalline surfaces, a correct picture of the internal domain boundaries can be deduced. Most interesting is the irreversible behaviour of the walls at the point of saturation of the centre of a bar, such as an iron whisker. An applied dc field H_o parallel to the bar which just saturates its centre, and therefore splits the previous walls, is called the departure field H_d.

A smaller field which just allows the reformation of some domain structure at the centre is called the nucleation field H_n.

2. AC Susceptibility Measurements

An ac susceptibility measurement of an iron whisker can be made by simply using the whisker as the core of a transformer. The primary coil can be a tightly wound single layer solenoid which is much longer than the whisker. Another possibility is to use a matched pair of Helmholtz coils properly spaced to produce as homogeneous a driving field as possible. A typical driving field is 10 mOe at a frequency from 0.25 to 25 kHz. The secondary coil is tightly wound and can be a long coil which averages the ac flux over the length of the whisker. Alternatively it can consist of as little as one turn and can be placed at any position z along the whisker's length.

The ac signal from this pick-up coil is input to a PAR 124 lock-in amplifier which can be used to separate two orthogonal components of this signal, an in-phase component ε' and an out-phase component ε''. With no whisker in the coil system, we can set the phase of the lock-in amplifier for a maximum detected signal. We call this the in-phase signal from the pick-up coil alone (for reasons which hopefully will be made clear below) despite the fact that this signal is 90° out of phase with the driving signal. (Actually it is 90° ahead of the driving signal for concentric coils wound in the same sense.) There is no out-phase signal orthogonal to it. Alternatively, rather than removing the whisker from the coil system, something which is

often inconvenient to do, a very strong dc field H_o can be applied parallel to the whisker axis. With a strong bias field the whisker is unable to respond magnetically to the ac driving field, and so in a similar manner, the phase of the lock-in amplifier can be adjusted for a zero out-phase signal. This phase setting may be slightly frequency dependent as will be seen below.

When the bias field H_o is made smaller than H_n, some domain structure is nucleated resulting in a strong pick-up signal ϵ. At sufficiently low frequency, the ϵ' signal is a measure of the magnetic stiffness, the ease with which magnetic domain walls oscillate in response to the ac driving field. A high intrinsic susceptibility χ_i corresponds to freely mobile domain walls which produce a large in-phase signal. Domain walls are very mobile if they involve little or no net rotation of moments away from easy directions. We shall see this is the case in the [100] and [111] whiskers for small dc fields. If locked or immobile walls are forced to bow, and spins are forced to rotate in response to the driving signal, a much smaller χ_i, and a comparatively smaller ϵ', will be detected. This is the case for whiskers in higher fields.

The out-phase signal ϵ'' is a direct measure of the losses in the transformer system. Since an iron whisker is a highly conductive core, the major source of loss, at the frequencies we use, is eddy currents. Provided that the flux penetration is complete, the power-loss/unit volume due to eddy currents is proportional to $\sigma\omega^2 M_s^2 A_{eff}$ where σ is the conductivity, ω is the frequency, M_s is the saturation magnetization, and A_{eff} is an effective cross-sectional area for the whisker dependent on the domain structure nucleated. (For a study of eddy currents generated by wall motions in iron-3% silicon picture frames, see the classic paper by Williams et al.

(1950).

There are several other sources of loss. At low frequencies, the most important mechanism is hysteresis. The origin of this is damping phenomena such as eddy currents resulting from irreversible wall motions or jumps, as well as irreversible spin rotation. In the Rayleigh region, the loss depends on the amplitude of the applied field H_o. Also at low frequencies, the magnetic after-effect due to the diffusion of interstitial gas atoms such as carbon or nitrogen is a source of power loss.

Intrinsic losses are also present in the form of some sort of friction which affects the free precession of spins in an internal field. These have been described by the equations of motion of Gilbert, and of Landau and Lifshitz, each postulating a damping phenomenon. This is currently an area of active research, particularly towards understanding the spin dynamics and fluctuations of a ferromagnet near its critical point.

Finally, at higher frequencies losses in the form of resonances become important. There are dimensional resonances due to the driving of electromagnetic standing waves in a specimen and the resonant absorption of microwaves at ferromagnetic resonance (FMR).

Now for the moment let us assume that the frequency is sufficiently small that $\varepsilon'' << \varepsilon'$. Consider a single turn pick-up coil at position z as shown in fig. (4). There are three contributions to the flux through this coil which induce the voltage ε':

$$\bar{\Phi}(z,t) = \bar{\Phi}(z)\, e^{i\omega t} = H_o A_c e^{i\omega t} + \left[4\pi \bar{\chi}_e(z)\, H_o A_w - H_D(z) A_c\right] e^{i(\omega t - \delta)} \qquad (1)$$

Here H_o is the applied field, $\chi_e(z)$ is the average effective susceptibility at position z, $H_D(z)$ is the average demagnetizing field, A_c is the cross sectional area of the coil, and A_w is the cross sectional area of the whisker. We can remove the $e^{i\omega t}$ time-dependence and just look at the amplitudes. The first term is the signal from the driving field itself, that is, the in-phase signal for a whisker in a very strong dc bias field. The second and last terms are due to the sample. The second term represents the ac flux from the net magnetization M averaged over the cross section of the whisker. The effective susceptibility $\chi_e = M/H_o$ is what we normally would like to determine. The last term represents the opposing flux through the coil due to the demagnetizing field. The sources for this field are magnetic charges distributed over the side and end surfaces of the whisker.

From Faraday's law of induction, the signal detected by a single turn at position z is

$$\mathcal{E}(z) = -\frac{1}{c}\left|\frac{d\Phi(z,t)}{dt}\right| = \frac{i\omega}{c}\,\Phi(z) \tag{2}$$

$$\mathcal{E} = \mathcal{E}' - \mathcal{E}'' = \frac{-i\omega}{c}\left(\Phi' - i\,\Phi''\right) \tag{3}$$

The in-phase signal is given by

$$\mathcal{E}'(z) = \frac{-i\omega}{c}\,\Phi'(z) =$$
$$-\frac{i\omega}{c}\left[H_o A_c + 4\pi\chi'(z) H_o A_w - H_D'(z) A_c\right] \tag{4}$$

where $\chi' = \chi_e \cos\delta$ and $H'_D = H_D \cos\delta$, while the out-phase signal is

$$\varepsilon''(z) = \frac{-i\omega}{c}\left[4\pi\chi''(z) H_0 A_w - H_D'' A_c\right] \qquad (5)$$

where $\chi'' = \chi_e \sin\delta$ and $H''_D = H_D \sin\delta$. If we call the in-phase signal from the whisker in a high bias field

$$\varepsilon_{hf} = \frac{-i\omega}{c} H_0 A_c \qquad (6)$$

then we can simply write the phase angle δ for the low frequency case as

$$\delta \approx \frac{\varepsilon''}{\varepsilon' - \varepsilon_{hf}} \qquad (7)$$

The phase angle δ is essentially proportional to ω. In the analysis we describe below, we assume that δ can be taken to be zero since the frequencies we use for our measurements are 500 Hz or less. ($\delta < 0.05$)

As well, if the diameter to length ratio d/l is sufficiently small, the contribution of the last term in eq. (1) is much smaller than that of the second and proportional to it, and therefore can be incorporated in it. The demagnetizing field is given by

$$H_D = 4\pi D M \qquad (8)$$

where M is the net magnetization and D is the demagnetizing factor, a geometrical factor mainly dependent on the dimensions of the whisker. D is roughly proportional to $(d/l)^2$ although there is a logarithmic term as well. (For an in-depth discussion and calculation of D factors for whiskers,

as well as of the distribution of magnetic charge on an iron rod, see the thesis by Bloomberg (1973) or the paper by Bloomberg and Arrott (1975).) Consequently for long thin whiskers,

$$\delta \approx \frac{\chi''}{\chi'} \qquad (9)$$

and the two signals are direct measures of the in-phase and out-phase susceptibilities of the whisker.

If we return once again to fig. (4) it is interesting to consider the effect of choosing different surfaces for determining the flux penetration of the coil at position z. In the figure there is shown a surface A which is simply the flat surface of the plane of the coil. Also shown is the cylindrical surface B of depth z with its bottom of area A_c at the centre of the whisker. The net flux Φ through each of these surfaces must be equal. The portion of the flux due to the applied field is the same through both surfaces, and therefore the total flux from the sample penetrating each surface, given by the second and last terms of eq. (1), are equal as well. However from Gauss's law, the flux through surface A due to the demagnetizing field differs by $4\pi Q$ from the flux through surface B, where Q is the magnetic charge enclosed by the two surfaces.

$$\Phi_{H_D}(\text{surface A}) - \Phi_{H_D}(\text{surface B}) = 4\pi Q \qquad (10)$$

From eq. (1), this leads also to

$$\chi_e(0) - \chi_e(z) = \frac{Q}{H_0 A_w} \,. \qquad (11)$$

The distribution of magnetic charge along the length of the whisker controls the distribution of the effective susceptibility and of the demagnetizing field along the length. Actually, inside the whisker, the demagnetizing field remains as uniform as possible to cancel the uniform applied field. Thus when we speak of the distribution of the demagnetizing field $H_D(z)$ along the length of the whisker, we are referring really to the change in strength of the external demagnetizing field outside of the whisker. As a whisker is magnetized, the magnetic charge which is created, expels itself from the centre, and resides in greatest concentration on the end surfaces. This results in a demagnetizing field which is weakest at the central cross section while strongest near the ends surfaces. As well, the effective susceptibility $\chi_e(z)$, and therefore the magnetization $M(z)$, is strongest at the centre and smallest near the ends.

As the bias field H_o is increased, the demagnetizing field increases to cancel it. This is accomplished by increasing the amount of charge on each half of the whisker. Accompanying this is an increase in the magnetization $M(z)$. Rewriting eq. (11), we can see that

$$M(0) = \frac{Q_{1/2}}{A_w} \qquad (12)$$

that is, the magnetization at the central cross section is simply the total magnetic charge on one half of the whisker divided by the cross sectional area. With further increases in the applied field, the centre of the whisker saturates at a value of $M(0) = M_s$ when $H_o = H_d$.

For $H_o > H_d$, the central volume of the whisker which is saturated grows. The charge on one half of the whisker remains fixed at

$$Q_{1/2} = M_s A_w \tag{13}$$

but is excluded from the side surfaces of the central saturated region. This results in an increasing charge density on the ends. In the infinite H_o limit, the charge density on the ends is M_s.

There is a possibility that at the two interfaces between the central saturated region and the unsaturated ends, a certain amount of magnetic charge may be located. This would cause a discontinuity in M(z) at the interfaces to occur. We have made attempts to observe these discontinuities with no success. If they exist, they must be small.

For $H_o < H_d$, the demagnetizing field H_D increases with H_o as the magnetic charge increases. However for $H_o > H_d$, the amount of charge remains fixed as it is driven away from the centre. This results in a decrease in H_D with increasing H_o. In the infinite H_o limit, H_D reaches a minimum value of

$$H_D(0, H_o \to \infty) \to 4\pi M_s \left[1 - \frac{1}{(1+\rho^2)^{1/2}} \right] \tag{14}$$

where ρ is the diameter to length ratio d/l of a cylindrical whisker. Near an end, $H_D = 2\pi M_s$ from Gauss's law.

In fig. (5), we show the continuously measured ac signal detected with a very short tightly-wound 2-turn pick-up coil as it is slid along a whisker. Curve A is for $H_o < H_d$, while curves B, C, and D are for successively larger fields which are greater than the departure field. For each curve, the coil has been moved from position 1 to position 3 as shown in the

diagram. As the central region of the whisker is saturated, the ac flux at the centre quickly drops. For further increases in the field, the only contributions to the flux are the driving field and the demagnetizing field. The former is simply an uniform background, independent of field, of voltage level equal to the level for the coil positioned outside the end of the whisker (i.e. position 3). The latter decreases at the centre as charge is expelled towards the ends. Note that in curve D, the signal at the centre (position 2) has decreased to the level that would be measured with no sample (position 3). From eq. (1), the ac flux in this case is

$$\frac{d\Phi}{dH_0} = \left[1 - \frac{dH_D}{dH_0}\right] A_c \qquad (15)$$

which approaches A_c with increasing applied field. In curves B and C, this high field limit has not been reached. Therefore a positive contribution to the signal from the demagnetizing field can still be seen. The rate of change of the demagnetizing field with applied field gradually decreases to zero as the magnetic surface charge is expelled to the end surfaces of the whisker and as more of its central region saturates.

The difference between the applied field and the demagnetizing field is called the internal field,

$$H_i \equiv H_0 - H_D \qquad (16)$$

It is identical to the Lorenz local field except for a term which is parallel to the local magnetization and therefore exerts no torque. The effective susceptibility is then given by

$$\frac{1}{\chi_e} = \frac{1}{\left(\frac{dM}{dH_o}\right)} = \left(4\pi D + \frac{1}{\chi_i}\right) \qquad (17)$$

where equation (8) has been used and $\chi_i = dM/dH_i$ is the intrinsic susceptibility. For $\chi_i \to \infty$, $H_i = 0$ and $\chi_e = 1/4\pi D$ is determined by the geometry of the sample alone. The smaller the d/l ratio, the larger the effective chi. A smaller χ_i has the effect of decreasing χ_e below the value corresponding to infinite χ_i. However, in some cases where an instability exists, χ_i actually goes negative (through infinity) resulting in an increased χ_e.

It is also important to note that the distribution of $M(z) = \chi_e(o)/H_o$ is dependent on the intrinsic susceptibility χ_i. This has been extensively studied by Bloomberg and Arrott (1975). For infinite χ_i, the applied field H_o must be cancelled by the demagnetizing field H_D. This can be approximated by a linear distribution of charge on the side of a cylinder with a uniform distribution of charge on the ends. A quadratic $M(z)$ along the length of the cylinder results.

For a finite χ_i, there is a net H_i field accomplished by having less charge at the centre. Both the surface charge distribution $\sigma(z)$ and $M(z)$ are represented by higher order polynomials which have profiles that are flatter at the centre and steeper towards the ends.

Ideally, one would like to measure the differential susceptibility χ_{diff} of a whisker. This is the signal one would get with a single sweep of the applied field taking the whisker from saturation in one direction to saturation in the opposite direction. When an ac technique as described

above is used, one measures the reversible portion χ_{rev} of the differential susceptibility. For each value of the dc bias field H_o, the whisker is swept on a small minor loop determined by the amplitude of the modulation field. As an illustration of this point, the trapping of the domain structure of a whisker by interstitially absorbed carbon gas results in such an amplitude dependence. When a very small 5 moe driving field is used to excite the whisker, a trapping can be observed in the form of a decreased χ_e compared to the expected $1/4\pi D$ value. However, if the driving amplitude is increased to say 50 moe, the trapping effect can be eliminated. As well there are often irreversible jumps observable in the χ_{diff} which would not show up in a χ_{rev} measurement. There is information to be had from both types of measurements, and it is important to compare them.

In this section we have outlined the behaviour of a whisker in a dc bias field with a small amplitude ac modulation. We have discussed what you would expect to see with a pick-up coil. We now turn to the task of describing the magnetic domain structure and behaviour of each of the three whiskers.

3. The [100] Whisker

This whisker, the most commonly grown of the three orientations, has four (100)-type side faces and a square or nearly square cross section. The end surfaces are usually cleaved square by us from a longer whisker. Typical length and thickness are 10 mm and 0.1 mm respectively. A slight taper along the length of the whisker is not uncommon.

The domain structure and magnetic behaviour of the [100]-oriented whisker have been studied for some time. The classic domain arrangement for this whisker is the Landau structure, which has been described in the introduction above. A diagram of this structure is shown in fig. (2).

The Landau structure and variations of it have been observed on the side surfaces of [100] iron whiskers using the Bitter technique. These have been extensively reported by Coleman and Scott (1957), and R.W. DeBlois and C.D. Graham (1958). Fig. (6) shows diagrams of some of the possible structures which we have observed such as diamonds and multiple structures in thicker whiskers. With a dc applied field, a bowing of the long Landau wall and displacement of the tie points near the ends can be observed with the Bitter technique.

A structure other than the Landau structure usually occurs at nucleation. This has been dubbed the "Coleman" structure by us since it was first described by R.V. Coleman. One or possibly two long 180 deg walls run the length of the whisker. Each wall nucleates in the corner where two side surfaces meet. As the applied field is decreased, the lines where a Coleman wall intersects two adjoining surfaces can be observed to move away from the edge with the Bitter technique. Thus the area of the Coleman wall increases with decreasing field in contrast to the Landau wall which has a relatively fixed area (ignoring the effect of bowing). The arrangement of closure domains at the ends of the whisker is still not known. The Coleman structure is metastable and eventually will jump into the Landau structure. This will be described below.

The in-phase and out-phase signals in an ac susceptibility measurement of a [100] whisker are shown in fig. (7). These would be typical traces at 1

kHz with a long pick-up coil. The changes in signal are more dramatic in the out-phase component and we now describe the steps by which this trace is made following the numbering in the diagram. Initially there is no out-phase signal at position I corresponding to a large applied field along the length of the whisker. The central region of the whisker is saturated. As the field is decreased, a slight increase in signal can be detected. The volume of the whisker at the ends which is not saturated increases resulting in increased eddy current loss. This increase is not seen with a very short tightly wound pick-up coil at the centre of the whisker. Finally when the nucleation field H_n is reached, there is a large discontinuous increase in the out-phase signal as the Coleman structure is nucleated.

Shown in the diagram is the case for nucleating two Coleman walls, probably in opposite corners. With further decrease in field in region II, the out-phase signal decreases roughly linearly with field. The two walls move inward toward each other increasing their respective areas and decreasing their amplitudes of oscillation. The net result is a decrease in eddy current loss. The 2-wall Coleman structure can persist through the M=0 state and is stable to increases and decreases in the applied field. However once a sufficiently large field is applied in the opposite direction (perhaps $H_o \sim H_{d/2}$), the structure will jump into the Landau structure denoted as region III. If a single Coleman wall had been nucleated, the jump into Landau structure would occur before the M = 0 state is reached. Otherwise the general behaviour is the same. Whether one or two Coleman walls are nucleated depends on the whisker and its magnetic history.

Once the jump to Landau structure has occurred, it can be stable over the full range of applied fields between departure in both directions. More

common behaviour is a jump back to Coleman just before departure is reached. The size of the hysteresis in field (H_d-H_n) is whisker dependent.

The Landau structure is characterized in the out-phase signal by having a maximum at $H_o = 0$. This is due to the fact that the greatest eddy current loss occurs when the Landau wall occupies the central plane of the whisker leaving large volumes of conducting metal on either side in which to induce eddy currents. At departure a very large spike in out-phase is generated due to the process of saturating the centre of the bar, which is sometimes discontinuous. The long domain wall breaks into two pieces, each of which retreats along the whisker towards an end as the applied field is further increased. If departure from the Landau structure occurs, saturation first takes place at the centre of a whisker face and then widens out cutting the Landau wall in half. The Coleman wall breaks right in the edge at the point of first contact.

The in-phase component of the signal is also shown in fig. (7). As can be seen this signal, which measures the magnetic stiffness of the structure, is independent of field. It is also independent of the structure nucleated, although we have observed a small spike occurs in a dc pulse measurement as the structure jumps from Landau to Coleman. For a tightly wound pick-up coil, the full height of the signal above zero voltage (not above the high field background) is a measure of $\chi_{eff} = 1/4\pi D$ for the sample. This assumes that $4\pi D\chi_i >> 1$. Once again large spikes occurring at nucleation and departure can be observed in the in-phase signal. High field tails can be observed in the in-phase signal for both long and short pick-up coils, although the size of the jump at departure is larger for the short coil. These tails relative to the high field background are a measure of χ_{eff} =

dH_D/dH_o. Note that this is a positive contribution to the effective susceptibility above departure. An increase in applied field expels charge from the centre of the whisker resulting in a decrease in the demagnetizing field, which is a change in flux in the direction of the applied field.

All of the above discussion about in-phase and out-phase signals applies only to the case of low frequency i.e. where $\delta >> 1$. As the frequency is increased, the loss angle δ is no longer small resulting in a mixing of the losses into the in-phase signal and the stiffness into the out-phase signal. For a complete discussion of these processes from dc to 200 kHz, see the paper of Heinrich and Arrott (1972).

The departure field of a [100] whisker is given by

$$H_d = 4\pi DM_s \qquad (18)$$

This can be seen from eq. (8) above since we know the internal field $H_i = H_o - H_D = 0$ and the demagnetizing field at saturation of the centre is $4\pi DM_s$. This has been verified by Heinrich and Arrott (1972) by measuring the dc hysteresis loop with an integrating photo-electric galvanometer. Thus it can be seen that a [100] whisker can be used to determine the saturation magnetization M_s by measuring the departure field and its effective susceptibility. This is precisely the technique which has been used by us to measure the temperature dependence of the saturation magnetization of iron, the results of which will be described below. However minor corrections for the anisotropy must be made.

4. The [111] Whisker

Most of the research reported in this thesis was conducted on [111]-oriented iron whiskers. These whiskers are relatively rare and many attempts were made to grow them before success was achieved. They tend to be longer and thicker than the [100] whiskers grown under the same conditions in the same boat. Lengths and thicknesses are typically 12 mm and 0.4 mm respectively. They can be slightly tapered as well.

The side surfaces are six (110)-type surfaces forming a right hexagonal prism with a [111]-axis. This hexagonal whisker can be thought of as a packed bundle of six whiskers, each with a equilateral triangular cross section. Once again the faces of these triangular prisms are (110) surfaces, one face of each of the triangles being one face of the hexagon. Viewing the hexagon in this way makes it easier to understand its domain structure. We will describe the domain structure of the triangular prism and then construct the same for the hexagonal prism from it.

The growth tip of a [100] whisker, if it is not tapered down to a point, is usually irregular. In contrast, a [111] whisker is usually terminated in a beautifully regular growth tip of three mutually orthogonal (100) surfaces. A diagram of a [111]-oriented whisker showing this growth tip appears in fig. (8).

We now turn to describing the domain structure. A simple domain pattern for a triangular prism consisting of 3 domains is shown in fig. (9). Each domain is magnetized in a [100]-type easy direction as represented by the orientation of a small beer can with an arrow. This pattern produces no free-poles on the outer surfaces or on any of the three domain walls. The

walls are 90 degree walls which are (112)-type surfaces. This pattern applies to the central cross section of the prism where there is no charge on the outer surface by symmetry. (Away from the centre there is a variation of the basal plane components that puts magnetic charge density on the surfaces as required by dM_z/dz. The contribution to the magnetic flux from this pattern is $A_s 4\pi M_s/\sqrt{3}$. During approach to saturation in the axial direction, the magnetization vectors continue to lie parallel to the external surfaces of each domain as they rotate. The domain walls are no longer 90 degree walls, but they still remain charge free.

The result of combining 6 of these triangular patterns is shown in fig. (10). This produces 12 domains, 6 of the original triangular domains and 6 diamond shaped domains where triangles join internally. The magnetic flux is still given by $A_s 4\pi M_s/\sqrt{3}$, and the approach to saturation is the same as for the individual triangular prisms. The 6 triangular prisms now share a mutual demagnetizing field.

The start of the reversal process is indicated in fig. (10). Reversal below the knee of the magnetization curve can proceed by nucleation of 180 degree walls in triangular trios. There are six sites where these nucleations can take place, namely the centre of the six triangular prisms. All six nucleations are required for the reversal to be complete.

Fig. (10) shows only the simplest pattern constructed by placing the triangles of fig. (9) in the hexagonal cross section. They can be made much smaller at the cost of wall energy. As saturation is approached, the wall energy gets less and less. In this limit one can gain a lot of entropy by creating fluctuating magnetization configurations based on these divergentless patterns. Each point in a cross section could find itself

sampling deviations from the [111] direction by rotating toward any of the three [100], [010] and [001] directions. The dipole-dipole constraints do not appear to violate the principle feature of the three state Potts model in that the vector has three choices. We will discuss this model below.

It is clear also that the number of reversal processes and demagnetizing states are limitless. This shows up dramatically in measuring the differential ac susceptibility for $M < M_s/\sqrt{3}$ as shown in fig. (11). In cycling the applied field over this restricted range (typically $|H_o| < 15$ oe), one detects a relatively large signal characteristic of a high effective susceptibility associated with wall motion. However in cycling the field one finds numerous sudden rises and falls in the signal as domain walls are nucleated, annihilated or become locked. What is reproducible, however, is that in making a monotonic sweep of the applied field, there are six peaks in the wall motion region. We identify each of these peaks with the nucleation of a trio of mobile 180 degree walls as they come in one at a time. In the figure, we show the signal for only one simple sweep of the field.

In this low applied field region, the response is mainly by reversible wall motion, but the mobility of these walls is not sufficient to produce the ac magnetization that completely cancels the applied ac field. Consequently, at all but the highest temperatures, the susceptibility in this region is less than expected for freely moving walls where the response would be determined by the demagnetizing field alone. This is in contrast to the dc loop measurement which shows a slope of $1/4\pi D$ for M plotted against applied field.

The knee of the magnetization curve at $M = M_s/\sqrt{3}$ corresponds to a steep drop of the measured ac response. With further increase in applied

field, the magnetization process involves rotation away from easy directions towards the [111] hard direction. Eventually a critical field H_c is reached where the susceptibility rises in a spike (at low temperatures) and then drops as the central cross section saturates. Fig. (12) shows a typical curve at room temperature. A typical value for H_c is 420 oe or more, depending on the thickness to length ratio of the whisker. This field, H_c, is related to the anisotropy field, H_k, and the demagnetizing field through the relation

$$H_c = H_k + 4\pi DM_s \qquad (19)$$

It is this rotational part of the susceptibility curve which is carefully studied in the next section. The temperature dependence is reported in the section after that.

Another factor to be considered while speculating on domain structures is the energy density of a wall. Both 90 and 180 degree walls can be oriented at any angle, but this angular orientation affects the energy density. The equilibrium condition is that the exchange energy density be equal to the anisotropy energy density everywhere in the wall. (This is a simplifying assumption which is true only if there is no pinning of the spins at the sides of the wall. Possible dipole-dipole energy is ignored as well.) However the anisotropy energy density, and therefore the total energy density, is dependent on the orientation of the plane of the domain wall. It is simple to calculate this angular dependence as shown in Chapter 9 of Chikazumi's book (1964). For the case of cubic anisotropy in iron, assuming $K_1 > 0$ to be the only important anisotropy constant, one finds the energy

density both of a 90 degree wall and of a 180 degree wall increases monotonically as the wall is rotated from lying in a (100) plane to lying in a (110) plane. The energy density of the (110) wall is 29% higher then that of a (100) wall in the case of 90 degree walls, while it is 38% higher in the case of 180 degree walls.

With this information one can wonder what is the orientation of a 180 degree Coleman wall described above. If it is nucleated in the corner of a [100] whisker at 45 degrees, it is a (110) plane which possesses the highest possible energy density. However if one rotates the wall to reduce the energy density, the area of the wall will increase. If one varies the angle of the wall while holding the magnetization of the whisker fixed, one finds the total energy of the wall is a minimum for the (110) orientation. This helps to account for the stability of Coleman walls over a range of applied fields.

These same considerations can be applied to the 90 degree walls of a Landau structure in a [100]-oriented iron whisker. DeBlois and Graham (1958) made observations of such walls and found them to be inclined away from the (110) orientation so as to minimize their total wall energy.

The energy density of a 90 degree wall is approximately one half of that of a 180 degree wall of the same orientation. This is exactly true for (100) walls. This is easy to understand since one can visualize a 180 degree being composed of two 90 degree walls. (The midpoint of the wall is an easy direction). As mentioned above, Kittel has pointed out that a 180 degree wall is not free to separate into two 90 degree walls. To do so would create a new domain with magnetization perpendicular to the domains on either side. Iron is no longer cubic when magnetic, but expands in the direction of

magnetization by 21 parts per million. This domain perpendicular to those on either side sets up a strain field which suppresses the separation of the wall into two parts.

Thus the walls with the lowest energy density in iron are (100)-oriented 90 degree walls. The (112)-oriented 90 degree walls of the triangular and hexagonal [111]-oriented whiskers have energy densities which are only 2% greater. This strengthens our view that the fundamental domain structure of the [111] whisker is constructed of these types of 90 degree walls.

All of this discussion about wall energy densities forces us to question the nucleation of trios of (110)-oriented 180 degree walls for the purpose of demagnetizing the [111] whisker. Is it not possible to find a demagnetized state using 180 degree walls of lower energy density, preferably (100) walls? First of all we can imagine a demagnetized state for the hexagonal whisker using no 180 degree walls at all. This is illustrated in fig. (13). However this state has two serious drawbacks. It is not easily magnetized and it is composed entirely of (110)-oriented 90 degree walls. We are better off by maintaining the structures of lower energy (112)-oriented 90 degree walls and searching for ways to introduce low energy 180 degree walls.

The introduction of (100)-type 180 degree walls would result in these walls intersecting the (110) faces of the whisker at an angle $\theta = 54.74$ degrees ($\cos\theta = 1/\sqrt{3}$) with respect to the [111] axis. Note that these are the first walls that we have mentioned which intersect the side surfaces of the whisker and therefore could be observed by the Bitter technique. In zero field, we have observed these walls on some of the (110) faces and at certain regions along the length of the whisker. From photographs we made, the walls appear to be at the expected angle with respect to the axis. In the region

on a face where these walls could be seen, they appeared in a regular pattern of equal spacing as illustrated in fig. (14). The ratio of the spacing between the walls, s, measured in the axial direction to the width of a face, w, appeared to be $1/2\sqrt{2}$. This ratio has the following interesting consequence: assuming that these walls exist on the three faces of a triangular whisker in a candy cane pattern, a single stripe would make one revolution in an axial direction of six wall spacings (6s). Thus every face of the triangular whisker is identical (a rotation by 120 degrees is a similarity transformation). The domains alternate in their polarization in a regular way on the faces, but the "sense" of the wall continues from face to face.

The application of a small field causes the walls to pair up, collapse together and vanish. Removal of the field allows the wall to return. It appears that these walls remain only in the demagnetized state. A stable arrangement of these walls with an applied field stronger than that of the earth can not be maintained.

For each candy stripe line observed with the Bitter technique on the central face, there are two possible orientations for walls internally. For example, consider a $(01\bar{1})$ face which has candy stripe lines running upward to the left in a [100] direction. Internally one of these lines could be the edge of either a (010) or a (001) 180 degree wall. A self consistent arrangement of these internal 180 degree walls which is charge free has not yielded to our attempts to determine it. It can be based on the whole hexagonal prism or on individual triangular prisms; more likely the latter since the candy stripe is observed only on some of the faces of a whisker.

5. The [110] Whisker

Without a doubt, the [110]-oriented iron whisker is the rarest of the three observed orientations. Indeed, in three years of growth and study of iron whiskers by us, only two which have [110] axis have been found. However this is partly due to us not knowing what geometry of side faces to expect for this type of whisker.

One of these whiskers we have examined carefully both by the Bitter technique and by ac response. This whisker has six faces, two much broader than the other four, producing a cross sectional shape as shown in fig. (15). The width and thickness are roughly 1.0 and 0.3 mm repectively while the length is about 10 mm.

By the Bitter technique we observed long regularly spaced parallel walls perpendicular to the sample axis on the broad faces. These walls which we have illustrated in fig. (16) extend almost across the full width of a face. Conceivably they could either be 90 degree walls on a (100) face or 180 degree walls on a (110) face. With closer examination, we can also observe patterns such as the one shown in fig. (17) which can only exist on a (100) surface. These patterns consist of 90 degree walls perpendicular to the (110)-axis and 180 degree walls at 45 degrees to this axis. Thus the magnetic structure clearly indicates that the two broad side faces are (100) surfaces.

The angle which the small faces makes with the broad ones was measured and was found to be 54 to 55 degrees in all cases. This was done by first reflecting a laser beam with a broad face onto a far screen. The sample was then rotated on a goniometer about its (110) axis until the beam was

reflected by an adjacent small face to the same point on the screen. The measured angles indicate that the four small faces are (111) surfaces.

The in-phase ac response of this sample as a function of field applied along its length is shown in fig. (18). There is a wall motion region of high susceptibility at low applied fields. There is little of the hysteresis displayed by the [111] whisker. The signal has a maximum at zero field, drops slowly initially, and then much more rapidly as the central cross section reaches a magnetization of $M_s/\sqrt{2}$. The field at this point, $H_1 = 4\pi DM_s/\sqrt{2} \sim 70$ oe is determined by the geometry of the sample. With further increase in field, the signal remains at a low, but field independent, value as the magnetic domains are rotated from easy directions into the [110]-direction. Finally, without a spike, the signal drops to background level at an applied field $H_z = H_k + 4\pi DM_s \sim 660$ oe. This indicates an anisotropy field $H_k = 550$ oe which is consistent with the anisotropy field determined for the [111] whisker according to mean field theory. In the next section we will describe this theory and our measurements on [111] whiskers.

IV. THE APPROACH TO SATURATION OF A [111]-ORIENTED IRON WHISKER

1. Introduction

Over 50 years ago Honda and Kaya (1926) produced magnetization curves for single crystal ellipsoids of iron. Their results are often reproduced in reviews, accompanied by curves showing the prediction of anisotropy theory in the mean field approximation. According to this theory there should be a first order jump in the magnetization for the approach to saturation in the [111] direction. The absence of a jump is discussed by Stewart in his monograph on Ferromagnetic Domains (1954). He recalls the argument of Cans and Czerlinski (1932). The magnetization in the [100] direction does not saturate in zero internal field. There must be some additional field, which may be due to internal stress, that has to be overcome to reach saturation. If this is true in the [100] direction it should also apply in the [111] direction. This explanation is satisfying, yet not intrinsically very interesting. Perhaps this is why most authors choose not to mention the difficulty.

Recently, the theorists Mukamel, Fisher and Domany (1976) have directed attention to the approach to saturation in the [111] direction of Fe. They feel that this, as well as several other magnetic and non-magnetic systems, are physical realizations of a statistical mechanical model of some interest called the 3-dimensional 3-state Potts model. They and many other researchers have studied this model both theoretically and experimentally with particular interest in determining the nature of the phase transition. We review the work that has been done on this model below, and compare the

findings with what we see in iron.

In this section we report our study of the approach to saturation of a [111]-oriented iron whisker at room temperature. For such a whisker there is no reason to expect internal stress or any other defects to influence the approach to saturation. If, from the same boat, we take [100]-oriented whiskers, we find that the magnetization in the central cross section saturates in slightly less than zero internal field (Heinrich and Arrott, 1972). The whisker we selected for study has a large length to diameter ratio to assure that the demagnetizing field was much smaller than the anisotropy field, and has little taper along its length.

The experiment we carry out is a simple measurement of ac susceptibility as a function of applied field for a number of positions of a short pick-up coil along the length of the sample. The extraction of the dependence of the magnetization vector on the local internal field is not simple. A series of questions needs to be answered in detail before we can develop full confidence in our principle result. Like Honda and Kaya and everyone who has published results, we do not observe a first order transition for iron.

Among the questions we discuss are the role of sample perfection, alignment of the [111] axis with the applied field, the effects of demagnetizing fields on the variation along the whisker length of the net magnetic flux in each cross section, the domain structure in the approach to saturation, and the role of dipole-dipole interactions in the magnetic fluctuations. Our technique of measurement is designed to help answer some of these questions.

2. The Phenomenological Theory of Cubic Magnetocrystalline Anisotropy

Internal energy in almost all ferromagnets is sensitive to the orientation of the spontaneous magnetization M_s in a crystal. An energy of magnetic anisotropy, one term in the magnetic part of the free energy, can be expressed as $E_k = f(\alpha_1, \alpha_2, \alpha_3)$ where α_i are the direction cosines of M_s. For cubic symmetry such as found in Fe and Ni, the anisotropy energy can be written in a polynomial expansion of the direction cosines,

$$E_K = K_1(T,H)\,S + K_2(T,H)\,P + K_3(T,H)\,S^2 + \cdots \tag{20}$$

where $$S = \alpha_1^2\alpha_2^2 + \alpha_2^2\alpha_3^2 + \alpha_3^2\alpha_1^2 \tag{21}$$

and $$P = \alpha_1^2\alpha_2^2\alpha_3^2 \quad . \tag{22}$$

The direction cosines are measured with respect to the [100] cube edges. Therefore in the case of iron ($K_1 > 0$), the six easy directions are $[\alpha_1, \alpha_2, \alpha_3] = [\pm1,0,0]$, $[0,\pm1,0]$ and $[0,0,\pm1]$ while the eight hard directions are $\sqrt{3}[\alpha_1, \alpha_2, \alpha_3] = [1,1,1]$, $[-1,1,1]$, $[1,-1,1]$, $[1,1,-1]$, $[-1,-1,-1]$, $[1,-1,-1]$, $[-1,1,-1]$, and $[-1,-1,1]$. The anisotropy constants K_i are measured or are calculated from theory, and in general are dependent on temperature and applied field. The form of each term in the expansion is the result of requiring it to be an invariant under all the symmetry operations for a cube. The leading term $\alpha_1^2 + \alpha_2^2 + \alpha_3^2$ does not appear in the expansion since it is equal to unity as required for the unit vector field M_s. This fact is useful for simplifying higher order terms into products

of the lower order terms. All terms which satisfy the cubic symmetry requirements but appear to be missing from the expansion can be expressed in terms of s, p, s^2 and constants.

An expression for the internal field H_i as a function of the direction of M_s can be obtained by minimizing the magnetic free energy. In our case, we are interested in the simple rotation of the magnetization, for example, in the (110) plane from the [001] easy direction into the [111] hard direction. Letting η be the direction cosine of M_s with respect to the [111] direction in this plane, the internal field is then given by

$$H_i = \frac{1}{M_s}\frac{dE_K}{d\eta} = \frac{K_1 + 2K_3 S}{M_s}\frac{ds}{d\eta} + \frac{K_2}{M_s}\frac{dP}{d\eta} \qquad (23)$$

taking terms of the energy expression to eighth order in the direction cosines. Expressed in terms of η,

$$S = \frac{1}{3}\eta^4 + \frac{1}{4}(1-\eta^2)^2 - \frac{\sqrt{2}}{3}(1-\eta^2)^{3/2} \qquad (24)$$

$$\frac{ds}{d\eta} = \frac{1}{3}\left(\eta(7\eta^2-3) + (2-2\eta^2)^{1/2}(4\eta^2-1)\right) \qquad (25)$$

$$\frac{dP}{d\eta} = \frac{1}{18}\left(\eta(1-16\eta^2+23\eta^4) - (2-2\eta^2)^{1/2}(1-9\eta^2+10\eta^4)\right) \qquad (26)$$

The expression for the anisotropy energy as a function of the direction cosines of M_s is a Landau expansion of the free energy in the order

parameter. (Landau proposed that such expansions of thermodynamic potentials could be made about the critical point for the purpose of determining the critical behaviour of a system.) Eq. (20) is also called a mean field theory because as in all mean field theories no knowledge of the details of the microscopic interactions between the individual moments is used. Each moment or cluster of moments feels an average torque due to all of the fields of the system. In a mean field theory each moment interacts equally with every other moment of the system. As can be seen in this calculation none of the details involving domain structure or the size and shape of the sample are used.

3. Measurements

A [111] Fe whisker with dimensions 0.3 x 0.3 x 12.7 mm is our principal subject for these measurements. It is placed in a glass capillary of 0.5 mm O.D. on which is wound 5 turns of closely spaced #50 wire. The coil acts as a secondary whose primary is a pair of Helmholtz coils carrying a 500 Hz current which produces an ac field of 10 millioersted. Care is taken to see that there is negligible coupling to the lead wires. There is a dc bias field supplied by an electromagnet with a 7 cm gap. The electromagnet is sufficiently hysteretic and sufficiently conducting that it does not respond to the field of the Helmholtz coils. The dc field is measured with a calibrated Hall probe.

The ac voltage from the secondary is measured with a phase sensitive lock-in amplifier as a function of dc bias field. The out-phase component is

negligible. Auxilliary experiments were carried out to give assurance that the differential ac susceptibility agrees with the slope of the magnetization curve measured on continuously increasing field. It does for fields sufficient to remove the 180 degree domain walls. These are present only below the knee of the magnetization curve, that is for $M < M_s/\sqrt{3}$.

The differential ac susceptibility is measured for increasing and decreasing dc bias field from 10 to approximately 1000 oersteds. The field is swept at 1 oersted/min. Readings are taken every 30 seconds using a time constant of 10 seconds on the output of the phase sensitive detector. The sweeps up and down in field are made for 15 positions of the secondary coil along the full length of the whisker. We thus map out the field dependence of the flux for the entire sample. This data can then be analyzed to extract only that contribution to the ac flux due to the magnetization of the sample.

4. Analysis

The measured voltage is equal to the rate of change of flux in the secondary. From equation (1), it can be seen that there are three contributions to the flux per turn

$$\Phi(z,H_o) = \int 4\pi \vec{M}(z,H_o)\cdot d\vec{s} + A_c H_o - \int \vec{H}_D(z,H_o)\cdot d\vec{s} \qquad (27)$$

where A_c is the coil area, $\vec{H}_D$ is the demagnetizing field, the element of area $d\vec{s}$ is along the applied field H_o, and $\vec{M}$ is the magnetization vector. The component of M along the [111] direction is the same throughout any

particular cross section if our model of the domain structure is correct. The driving frequency is sufficiently small that we can take the loss angle δ to be zero. If we assume that the z component of H_D does not vary across the coil, we can write

$$\Phi(z) = 4\pi M_z(z) A_s + H_o A_c - H_D(z) A_c \qquad (28)$$

where A_s is the cross sectional area of the sample. This is only a good assumption for a tightly wound pick-up coil. One of our coworkers, T.L. Templeton, with a computer calculation, determined the z and radial components of the internal and external demagnetizing field for a cylindrical bar of given susceptibility. From his results we determine an effective value for A_c in eq. (28).

We use all of our data to determine $M_z(z)$ and $H_D(z)$ self-consistently for each applied field. We need

$$H_D(z) = f(H_o, z) \qquad (29)$$

in order to calculate the internal field

$$H_i(z) = H_o - H_D(z) \qquad (30)$$

Further we need $dH_D(z)/dH_o$ to calculate the intrinsic susceptibility from $d\Phi/dH_o$ which we measure. We use the result

$$\chi_i = \frac{dM_z}{dH_i} = \frac{1}{4\pi A_s}\left[\frac{d\Phi/dH_o}{1 - dH_D/dH_o} - A_c\right] \qquad (31)$$

Note that one corrects the entire flux for the effect of the demagnetizing field and then subtracts the high field contribution from the driving coil!

What we measure, of course, is the voltage induced in our pick-up coil of n turns,

$$V = \frac{-i\omega n h_o}{c} \frac{d\Phi}{dH_o} \tag{32}$$

The factor $\omega n h_o/c$ can be determined by measuring the induced voltage with a standard [100] iron whisker in the pick-up coil with the same driving conditions and in zero applied field. A thick and long [100] whisker of cross sectional area A_o is used to minimize the area $A_c - A_o$ outside the coil. This whisker is of sufficiently high susceptibility that we can assume that the induced standard voltage is

$$V_o = \frac{-i\omega n h_o}{c} \frac{4\pi D M_s}{H_d} A_o \tag{33}$$

where H_d is the departure field of the standard whisker and M_s is the room temperature value of the saturation magnetization of iron.

Therefore we can rewrite equation (31) in terms of the measured voltage $v(z,H_o)$, the standard voltage v_o and the high applied field voltage $v_{hf} = -i\omega n h_o A_c/c$,

$$\chi_i = \frac{A_o M_s}{A_s H_d} \frac{1}{V_o} \left[\frac{V}{1 - dH_D/dH_o} - V_{hf} \right] \tag{34}$$

We obtain the function in eq. (29) from the experiment and the

following computation. If we know $\Phi(z)$ at a given H_o, then eq. (28) gives one relation between $M(z)$ and $H_D(z)$. A second relation is obtained by assuming one knows $M(z)$ in order to calculate the sources of $H_D(z)$, and therefore $H_D(z)$ itself. One does this iteratively to find self-consistent values of $H_D(z)$ and $M(z)$. To obtain $\Phi(z,H_o)$ at each H_o we first calculate $\Phi(z,\infty)$ for the completely saturated whisker. Then we numerically integrate our measured $d\Phi/dH_o$ down from saturation to get

$$\Phi(z,H_o) = \Phi(z,\infty) - \int_{H_o}^{\infty} \frac{d\Phi}{dH_o}\, dH_o = \Phi(z,\infty) - \frac{4\pi M_s}{H_d}\,\frac{A_o}{V_o}\int_{H_o}^{\infty} V(z,H_o)\, dH_o \quad . \tag{35}$$

Here we subtract the high field background first before carrying out the integration to obtain the portion of the flux due to the sample. This integration is performed for each of the 15 positions of the coil.

For the purposes of the computation we treat the sample as if it were a right-circular cylinder with the same cross sectional area as the [111] sample being studied. The magnetic charges which are the sources of the demagnetizing field are all on the surfaces because div M = 0 as long as χ_i depends only on H_i and not on position. The charge density on its sides is given by

$$\sigma_s(z) = -\frac{1}{2}\left(\frac{A_s}{\pi}\right)^{1/2}\frac{dM_z(z)}{dz} \tag{36}$$

There is also charge density on the end surfaces equal to M_z evaluated at the ends. We calculate the z-component of the demagnetizing field $H_D(z)$

on the axis of the cylinder. The cylinder is given the taper of the measured whisker if it is significant. From magnetostatics,

$$H_D(z) = \int_{-1}^{+1} \frac{\lambda(z')(z'-z)\,dz'}{\left[(z'-z)^2 + R^2\right]^{3/2}} + \qquad (37)$$

$$2\pi \int_0^{R(+1)} \frac{r\,\sigma_e(+1)(1-z)\,dr}{\left[(1-z^2)^2 + r^2\right]^{3/2}} -$$

$$2\pi \int_0^{R(-1)} \frac{r\,\sigma_e(-1)(1+z)\,dr}{\left[(1+z^2)^2 + r^2\right]^{3/2}} .$$

Here $$\lambda(z) = -\frac{d}{dz}\left(M(z)A_s(z)\right)$$

$$\sigma_e(\pm 1) = M_z(\pm 1)$$

$$A_s(z) = \pi R^2 (1+tz)^2$$

$$R(z) = \frac{2\rho}{\ell}(1+tz)$$

where ρ is the radius of the cylinder at the centre, ℓ is the length and t is the taper. Initially in the calculation it is assumed that the flux $\Phi(z,H_o)$ in eq. (35) represents $M(z)A_s(z)$. This is fitted to a twelfth order polynomial in z, which is used to calculate $H_D(z)$ according to eq. (37). Then using eq. (28), a corrected value for $M(z)$ is calculated and the process is repeated.

The function of eq. (29) which is the result of this calculation is

shown in fig. (19). Also shown is the fit that we use to determine the derivative dH_D/dH_o. It should be noted that H_D is not a monotonic function of H_o. It increases as the magnetic charge on the surfaces increases until a maximum value is reached near the saturation of the central cross section. Then with further increase in H_o, the charge on each half of the sample remains the same, but moves towards the ends, resulting in a decrease in H_D. Note that greatest correction to the data both in field and in signal occurs at the critical point.

The results of the analysis are shown in figs. (20) and (21) which give χ_i and M as a function of H_i, respectively. Ideally χ_i should remain slowly varying right down to $H_i = 0$. The apparent increase in χ_i for low fields will probably go away when we carry out the demagnetizing field corrections for the end of the field range. The function we used in eq. (29) is obtained from data taken above 100 oe. This low field discrepancy does not hinder our efforts to study the critical behaviour at higher fields.

5. Results

Mean field theory predicts the dashed curves shown in figs. (20) and (21). The values used for K_1, K_2 and K_3 are the torque curve values of Cengnagel and Hofmann (1968) who give $K_1 = 472 \times 10^3$ erg/cm^3, $K_2 = -7.5 \times 10^3$ erg/cm^3 and $K_3 = 19.0 \times 10^3$ erg/cm^3. They extrapolate to high fields to overcome the effects of sample imperfections. The curve of fig. (21) is a plot of equation (23) where $\eta = M_z/M_o$. As can be seen from the details of the inset, the phase transition is first order. There is a critical field Hc_1

= 410 oe for increasing internal field and a critical field Hc_2 = 367 oe for decreasing internal field. These are analogous to supercooling and superheating. If nucleation and growth occur to achieve a thermal equilibrium of two phases in a first order transition they should occur at $H_{f.o}$ = 403 oe where the two phases can coexist. The derivative of the theoretical curve of fig. (21) is the dashed curve of fig. (20).

The results of our measurements and analysis are the solid curves of fig. (20) and (21). In fig. (20), the data has been corrected for the demagnetizing field contribution to the magnetic flux changes, except at low fields. This curve of data is integrated from high field down to obtain the solid curve of fig. (21). No discontinuous jump in this curve near saturation can be seen.

In a material as near perfect as our whisker we might reasonably expect to observe Hc_1 and Hc_2 and a pronounced hysteresis. If Hc_1 could be reached without a nucleation of saturation, then $1/\chi_i$ should go linearly to zero with η = .9799, for the chosen values of K_1, K_2 and K_3. Fig. (22) compares $1/\chi_i$ as a function of η from experiment with the prediction of theory. There is an indication in the experimental curve that something happens at Hc_1 even though the maximum in χ_i is at a higher field.

6. Discussion

Our results fail to show the first order jump predicted by mean field theory. Adding terms to the free energy which are proportional to η or any power of η cannot completely suppress the first order change because the

anisotropy has a term in $(1-\eta^2)^{1/2}$ which is linear in the angular deviation from the [111], whereas the terms in η are quadratic in the angle. An internal stress field not parallel to the [111] direction can suppress the jump, just as can an applied field sufficiently misaligned with respect to the [111] axis. Though we doubt that either internal stress or misalignment are playing a role here, we have yet to demonstrate this. We can only point out the perfection of our samples and state that care was taken in aligning them. As well any small component of the applied field perpendicular to the axis of the whisker is cancelled by the large demagnetizing field $2\pi M_x$.

The gradient of the magnetization along the length of the whisker contributes to both the exchange energy and the demagnetizing energy. The latter yields a field in the [111] direction and therefore should not suppress the transition. The exchange will produce a torque away from complete alignment, but its magnitude is entirely negligible with respect to the anisotropy terms.

It is our conclusion that the first order transition is not there because the mean field theory is not applicable. This is in contrast to the conclusions of Barbara, Rossignol and Bak (1978) who study highly anisotropic $DyAl_2$ in high fields at low temperatures. They find excellent agreement with the theory. The jumps occur even at higher temperatures where much of the magnetization comes from the applied field aligning moments against thermal agitation. $DyAl_2$ has single ion anisotropy; Fe does not. The predicted jump for iron is from $\eta = 0.964$. In $DyAl_2$ the measured jump is from $\eta = 0.73$. K_2 must be important in $DyAl_2$. There is very little hysteresis in $DyAl_2$ and one never gets close to Hc_1 or Hc_2, so the fluctuations do not get a chance to play a significant role.

7. The (q = 3)-State Potts Model

It has been suggested that cubic ferromagnets with three easy axes of magnetization, such as Fe and the (rare-earth)-Al_2 compounds, in a diagonal [111]-oriented field are possibly accurate manifestations of what is called the (q = 3)-state Potts model (Mukamel et al. 1976,1977). In this section we discuss this proposition as well as the question what is required of a physical system to qualify it to be labelled a realization of a particular model.

The more familiar Ising model is a d-dimensional lattice, each site of which can be in one of two states. An example of its application is to model a binary alloy where each site can be occupied by an atom belonging to one of two elements. In 1952, R.B. Potts generalized this model so that each site can be in one of q distinct states (Potts 1952). Using a matrix approach, he discovered a duality transformation which successfully locates the transition temperature T_o for the case of the square lattice (i.e. d = 2) and for general q. As in the case of the Ising model (which happens to be the (q = 2)-state Potts model), only nearest neighbours interact, either with an energy E_o if they are in the same state or with an energy E_1 if they are not. External fields $\zeta_1,\zeta_2,\ldots,\zeta_q$ can influence a site to be in one of the q possible states. There can be as many fields as sublattices. For q = 2 there need be only one field.

Recently there has been much theoretical interest in the (q = 3)-state Potts model. As discussed by Blote and Swendsen (1979a, 1979b, 1979c), it is apparently relevant for the description of several kinds of physical problems which are currently being studied. The investigation of noble gases adsorbed

on graphite (Bretz 1976), certain stress-induced crystallographic transitions (Aharony et al. 1977), and ferromagnets with cubic anisotropy in a magnetic field (Barbara et al. 1978, Hanham et al. 1979) are some examples.

The degree of success in solving the 3-state Potts model depends on the spatial dimensionality of the model. For (d = 1)-dimension, the model is solvable, but has no phase transition except at zero temperature. In (d = 2)-dimensions, the Potts model undergoes a continuous (second or higher order) phase transition in zero field for $q \leq 4$. This is shown by high temperature series studies (Straley and Fisher, 1973) and by an exact calculation of the latent heat (Baxter, 1973). In contrast, however, Potts (1952) has shown that the transition is first order when a phenomenological approach is taken. A term in the free energy is third degree in the order parameter, thus necessarily predicting a discontinuous transition by Landau theory.

For the (d = 3)-dimensional model, the order of the transition is as yet undetermined. It can be either first order as suggested by mean field theory (which does not take the dimensionality d into account, but which is supposedly correct for $d \geq 4$) or second order (as for d = 2). Extensive theoretical work has been carried out on the (d = 3, q = 3)-Potts model to resolve this question (see Blote and Swendsen, 1979a; as well as references 4 to 20 found therein).

The conclusion of Blote and Swendsen (1979b) from their Monte Carlo renormalization group calculations is that the transition in 3-dimensions is "nearly second order". It is apparently first order. However, a second order fixed point located in the metastable region causes substantial fluctuations and thus dominates the flow of the renormalization procedure

near the transition.

A sufficient condition for a first order transition is a discontinuity fixed point. No discontinuity fixed point is found. Rather the only grounds for designating the transition as first order are the same as in Landau theory. The free energy of both phases is the same at the transition temperature, so that they can coexist as in a nucleation and growth process. The transition is driven by the critical fluctuations revealed by the Monte Carlo calculation. The chance of such a fluctuation is $e^{-\Delta S/K}$ where ΔS is the deviation of the entropy from the equilibrium value. If ΔS is not too large, spontaneous nucleation of a new phase can occur. Mean field theory, or Landau theory, which leads to a first order transition does not take these fluctuations into account. On carrying out the same calculation for the (d = 4)-dimension model, Blote and Swendsen find the fluctuations are substantially reduced, and the transition is clearly first-order. A summary of the nature of the transition is shown in table 2.

Returning now to ferromagnetism, we raise the obvious question: what does the Potts model have to do with our problem? Mukamel et al. (1976, 1977) claim that a cubic ferromagnet with three easy axes provides a rather accurate realization of a q=3 Potts model. Since the exact nature of the transition in 3 dimensions has not yet yielded to theoretical research, they feel the problem may be solved by experimental study of such ferromagnets. They show that the form of the anisotropy term in a Landau-Ginzburg-Wilson Hamiltonian for the cubic ferromagnet is the same as the cubic term in the corresponding LGW Hamiltonian of the Potts model. As well, they show the topology of critical points, edges and surfaces of the phase diagram, both for mean field theory results and for results obtained for the

(d=2)-dimensional model. However, the discovery of which of these diagrams is correct is left up to the experimentalist.

Experimental work, which is claimed to be evidence for the physical realization of the (q = 3)-state Potts model, lies in three areas. Two of these we only mention. The third, the subject of this thesis, is discussed in more detail.

Bretz (1976) measures the heat capacity of the ordering transition of helium films on highly uniform graphite surfaces. The critical exponent α which they obtained is substantially different from that calculated for the (q = 3)-state Potts model in two dimensions. A second order transition is indicated in agreement with the theory.

Aharony et al. (1977) study the structural phase transitions in $SrTiO_3$ as a function of temperature and stress applied along the [111] diagonal direction. At constant stress p(>0) with decreasing temperature, they observe a second order transition from "pseudocubic" to trigonal phases followed at a lower temperature by a first order transition to a "pseudo-tetragonal" phase. As the stress p is reduced to zero, the temperatures of these two transitions approach each other finally meeting at a bicritical point at p = 0. The claim that they make is that the second order transition is Ising-like (see page 496 of Bruce and Aharony, 1975) while the first order transition is described by the continuous version of the three-state Potts model. The rotational order-parameter $\vec{\Phi}$ alters from being along the [111] direction in the trigonal phase to having components in the (111) plane as the stress is reduced. This plane has three-fold symmetry because of preference for ordering along cubic [100] axes. Using the variables of temperature and stress, the experimenters are able to examine the transition

at different values of the order parameter $M \propto \langle \phi_{[111]} \rangle$ and at different values of the cubic anisotropy coefficient v. They obtain a value of the critical exponent δ which agrees well with theory (Golner, 1973; Rudnick, 1975). The theory shows for small values of w (the symmetry-breaking term in the reduced Hamiltonian) which is proportional to v, the transition is no longer described by mean field theory. Critical fluctuations cause the transition to become nearly second order.

The third case is the study of cubic ferromagnets with three easy axes of magnetization. These are studied as a function of field H parallel to the [111] direction and as a function of temperature below the Curie point. Barbara et al. (1978) report magnetization measurements on $DyAl_2$ in extremely high magnetic fields at several temperatures below T_c ($T_c \sim 50K$). They find that the transition is first order in agreement with mean field theory. However, the hysteresis they measure is much smaller than would be expected from mean field theory alone. As well, the size of the jump in magnetization is more than 25% compared to 3.66% predicted by mean field theory if only the fourth order anisotropy term is assumed.

There are many difficulties and some errors in this work by Barbara et al. The reason that the discontinuity in magnetization at the transition is so large is that the second anisotropy constant K_2 is of the same order of size as the first anisotropy constant K_1. This is in contrast to the case of iron where K_2 can be ignored in comparison with K_1 at all temperatures from zero to T_c. This huge jump is clearly not supported by the work of the theorists on the (q = 3)-Potts model. Blote and Swendsen conclude that the transition is nearly second order for the (d = 3)-dimensional model. Their results imply that thermodynamic quantities are analytically continuable into

the metastable region. Thus no huge jump in the magnetization is expected for this model.

In explaining their data, Barbara et al. show the results of classical calculations in which they use the values of the phenomenological anisotropy constants, $K_1 = -1$ and $K_2 = 0.5$. They feel that these calculations represent a behaviour as shown by their data i.e. a similar size of jump as the field is applied in various directions. We can only point out that the signs and magnitudes of the anisotropy constants which they use are identical to the constants measured in nickel at room temperature. As is well known, nickel has four easy directions of magnetization, namely the [111], $[\bar{1}11]$, $[1\bar{1}1]$ and $[11\bar{1}]$ directions. Nickel is not a physical realization of the (q = 3)-Potts model. If the values of the constants used by Barbara et al. are even moderately accurate, then $DyAl_2$ is not a Potts model either.

The anisotropy field H_K of $DyAl_2$ is approximately 58 Koe at 4.2° K while the saturation magnetization M_s is $10\mu_B$/Dy($\sim 10^3$ magnetic moment cm^{-3}. This compares with H_k = 403 oe and M_s = 1714 magnetic moments cm^{-3} for Fe at room temperature. Iron at 4° K has H_k = 446 oe and M_s = 1760 magnetic moments cm^{-3}. The anisotropy field of $DyAl_2$ is over two orders of magnitude larger than that of iron while their saturation magnetizations are comparable. Caution should therefore be exercised in considering $DyAl_2$ as a Potts model. The analysis and mean field theory phase diagram outlined by Mukamel et al. are for small anisotropy. Barbara et al. add sixth order terms to the theory, as they should, but they assume the equivalence of $DyAl_2$ and the Potts model is justified based on symmetry considerations only. The correctness of this is not clear and may be difficult to justify. The analogy that Mukamel et al. make between the continuous (q = 3)-Potts

model and a cubic ferromagnet considers only the fourth order anisotropy terms. This makes iron a much better candidate for being a Potts model.

This leaves us with the question: what can we say about the Potts model from our data? The anisotropy of iron, not single-ion anisotropy as in the case of $DyAl_2$, seems to fit the Potts model picture. However there seems to be a definite difference; in high fields, the spins in iron align in the [111] direction whereas in the Potts model, the average values of the spin components perpendicular to the [111] direction go to zero at the Potts transition temperature. There may be the same coupling in the two cases, but the constraints on the spin directions are different.

In our experiment we do not see a first order jump in the magnetization at room temperature or at higher temperatures. Nevertheless we cannot conclude that the transition is higher order. The transition could be "nearly second order". It could be the limit of stability of a phase superheated beyond a first-order transition. Like Barbara and coworkers, we do not measure the order parameter, that is, the spin components in the (111) plane. We measure the average value of the z-component of the magnetization. In particular we measure the magnetization in the central cross section of the sample plus the contribution to the internal field from all the sources of the demagnetizing field. We can analyze for each of these contributions using all of our data measured along the length of the sample. As well, even though our three turn pick-up coil is short (~0.2 x sample diameter), we measure an average over a certain length of the sample.

Finally this brings us to the general question of comparing real systems with models. A model is an approximation of a real system. The simpler the model, the more likely we will know its behaviour, but the less likely it

will represent the real system which we are trying to understand. To say that a real system is a physical realization of a particular model demands that we outline the limitations of the comparison that we are attempting to make.

In making these kinds of comparisons there seem to be two fundamental criteria, symmetries and critical behaviour. With the discovery of renormalization group theory, we now know that critical behaviour is a result of further symmetries which had not been previously fully appreciated. If a model and a real system display the same symmetries and critical behaviour, then it could be argued that one is a physical realization of the other. Further theoretical and experimental research could be pursued to discover the similarities and differences.

However to say that a real system is a manifestation of a model based on symmetry arguments alone is questionable. It is further questionable to conclude that a model has a particular critical behaviour based on measurements of the real system it is supposed to represent. The critical behaviour of the 3-dimensional 3-state Potts model hopefully will be determined by the theorists. The experimentalists will then seek real systems with the proper symmetries and critical behaviour revealed for that model.

V. THE TEMPERATURE DEPENDENCE AND MAGNETIZATION DEPENDENCE OF THE MAGNETIC ANISOTROPY OF IRON

1. Introduction

Iron whiskers which are grown with their axes parallel to the [111] direction have magnetic properties which are more dependent upon magnetic anisotropy than those grown with the [100] orientation. In the previous sections we reported our findings concerning the domain structure and the approach to saturation of [111] whiskers as they are magnetized in the hard [111] direction. In this section we describe our measurements of the anisotropy as a function of temperature from room temperature up to the Curie point. As well we use the results of our measurement of the temperature dependence of the spontaneous magnetization M_s to arrive at the M_s dependence of the anisotropy over the same temperature range. In the critical region just below T_c ($0 < T_c - T < 12^o$ K), our method of analysis gives the anisotropy as a function of M_s directly.

The most complete data on the anisotropy constants, K_1, K_2, and K_3 of iron are the torque measurements taken in the (100) and (111) planes of single crystal spheres by Gengnagel and Hofmann (1968). They give the temperature dependence of the anisotropy constant K_1, obtained by linear extrapolation to $H = \infty$ and to $H = 0$ in plots of K vs 1/H, for temperatures from 20^o K up to $T_c - T = 92^o$ K. They conclude that "the crystal energy constants K_2 and K_3 can be neglected in relation to K_1 of iron within the whole temperature range in magnetocrystalline energy expressions".

Here we present results on the magnetocrystalline anisotropy for the

previously unexamined critical region of a cubic ferromagnet. Our data yield K_1 up to within 0.5 degrees of T_c. These data are analyzed to obtain the dependence of K_1 on temperature and a power law relation between K_1 and the spontaneous magnetization M_s in the critical region. From Landau theory one expects K_1 to be proportional to M_s^4 in the limit of small anisotropy. The analysis is in terms of the anisotropy field $H_k \sim K_1/M_s$ which is deduced in two separate experiments by two different methods of analysis. The results are in good agreement. The more precise set of data indicates that H_k is proportional to M_s^n with $n = 3.11 \pm 0.05$ using as a level of confidence a 10 per cent increase in the mean square deviation of the fit. In terms of temperature dependence we find

$$H_K \sim (T_c - T)^{3.1\beta} \qquad (38)$$

where β is the critical exponent for the temperature dependence of the spontaneous magnetization.

The analysis of our data from room temperature up to the critical region is complicated by the field dependence and temperature dependence of the demagnetizing field. In the section on the approach to saturation above, we have shown how to handle this problem in analyzing our room temperature results. Using the room temperature results and a similar method of analysis, we have extracted the temperature dependence of H_k up to approximately 12 degrees below T_c. The uncertainty in the data, however, due to the rapid decrease of H_k compared to H_D makes extension of the analysis to even higher temperatures inaccurate. The technique which we use in the critical region gives by far the more accurate results.

2. The Experiment and Measurements

The sample investigated is a [111] iron whisker, hexagonal cross section with 0.118 mm edges and 12.6 mm length, hermetically sealed in vacuo in a quartz capillary. This is placed in a long single-layer driving coil of ceramic insulated platinum wire. Concentric pick-up coils of different lengths are used in the two experiments reported here. This assembly is mounted in a boron nitride chamber in an evacuated furnace with radiation shields. The temperature of the water jacket is controlled to ± 1 mK (Heinrich et al., 1978). The heating coil is energized by a dc power supply stabilized to ± 2 ppm. A type S thermocouple measures the temperature of the sample relative to the controlled water jacket temperature. With this system, temperature control relies on the fact that the drifts in water control point and room temperature, as well as in the power supply, are sufficiently long in time and small in size that they can be ignored. Stability to better than 0.01° K over 2 hours can be achieved with mK stability over shorter periods. The furnace sits in the 20 cm gap of an electromagnet which applies a dc field parallel to the sample axis. A Hall probe outside the furnace monitors this field.

Two different experiments have been carried out. In the first, a multilayer 150 turn pick-up coil is used while the driving coil is exciting the sample with a 10 millioersted field typically at 2 kHz. The in-phase and out-phase ac response are measured with two lock-in amplifiers as a function of dc field and temperature. Frequency is swept as well to obtain information on loss mechanisms, but this work is not discussed here.

In the second experiment, small three turn coils at several places along

the whisker are used. Typical experimental results are shown in fig. (23) for a series of temperatures with a small coil about the central cross section of the whisker. These results for the intermediate temperature range 630 to 760° C have been normalized at each temperature to the critical field H_c at which the centre of the sample saturates. The temperature dependence of H_c over the full temperature range from room temperature to T_c is shown in fig. (24). This field is related to the anisotropy field H_k and the demagnetizing field through the relation given by eq. (19).

The difficulty is that the demagnetizing factor D itself is dependent on the anisotropy, although this can be neglected in the limit of very low anisotropy in the temperature interval 12 K below T_c. Using the temperature dependence of H_c shown in fig. (24) one can deduce H_k once $4\pi DM_s$ is determined, either independently or self-consistently from the measurements of the field dependence with the several small coils. The first part of the analysis reported here will be for the 12 K temperature range immediately below T_c, for in that region D is constant up to saturation, and furthermore, the shape of the curves of in-phase responses vs applied field can be interpreted more readily. The second part of the analysis treats the rest of the data down to room temperature, extracting H_k from H_c.

In the second run, three short pick-up coils, each 3 turns of platinum wire, are used, one at the central cross section position of the sample and the others 3 mm and 4 mm respectively along the sample away from the first. The sample is driven by a 68 millioersted field at 2 kHz. At higher temperatures, where the fall-off field of the spike at H_c becomes comparable with the driving amplitude and the eddy current losses become more significant, the sample is then excited by a 10 millioersted field at 0.5

kHz. At low temperatures the sample is driven by a 0.75 oe field at 30 Hz in addition to the 2 kHz measuring field. This extra drive prevents the decrease of the susceptibility due to the interaction of domain walls with interstitial gas atoms of carbon. This is the phenomenon called the magnetic after-effect, descibed above. As the temperature is increased, the hopping frequency of the gas increases, and this drive becomes unnecessary above 200° C.

Digital data is collected for the 3 coils as measured by 3 lock-in amplifiers. The dc field is monitored and stepped in 0.5 oe increments over a sufficient range to saturate the central portion of the whiskers in both directions. As can be seen in fig. (24), H_c is a strong function of temperature. To compensate for this, the field step size is changed to 0.2 oe and then again to 0.08 oe.

The large drop in signal at H_c results in a sharply peaked second harmonic signal detected by the lock-in amplifier (Heinrich and Arrott, 1975; Heinrich et al., 1978). This is the best means for determining H_c, especially near T_c where the spike in the fundamental signal is not present. Using second harmonic detection with the large coil, we measure H_c during a sweep in temperature which is linear in time. The rate of change of temperature is determined by the thermocouple voltages averaged over the run, and time is used to give the temperature change on the scale of fractions of a mK. The results of such an experiment are shown in fig. (25). In constant temperature runs we use the value of H_c as a magnetic thermometer with fig. (25) serving as a calibration curve.

3. Analysis: High Temperatures

The analysis described in this section is applied to our data in the temperature interval $0 < T_c - T < 12$ K. The anisotropy field can be deduced from the integral of the measured ac susceptibilty. One takes the measured signal v minus the signal at higher fields v_{hf} where the sample no longer contributes, and normalizes it to $V_o - V_{hf}$ where V_o is the signal in the region where the magnetic response is completely determined by the cancelling of the applied field by the demagnetizing field. The relation for H_k from equation (19) gives

$$H_K = \int_0^{H_c} \left(1 - \frac{V - V_{hf}}{V_o - V_{hf}}\right) dH \qquad (39)$$

For this analysis to be correct it is necessary that the demagnetizing field scale with the magnetization i.e. the third term must scale with the first term in eq. (1). This is true as long as $V_o - V$ is small compared to V_o. It is also necessary that the differential susceptibility measured corresponds to the differential susceptibility of the dc magnetization curve. The lowest temperature points considered in our analysis of the high temperature behaviour of H_k are the two highest curves in fig. (23). The higher temperatures have $V_o - V$ approaching closer and closer to zero. The closer the signal in low fields is to the value it would have for the demagnetizing effect alone, the more we can be confident in the use of eq. (39).

By carrying out the analysis using eq. (39) we obtain H_k at a series of fixed temperatures. H_c is determined directly from the field at which

the saturation takes place. $4\pi DM_s$ is then calculated from eq. (19). Fig. (26) is a plot of H_k as a function of $(4\pi DM_s)^3$ for 12 data points in the interval $0.5\ K < T_c - T < 2\ K$. A power law fit (solid line) to these points yields an exponent $n = 3.11 \pm 0.05$. The dashed straight line is for a fit to the 8 higher temperature points using $n = 3.00$. It is known that the power law exponent at lower temperatures is much greater than this. (This is discussed below; see fig. (28). Indeed already in the range down to 11^o K below T_c there is evidence that H_k increases faster than for this more limited range. Perhaps the power $n = 3.00$ applies asymptotically as we approach T_c, but it is difficult to conclude this from our data.

Using the value of H_c for each constant temperature run we can convert the data to plots of $4\pi DM_s$ and H_k vs temperature. These are shown in fig. (27) where the solid curves are for $\beta = 0.371$ and $n = 3.11$ in the expressions

$$H_k = a(T_c - T)^{n\beta} \tag{40}$$

and

$$4\pi DM_s = b(T_c - T)^{\beta} \tag{41}$$

By taking $n = 3.11$ from the data of fig. (26) and varying the remaining 4 parameters, a, b, T_c and β, one can produce the best fit lines of fig. (27). The increase in n with decreasing temperature can be seen.

One can perform this analysis on H_c without using the integral method to obtain H_k. By assuming that the form of H_k and $4\pi DM_s$ is as given in

eq. (40) and (41) and using eq. (19) one can vary all five parameters. The precision of this method is much less, but it has the merit that it is independent of the integral method. In this analysis it is necessary to take β as known. Whether we use the value $\beta = 0.368$, which has been assumed in this laboratory over many years in previous analysis of data for [100] whiskers, or $\beta = 0.371$ from the above analysis makes little difference in what we obtain for n. This is because the error in n is large from the statistics of extracting the small anisotropy contribution in the presence of the larger $4\pi DM_s$ contribution to H_c. Nevertheless one obtains in this manner $n = 3.3 \pm 0.6$.

The lower curve in fig. (25) shows the extracted values of H_k if one assumes $n = 3.11$ and $\beta = 0.371$ in fitting the data using eq. (19), (40) and (41). This shows that despite the accuracy of the data for H_c, it is difficult to be precise in the fit to H_k because it is such a small part of H_c. This is why it is necessary to use the integral method for precision.

4. Analysis: Low Temperature

The data in the large temperature interval between room temperature and 12° K below T_c cannot be analyzed by the integral method. The demagnetizing field does not scale with the magnetization and a cancellation of the applied field by the demagnetizing field does not occur. The analysis requires a correction for the dH_D/dH contributions to the signal.

Our approach is to model the demagnetizing field sources with a self consistent distribution of magnetic charge on the surface of a cylinder. The

validity of this can be checked by using the measured signals of the 3 coils. The method relies on our knowledge of the temperature dependence of M_s of iron over the full temperature range. This we have measured and report in the next section.

As at high temperatures, the problem is to extract H_k from the measured value of H_c at each temperature according to eq. (19). In other words, the problem is to determine the demagnetizing field $H_D = 4\pi DM_s$ at each temperature. The temperature dependence of M_s has been measured in a separate experiment. As well the demagnetizing factor D, through its dependence on on χ_i, is dependent on temperature. As the temperature of an iron whisker is increased, the anisotropy quickly decreases causing an increase in χ_i. This causes the distribution of magnetization along the length of a whisker, just saturated at its centre, to become more quadratic, bringing a greater fraction of the charge from the ends to the centre. This results in an increased D and H_D at the centre. Thus, as temperature is increased from room temperature to the Curie point, the strength of H_D which is opposing the applied field first increases in strength due to an increased D, and then subsequently decreases as M_s more rapidly approaches zero near T_c. Our calculation below shows that H_D at the centre reaches a maximum value at $T/T_c = 0.92$ ($T = 690^o$ C).

We model the whisker as an untapered long cylinder of diameter/length ratio ρ and uniform intrinsic susceptibility χ_i. An effective diameter for the cylinder is calculated so that the cross sectional area of the cylinder is equal to that of the sample. A uniform field H_c is applied so that the cylinder is just saturated at its central cross section. This results in a distribution of magnetic charge/unit area σ along the cylinder which is

assumed to reside only on the side surfaces and the ends. These charges act as the sources of a demagnetizing field H_D which opposes the applied field. The sum of the two is called the internal field given by eq. (16)..

We assume that χ_i is independent of H_i. From our previous work at room temperature, we find that this is roughly true, except near the critical point where $H_i = H_k$. Here χ_i rises in a sharp spike (see fig. (20)). Therefore in our model this assumption is correct except at the region of the central cross section where $H_i = H_k$. As temperature is increased, the validity of this assumption only improves, as can be seen in fig. (23), until the critical region just below T_c is reached.

For the [111] whisker, the knee of the magnetization curve occurs for $M_z = M_s/\sqrt{3}$. The cosine of the angle between the [111] z-axis and say the [100] direction is $1/\sqrt{3}$. Using the above assumption, we can say

$$M_z = \chi_i\left(H_o + H_D(z)\right) + \frac{M_s}{\sqrt{3}} \quad . \tag{42}$$

M(z) takes a maximum value at the central cross section of the cylinder (z = 0) and drops off monotonically toward the ends. Near the ends of the whisker, $M_z < M_s/\sqrt{3}$, and H_i approaches zero as χ_i approaches infinity. However, we assume a constant χ_i for the cylinder and allow H_i to go negative. This results, as will be seen below, in an inaccuracy of the value of H_i over a distance of 4% of the length of the whisker at room temperature. Once again the error resulting from this assumption is small and decreases with increasing temperature. Assuming that the χ_i is smaller at the ends than it actually is, has the effect of excluding charge away from the centre. This means that the value we calculate for $H_D(0)$ is too small,

and therefore we overestimate H_k. However as temperature is increased, the χ_i at the middle of the whisker approaches the χ_i at the ends, and this error goes away.

It is possible in our calculation to introduce an interface at the position where $M(z_{IF}) = M_s/\sqrt{3}$. For $z > z_{IF}$, we can allow $H_i = 0$ and χ_i to go to infinity. We would have to postulate how to handle this interface in terms of its shape and the distribution of charge on the interface and on the sides. This would be highly artificial since we have no evidence that such interfaces exist in a particular form. The small improvement in the accuracy of the calculation does not warrant this approach.

The computer calculation we describe here is analogous to the one used by Bloomberg (1973) (also Bloomberg and Arrott (1975)) for [100] oriented cylinders. However several differences are necessary to accommodate the [111] orientation and the above assumptions.

Rewriting eq. (42) we have

$$-H_c = H_D(\bar{z}) - \frac{1}{\chi_i}\left[M(\bar{z}) - \frac{M_s}{\sqrt{3}}\right] \qquad (43)$$

where we have set the applied field to the critical field H_c, that just saturates the centre of the whisker, which we have measured. We let the charge density on the sides be $\sigma(z)$ and we assume a uniform charge density on the ends equal to σ_{end}. These act as the sources of the demagnetizing field which can be expressed as

$$H_D(\bar{z}) = 2\pi\rho\int_0^1 \sigma(\bar{z}')\,K(\bar{z},\bar{z}')\,d\bar{z}' - 2\pi\sigma_{end}J(\bar{z}) \qquad (44)$$

where the geometric factors are

$$K(z,z') = \frac{z-z'}{\left[(z-z')^2+\rho^2\right]^{3/2}} - \frac{z+z'}{\left[(z+z')^2+\rho^2\right]^{3/2}} \qquad (45)$$

and

$$J(z) = 2 - \frac{1-z}{\left[(1-z)^2+\rho^2\right]^{1/2}} - \frac{1+z}{\left[(1+z)^2+\rho^2\right]^{1/2}} \qquad (46)$$

in terms of dimensionless variables. From Gauss' law, we also have

$$M_z = \sigma_{end} + \frac{2}{\rho}\int_z^1 \sigma(z')\,dz' \quad . \qquad (47)$$

Since the centre of the cylinder is just at saturation we can use eq. (47) to express M_s in terms of the charge densities, namely, $M_s = M_z(0)$. Thus we have

$$-H_c = \int_0^1 \sigma(z')\left[2\pi\rho K(z,z') + \frac{2}{\sqrt{3}\,\rho\,\chi_i}\right]dz' - \frac{2}{\rho\chi_i}\int_z^1 \sigma(z')\,dz' - \left[2\pi J(z) + \frac{(1-1/\sqrt{3})}{\chi_i}\right]\sigma_{end} \quad . \qquad (48)$$

For the purposes of the computer calculation, the cylinder is divided into 200 disks. The calculation is done on 1/2 of the cylinder since it is symmetric about its central cross section. Thus there are 101 linear equations in 101 unknowns, the 100 side charge densities $\sigma(z)$ and the end charge density σ_{end}. The FORTRAN-called subroutine LEQT1F which resides in

the IMSL (International Mathematical and Statistical Library) is used to solve the equations. The routine performs Gaussian elimination with equilibration and partial pivoting. Once the equations are solved, we calculate H_D, H_i and M_z along the length of the cylinder. The required inputs to the program are the diameter/length ratio ρ, the intrinsic χ_i, and the critical field H_c. If H_c is given in oersteds, then so are H_D and H_i while M_z is in terms of emu magnet moments/cm^3 and σ is in emu charge/cm^2. All three of these units are the same.

The value of ρ which we use is obtained by measuring the length and width of our hexagonal whisker using an optical microscope. The widths are measured with 1% accuracy at best. The value of χ_i which we use is varied to obtain the value $M_z(0) = M_s$ which we have measured at each temperature. This analysis has been carried out for three different [111]-oriented whiskers at room temperature. The results are shown in table (3). Samples 1 and 3 have H_k values which agree within 0.6% while samples 1 and 2 agree within 2.3%. Sample 1 is the whisker used in the approach to saturation measurements. Sample 2 is the whisker used for the temperature dependence measurements reported in this section.

We can point out that this approach can be applied to [100] whiskers to magnetically determine ρ. Since χ_i is very large, one can vary ρ to obtain the proper value of M_s at the centre. Thus the measurement of the length of a [100] whisker and its departure field can be used to compute an effective "diameter" for the whisker.

In our case we first analyze the highest temperature data where we have previously determined H_k and χ_i by the integral technique described in the section above. Thus we can vary ρ to obtain the appropriate value of

$M_z(0)$ for the particular temperature data being examined. The value of which we obtain in this way is 1.68×10^{-2} which is in good agreement with the measured value reported in table (3). We can use this value to analyze all of the data down to room temperature since it is temperature independent.

5. Discussion of Measurements

The final results of our measurements and analysis are given in tables (4) and (5). The first table contains the results of the low temperature measurements up to 18° K below T_c, and the second table the results at higher temperatures up to 0.5° below T_c. In this section we describe the origin and uncertainty of each of these quantities. The fundamentally measured quantities in these tables are the temperature ratio T/T_c and the critical field H_c. The measurement of M_s is described in the next section. The anisotropy field H_k and demagnetizing field H_D are obtained by two methods of analysis, one for the high temperature data and one for the low temperature data. These methods have been described in the last section.

T/T_c

After sufficient time is allowed for the furnace system to stabilize, the drift of temperature in time becomes negligibly small. This is particularly true for the time it takes to measure the critical departure field of the whisker in both directions which is less than one minute. Two measurements of temperature are made simultaneously. A quartz thermometer

monitors the reference junction of the thermocouple which is in thermal equilibrium with the water jacket of the furnace. The quartz thermometer measures in absolute degree Celsius to better than one millidegree. It is periodically checked against distilled water at its ice point. The water jacket is typically at 20° C.

The second measurement of temperature is the thermocouple voltage. A type S thermocouple (Pt-Pt10%Rh) is used which when calibrated is still an international standard of thermometry in the temperature interval 600 to 900° C. Unfortunately this material "ages". The sensitivity of the thermocouple slowly decreases with time as the rhodium forms an oxide on the surface of the thermocouple wire. This process is very atmosphere dependent. A type S thermocouple which has been calibrated in air, which is the usual case, should be used in air for a measurement. Obviously this creates difficulties in experiments such as ours which are done in vacuum.

Type S thermocouples are calibrated by the Heat and Thermometry Division of the National Science and Engineering Research Council of Canada (NSERC). This is done in a furnace which is regularly checked against primary standards such as the melting point of silver. If care is taken not to stress the thermocouple and to employ the same experimental environment, a measurement of 770° C can be made with an uncertainty of 0.5°. This is done with a fit curve of a particular functional form which is provided by NRC with each calibration. This fit remains reliable only over a few high temperature runs and over a few months. It is dependent on run duration, temperature cycling and experimental atmosphere. Clearly this leaves room for plenty of improvement in thermometry in this temperature region. NSERC is presently studying the reliability and accuracy of high temperature

platinum resistance thermometers for use as a standard above 600° C.

At this point we can mention the lack of a primary standard temperature point in the vicinity of the Curie point of iron (770° C). This invites the suggestion of Arrott and Heinrich to establish the Curie point of high purity iron as such a primary point. There has been some interest from standards agencies along these lines. The problem is not the lack of sample material. Heinrich and Arrott have been studying [100] oriented iron whiskers near the Curie point over many years. They have studied whiskers grown in at least three different laboratories. In an experiment they can take three whiskers of different diameter to length ratios and simultaneously monitor the temperature dependence of the three departure fields. Temperature is allowed to drift at a constant rate in time upward and through the Curie point. The temperatures at which the the departure field of each of these whiskers goes to zero agree to within 3 millidegrees at 1043° K. (This same measurement has been conducted with one [111] oriented iron whisker and two [100] oriented whiskers. The T_c of the [111] whisker was 70 mdeg lower than the T_c's of the [100] whiskers which agree within 10 mdeg with each other.) The establishment of the Curie point of iron as a primary temperature point awaits only the careful and repeated measurement of such departure fields against a reliable thermometer.

In our measurements we use the thermocouple in vacuum. The thermocouple voltage is measured with a 6 digit voltmeter in both senses to check the zero offset of the voltmeter. The measurement is made to an accuracy of 1 microvolt which corresponds to 0.1° near T_c. Along with the reading of the quartz thermometer this measurement is converted to temperature in °C using a standard thermocouple table.

As well, the apparent T_c is measured by allowing the temperature to drift linearly in time up and through T_c. The critical field H_c, thermocouple voltage, reference temperature and time are recorded in regular intervals. The sweep in temperature is made over approximately 3^o C in a period of time of about 4 hours. Initially the interval between measurements is 3 minutes. However this is gradually decreased. When H_c is changing most rapidly just below T_c, a measurement is taken every 10 seconds. Ideally the sweep in temperature is linear in time and so time itself becomes the measure of temperature. As well, the reference junction temperature has not changed by more than a few hundredths of a degree. By making a plot of $(H_c)^{1/\beta}$, where the critical exponent $\beta = 0.368$, versus time, the time when T reaches T_c, and therefore T_c is determined.

For the data reported in tables (4) and (5), the apparent T_c which resulted is 763.7^o C. This is clearly different from the traditionally accepted value of 770^o C. The sensitivity of the thermocouple is decreased due to the rhodium oxidation on the surface of the thermocouple mentioned above. To handle this difficulty, we carried out the following calibration procedure. We fit the following function to a standard type S thermocouple table:

$$V(T)\,[mV] = aT + bT^2 - T(T - T_1)(T - T_2)(c - dT) \qquad (49)$$

With our fit parameters,

$$a = 0.68666 \times 10^{-2}$$

$$b = 0.29225 \times 10^{-5}$$

$c = 0.55205 \times 10^{-8}$

$d = 0.56042 \times 10^{-11}$

$T_1 = 300^{\circ}$ C

$T_2 = 770^{\circ}$ C

we can generate the standard table to within 5 microvolts over the full range from 0 to 770° C. The standard type S thermocouple table which we use is table 53 on pages 204-5 of the "Manual on the Use of Thermocouples in Temperature Measurement, 1974". The table is in 1° C intervals from -50 to 1760° C with the reference junction at 0° C. The emf values are given in absolute microvolts to an accuracy of one microvolt and temperatures are in degrees C (IPTS 1968).

We can make the above fit using just the first two terms of eq. (49) to the Pt-Pt13%Rh thermocouple in the same manual. We find that a is insensitive to the the difference in the rhodium content. Therefore we can do a one parameter fit of eq. (49) adjusting only b to obtain the emf at 770° C in this table. This fit agrees with the Pt-Pt13%Rh thermocouple table to within 1° C over the full range.

In light of this success we simply calculate a value b so that our emf at T_c corresponds to 770° C and generate our own thermocouple table. This table is used to determine the T/T_c values of table (4). The value of b used is

$b = 0.26610 \times 10^{-5}$

The maximum uncertainty in T/T_c values is estimated to be 0.1% for the

values of table (4).

The uncertainty in the T/T_c values at higher temperatures shown in table (5) is much smaller. Here the values of T_c-T are determined very accurately from the measured H_c values and the power law fit of H_c vs T_c-T for the linear temperature sweep. The uncertainty values in T/T_c are estimated assuming an uncertainty in T_c of one degree.

H_c

The measurement of the critical departure fields is made with a Bell model 620 Hall probe with a 1X probe. The instrument is used on the 1000, 300, 100, 30, or 10 oe range according to the size of field to be measured. Full scale deflection corresponds to one volt output which is measured to one millivolt with a Fluke 4.5 digit multimeter. The linearity of the Hall probe is tested against the current producing a field in a pair of matched Helmholtz coils. A random scatter of data about a straight line fit over a range of FS deflectiion in both directions is found. The scatter is within 0.1% of full scale. This test also compares the scale deflections for the same field on different range settings.

Measurements of the dc field applied in both directions along the length of the whisker which just saturates the centre of the whisker are made. The magnitudes of these fields are averaged to eliminate the zero offset of the Hall probe. The probe is not in close proximity to the sample since they are separated by the radius of the furnace. A separate measurement of H_c is made before the sample is mounted in the furnace. The field measurements made with the sample in the furnace are then scaled accordingly. This

compensates for the effect of the field gradient over the distance between the sample and the Hall probe.

The Hall probe is calibrated in the following way. A flux probe is used to measure the field of a large face, small gap electromagnet while a simultaneous measurement is made with the Hall probe. Measurements are made for the nominal fields of 0 to 1500 oe in 100 oe intervals. The flux probe consists of a small cylinder of aluminum of very uniform diameter on which is wound 380 turns of no. 50 copper wire. Upon reversing this coil in the field of the magnet the change in flux is measured with an integrating digital voltmeter in mVs. For each field, several measurements are made, averaged, and a field value is calculated. This provides a straight line calibration curve for the Hall probe. This in turn is used to measure the departure field of our sample which then becomes a suitable instrument standard itself. The departure field of our sample is

$$H_c = 417.0 \pm 0.4 \text{ oe}$$

at room temperature. This more or less represents the accuracy of the H_c values given in tables (4) and (5). The accuracy is maintained to the smallest fields in table (5) with power law fits of the field against temperature.

M_s

These values of the spontaneous magnetization of iron are obtained at each temperature from a fit of the departure field of a [100]-oriented

whisker versus temperature. This experiment and fit are described in the following section on the temperature dependence of M_s for iron. These values have an uncertainty of 0.1%.

$H_D(0)$

The uncertainty in $H_D(0)$, the calculated demagnetizing field at the centre of the whisker, can be estimated in a simple way. The greatest contribution to its uncertainty within the limitations of our model is the uncertainty in our measurement of the thickness of the whisker. Doubling this, since H_D is proportional to the thickness squared, gives us $\delta H_D/H_D = 3.3\%$. From our room temperature data, $H_D = -3.98 \pm 0.13$ oe. Combining this with the uncertainty in H_c gives us $H_K = 413.0 \pm 0.5$ oe (or + 0.12%). For the highest temperature point in table (4), $H_D = -7.60 \pm 0.25$ oe, giving $H_K = 1.00 \pm 0.3$ oe. This is a gross overestimation of the uncertainty in H_K at this temperature since we did not rely solely on the measured value of ρ. We actually use a value of ρ which allows the low temperature to extrapolate smoothly upwards into our more precise high temperature data. The value of ρ we choose is within the error bars of our measured value.

In the integral method which we use for the high temperature data we do not need to calculate $H_D(0)$. H_K is determined directly, and then if desired, $H_D(0)$ is calculated by simply subtracting H_K from H_c.

H_K

For the low temperature analysis based on our model, H_K is calculated by simply subtracting the calculated $H_D(0)$ from the measured H_c. Estimates of errors are given above.

However for the high temperature data, H_K is determined more directly using the integral method. Since H_c and the signal at zero field V_o are determined most accurately, the main cause of uncertainty is the inaccuracy of performing the integration of the small signal V_o-V against field. We estimate the uncertainty is no greater than 10%.

6. Results

The critical departure field H_c for a [111]-oriented whisker has been measured as a function of temperature from room temperature to just below the Curie point T_c. This field has been analyzed to extract the anisotropy field H_K at each temperature. These results are given in tables (4) and (5). Table (4) contains the results from room temperature to 18^o K below T_c. These data are obtained by a method of analysis which models the whisker as a cylinder of uniform susceptibility. Table (5) contains the results from 11^o below T_c to 0.5^o below T_c. These data are analyzed by integrating the area under the measure susceptibility curves.

Also given in the tables is the demagnetizing field $H_D(0)$ at the centre of the whisker just as the whisker is saturated at its centre. In table (5), the anisotropy is sufficiently small that $H_D(0)$ follows the

magnetization M_s. However this is not true for the values in table (5) at lower temperatures. Here the demagnetizing factor D is changing significantly with temperature as the distribution of magnetic charge along the whisker alters.

For completeness, values of the spontaneous magnetization M_s are given in both tables. These values are used as part of the analysis of the data of table (4), but not in the analysis of table (5) at higher temperatures. These values are obtained from a fit to our measurement of M_s described in the next section.

Graphs of the higher temperature data have been described above. Fig. (26) shows a plot of H_K versus $H_D(0)$ raised to the third power. Data over the 1^o K interval below T_c indicate a third power law while a power of 3.11 fits better to the data in the 2^o K interval below T_c.

Fig. (27) shows plots of H_K and H_D versus $T-T_c$ over the 11^o K interval below T_c. This data is contained in table (5). The solid curves are the appropriate power laws using the exponents $n\beta$ and β where $\beta = 0.371$ and $n = 3.11$. Even in this small temperature interval there is an indication that n is increasing as temperature decreases.

Fig. (28) shows a log-log plot of H_K versus M_s normalized to their respective zero temperature values. The zero temperature value for H_K was calculated from the data of Gengnagel and Hofmann (1968) and for M_s from the data of Crangle and Goodman (1971). All of the data of table (4) at lower temperatures and five points from table (5) are shown. The temperature T/T_c of each point is indicated although more accurate values can be obtained from the tables. Straight dashed lines at high and low temperatures indicate the value of the power law exponent n. The value $n = 11$ at lower

temperatures is much higher than the usually expected value n = 9.0. At high temperatures n = 3.1 is very close to the expected value of n = 3.0.

Also shown as a solid curve is the theoretical curve of Callen and Callen (1966). This calculation is expected to work well for a ferromagnet with localized moments, but not for an itinerant ferromagnet such as iron. The calculation does produce the third and ninth power laws at high and low temperatures. A brief review of the theoretical work in this area is given in the discussion below.

Finally in fig. (29) a comparison is made of our results with those of Gengnagel and Hofmann. A plot of our lower temperature H_k data from room temperature to 18^o below T_c is given. The resolution of the graph does not allow us to show our higher temperature values just below T_c. Also shown are the results of a mean field calculation using the K_1, K_2 and K_3 values of Gengnagel and Hofmann. We have fit their K_2 and K_3 data against temperature. Then for each temperature where they report a K_1 value, we have calculated the upper critical field H_{c_1} according to the mean field theory described previously. The agreement between our results and these calculated values is good, despite the fact that the techniques of measuring the two sets of data are quite different. A discussion of the torque curve method used by Gengnagel and Hofmann and others is given next.

Bhagat and Rothstein (1972) have reported 5 values of K_1/M_s determined from their FMR measurements on iron whiskers. We have calculated upper critical field values for these and plotted them in fig. (29) as well. Good agreement with our results is found as well. This technique of determining the anisotropy is discussed also in the next section.

Finally we show in fig. (29) two calculated curves of the anisotropy

field versus temperature. These are based on the single ion theory of Callen and Callen. Good agreement with the experimental data is not found, but this is not expected. An explanation of these curves is given below in the section on the discussion of the results.

7. Other Methods of Measuring the Anisotropy

Here we briefly describe two other methods of measuring the anisotropy constants of a ferromagnetic material. Each has its own advantages. Both methods produce results which are in agreement with ours.

The Torque Curve Method

The most commonly used technique to extract the temperature dependence of the anisotropy constants is the torque curve method. This technique was used by Gengnagel and Hofmann (1968) to determine the temperature dependence of K_1, K_2 and K_3 of iron over a wide range of temperature from 20° K to approximately 950° K. This is the most complete set of data on the anisotropy of iron to date which has been reported in the literature. As can be seen from fig. (29) our results are in agreement with theirs.

Klein and Kneller (1966) report torque curve measurements of K_1 which are in agreement with those of Gengnagel and Hofmann. They emphasize that it is important to report the field in which the anisotropy is measured. They extrapolate their measurement to obtain zero field results and report the field dependence of K_1.

Westerstrand et al. (1975) have measured K_1 of iron and of iron-silicon alloys at low temperatures. They have studied the dependence of K_1 on the concentration of silicon in iron.

There are numerous earlier measurements of the anisotropy of iron (Bozorth 1936, Bozorth and Williams 1941, Sato and Chandrasekhar 1957, Graham 1958). Several of these centred on the controversy about the magnitude and sign of K_2. It is now generally accepted, based on the results of Gengnagel and Hofmann, that K_2 is negative and K_3 is positive over the full temperature range. However both are sufficiently small that for most applications they can be ignored compared to K_1 in micromagnetic expressions of the energy. In fig. (29) we have graphed the anisotropy field calculated according to eq. (23) using all three anisotropy constants. If only the K_1 term had been used, the calculated anisotropy field would have been two percent smaller at the lowest temperatures. As well, the K_1 values used in this calculation are those obtained from an extrapolation to infinite fields. If the zero field values of Gengnagel and Hofmann had been used, the calculated anisotropy would have been two percent smaller at low temperatures.

The torque curve method involves using a device called a torque magnetometer. A single crystal sample is suspended on a fibre with good torsional properties between the pole faces of an electromagnet. The sample is allowed to twist on the fibre, but not allowed to move towards one of the pole faces. The crystal is cut into the shape of a sphere or disk so that corrections for demagnetizing effects can be made easily. The crystal is oriented so that the plane of rotation is one of the symmetry planes with low Miller indices. In the case of a cubic ferromagnet such as iron or nickel

this would be a (100), (110) or (111) plane.

A strong field is applied to the sample which causes the magnetization of the various domains to align as nearly parallel to the field as possible. Because of the anisotropy, this results in a torque on the sample which causes it to rotate on the fibre. The torsion constant of the fibre is selected so that small angular displacements of no more than 5 degrees are achieved. This angular displacement is a measure of the torque on the sample. Alternatively a compensating torque can be applied to the sample so that there is no angular displacement in the laboratory. The magnitude of the compensating torque is then the torque on the sample due to magnetocrystalline anisotropy.

The torque on the sample is measured as a function of the angular direction of the applied field. As a simple example consider the (100) plane of iron. This has four-fold rotational symmetry. If φ is the angle that the magnetization M_s makes with one of the four easy directions in this plane, then the torque/unit volume due to the anisotropy is given by

$$\tau = -\frac{dE_K}{d\varphi} \qquad (50)$$

where E_k is given in equation (20). In terms of φ,

$$E_K = \frac{1}{4} K_1 \sin^2 2\varphi + \frac{1}{16} K_3 \sin^4 \varphi \qquad (51)$$

Note that no information about K_2 can be obtained from measurements in the (100) plane. From eq. (50) and (51), the torque is

$$\tau(\varphi) = -\left(\frac{1}{2}K_1 + \frac{1}{8}K_3\right)\sin 4\varphi + \frac{1}{16}K_3 \sin 8\varphi \quad . \quad (52)$$

From this it is seen that the measured torque curve is a periodic function of the angle φ. By carrying out a Fourier analysis, the coefficients can be extracted and from these the anisotropy constants K_1 and K_3 can be determined.

In practice, the analysis is more complicated than is stated here. Lower order terms in the Fourier analysis may be required due to a possible induced uniaxial anisotropy which may be present. As well, the analysis must take into account the possible angle between the M_s vector and the applied field direction if the field is not sufficiently strong to align the magnetization against the anisotropy. This is always the case for a finite applied field which is not along a principle symmetry direction.

The measurement of torque curves and the analysis is usually carried out for a series of applied fields so that an extrapolation of the K_1 value can be made to zero or infinite fields. The infinite field value is higher since this is analogous to lowering the temperature, but the zero temperature anisotropy constant is not achieved, anymore than the zero temperature M_s value can be achieved. The susceptibility for increasing M_s in magnitude with a strong field is very small, but does increase with temperature. Thus it would be expected that the percentage increase in K_1 values at infinite fields over the same at low fields would be larger at higher temperatures. This can be seen from Gengnagel and Hofmann's data. However the 2% discrepancy between their K_1 values at low temperatures is more likely due to defects.

The advantage of the torque curve method is that it lends itself to the

determination of the anisotropy constants which are scalers. These then specify the anisotropy energy as a scaler function of the direction cosines of M_s. This in turn allows the calculation of all of the components of the anisotropy field. A disadvantage is that the method is not sensitive enough for measurement of very small anisotropies such as the case of iron in the last 100^o K below T_c.

The FMR Method

Ferromagnetic Resonance (FMR) is the resonant absorption of microwaves by a ferromagnet in an external dc field. The magnetic moments of the material precess about the effective field direction with a frequency determined by the effective field inside the material,

$$\omega = \gamma H_{eff} \tag{53}$$

where $\gamma = |ge/2mc|$ is the magnetomechanical ratio. However because of damping due to the lattice, this precessional motion requires energy. If energy is supplied in the form of incident microwaves, the applied field can be adjusted to find a resonant absorption of microwave power by the ferromagnet.

When an anisotropy field H_k is present parallel to the applied field, the relationship in eq. (53) must be modified to

$$\omega = \gamma(H_{eff} + H_k) \ . \tag{54}$$

In other words the resonant field, the applied field at which resonance occurs, is reduced or increased by the magnitude of H_k depending on its sign.

Bhagat and Rothstein (1972) have studied FMR in [100] and [111] oriented iron whiskers from 300 to 1090° K. Using a 9.6 GHz microwave system they have measured the resonant field and line width as a function of temperature for each of these samples. In each case the applied field was parallel to the axis of the whisker. The resonant field in the [111] direction is greater than that in the [100] direction by an amount $3.33\ K_1/M_s$, according to mean field theory. Thus they report K_1/M_s values for five temperatures in the range 520 to 870° K. We have calculated H_k values (upper critical point: $H_k = 1.48\ K_1/M_s$) for these and plotted them in fig. (29). It can be seen that the agreement with the torque curve and our data is good.

The advantage of FMR as a method of measuring anisotropy is that small samples can be used, as is the case with our method. This allows the use of whiskers which have high purity and few defects. However, as with the torque curve method, small anisotropy fields cannot be measured.

8. Discussion of Results

Our values of the anisotropy field H_k versus temperature agree well with those determined by other methods in the temperature range where these data coexist as can be seen in fig. (29). This is despite the fact that three different techniques of measurement of the three sets of data have been

used. The samples in the FMR measurements were iron whiskers as in our experiments, while the torque curve measurments were conducted on single crystal spheres cut from strain and annealed high purity iron.

No complete theory which calculates K_1 versus M_s or versus T, and which is suitable for iron, presently exists. This is unfortunate since the combined data of fig. (29) represents a good set of experimental measurements with which to compare such a theory. The combined data span a temperature range from 20^o K to 0.5^o K below the Curie temperature.

The good agreement amongst these data is not found with an earlier measurement by Bozorth (1951). In fig. (30) we show a composite plot of the data of fig. (29). H_k values which have been calculated using Bozorth's K_1 values are shown as well. The agreement is poor at low temperatures but improves as temperature is increased. We feel that Bozorth's data did not yield to a good torque curve analysis for K_1 and K_2 at low temperatures. In particular, his K_2 values are positive over the full temperature range, and show a slight peak in magnitude at approximately 100^o C. This is in contrast to the findings of Gengnagel and Hofmann which show a negative K_2 with no peak.

Also shown in fig. (30) are H_k values from the reported $K_1(T)/K_1(0)$ values of Yang et al. (1973). We have normalized these using the low temperature extrapolated value $K_1(0)$ of Bozorth. Once again these values show poor agreement with the composite data at low temperatures. The method by which their data was measured and the source of their data are unknown. This set of data is of some interest because they claim to find excellent agreement with Callen and Callen's theory. We do not find a good agreement between this theory and their data. This discrepancy is based on

our measurement of the temperature dependence of the spontaneous magnetization. The solid line in fig. (30) is the theoretical curve suitably normalized at zero temperature.

Before we discuss the Callen theory, we wish to point out recent progress made by Mori et al. (1974). In their paper they discuss the calculation of Mori (1969) in which he finds qualitatively good agreement with the data of Bozorth for both K_1 and K_2 versus temperature for iron and for nickel. He calculates the anisotropy energies for iron and for nickel using perturbation theory on the basis of the energy bands of these metals. The spin-orbit interaction is included in the tight binding approximation up to fourth and sixth order. Mori finds that doubly degenerate energy levels in the bands which intersect the Fermi level produce the dominant contributions to the anisotropy energy. Variations of the spin-orbit interaction, the magnitude of the spontaneous magnetization and the Fermi level are taken into account. The temperature dependence of the anisotropy constants of nickel are explained by the temperature variation of the Fermi level. The zero crossing of K_1 in nickel is produced. In iron the temperature dependence of the constants is understood in terms of the decrease of the exchange splitting.

It is remarkable that this theoretical calculation agrees with Bozorth's data so well. This is especially true to the extent that the peak in K_2 is produced and the sign of this constant is positive. Clearly the approach of this calculation is much more suitable for itinerant 3-d transition ferromagnets than others attempted in the past. The results are most encouraging. However an attempt should be made to find suitable values of the parameters of the theory which emulate the data of Gengnagel and Hofmann.

The theoretical calculation of Callen and Callen (1966) is a single ion theory most suitable for comparison with ferromagnets with localized moments. Each spin is assumed to to have a direction-dependent energy density of the form

$$\varepsilon(s) = \varepsilon_0 + \sum_{\ell} K_{\ell}(0) \sum_{m} q_{\ell}^{m} Y_{\ell}^{m}(s) \qquad (55)$$

where s is a unit vector in the direction of the spin, $K_{\ell}(0)$ are anisotropy constants at zero temperature, and a_{ℓ}^{m} are constants determined by the crystal symmetry. If the expansion is made in terms of the direction cosines of s, as in equation (20), rather than in terms of the spherical harmonics, one finds

$$K_4(T) = K_1(T) + \frac{1}{11} K_2(T) \approx K_1(T) \qquad (56)$$

The summation over ℓ in equation (55) is restricted to even values of ℓ in order to preserve time-reversal symmetry. The results of their calculation are

$$\frac{K_{\ell}(T)}{K_{\ell}(0)} = \hat{I}_{\ell+1/2}(X) \qquad (57)$$

and

$$m(T) = \hat{I}_{3/2}(X) \qquad (58)$$

where $m(T) = M_s(T)/M_s(0)$ and

$$\hat{I}_{l+1/2}(X) \equiv I_{l+1/2}(X) / I_{1/2}(X)$$

a ratio of hyperbolic Bessel functions. The quantity X is an independent parameter.

If the parameter equations (57) and (58) are examined in the limit of large X (low temperatures), one finds the famous 10th power law in its general form

$$\frac{K_l(T)}{K_l(0)} = [m(T)]^{l(l+1)/2} . \qquad (59)$$

This power law has been derived by many authors using many different methods over many years (Akulov 1936, Zener 1954, Keffer 1955). Callen and Callen (1966) have reviewed admirably the status of this low temperature power law giving their own generalized derivation.

Callen and Callen also point out that there is a corresponding high temperature power law. In the limit of small X (T close to T_c),

$$\frac{K_l(T)}{K_l(0)} = [m(T)]^{l} . \qquad (60)$$

In other words the 10th power law of low temperatures becomes the 4th power law near T_c with a continuous variation between.

We have plotted the parametric equations (57) and (58) in terms of anisotropy field and magnetization in fig. (28) as a solid curve. In this case the power laws are the 9th and the 3rd power at low and high

temperatures respectively. Our data does not extend to sufficiently low temperatures to make a comparison with the first of these power laws. We can only point out that our power law at room temperature is two powers higher (n=11). Duplessi (1971) has taken the anisotropy and magnetization data of other researchers and has found power laws which are much smaller than the 10th power at low temperatures. Graham (1958) has reported a 4th power law below room temperature. We have little to contribute in this matter since we have data only at high temperatures.

At high temperatures, the agreement between theory and our data is good as far as the power law in concerned. To our knowledge this is the first demonstration of the 4th power law in a cubic ferromagnet just below the Curie point. This power law should be quite general in its validity since it depends only on the cubic symmetry and not on a detailed accounting of the microscopic interactions of the system. Deviations from this power law occur quickly with decreasing temperature. Our data show that it holds only within the last few degrees below T_c, which is approximately 1043^{o} K.

This theory is also plotted as H_k versus temperature in fig. (29) as two solid curves. For the curve that agrees more closely with the data, the temperature values are obtained from our fit of spontaneous magnetization versus temperature reported below. The other curve is obtained by calculating temperature values according to

$$\frac{T}{T_c} = \frac{3}{X}\hat{I}_{3/2}(X) \qquad (61)$$

where X is the independent parameter. This is a result of Weiss molecular field theory using the Langevin function $\hat{I}_{3/2}(X)$. This poor approach is

shown here only to emphasize the importance that the assumed M_s versus T data plays in making such plots of anisotropy versus temperature. As well, we have shown the Callen theory here in the classical limit ($s = \infty$). Assuming a finite spin does not improve the agreement with our data. If $s < 2$ the term of cubic symmetry in the calculation vanishes identically (Wolf, 1957).

It is possible to include two-ion terms in the calculation which are pseudo-quadrupolar in structure. The ground work for doing this was laid by Van Vleck (1937) and has been extended by Keffer (1955). Reviews of the microscopic origins of magnetic anisotropy have been written by Kanamori (1963) and Yosida (1968). These studies are applicable once again to ferromagnets which have localized moments and not to the iron-group metals and alloys.

The theory of magnetic anisotropy in 3-d transition metals seems to be waiting for further developments in the theory of ferromagnetism itself. Calculations such as Mori's based on the energy bands of the metal are encouraging and hopefully will be extended.

VI. TEMPERATURE DEPENDENCE OF THE SPONTANEOUS MAGNETIZATION OF IRON

1. Introduction

The measurement of the spontaneous magnetization of iron has a long history. The earliest absolute measurements on iron and nickel were those of Weiss and Forrer (1926, 1929) by an axial extraction method. Since then the measurements have been repeated many times on both materials using the extraction method and force methods. The results of these studies have been summarized by Danan et al. (1968). The mean measured value for the absolute saturation of iron is $\sigma_o = 221.71 \pm 0.08$ emu/g corresponding to $M_o = 2.216\ \mu_B$.

The first study of the temperature dependence of the magnetization of iron from room temperature to the Curie point is that of Potter (1934). He employed a force method using a Sucksmith ring balance. More recently this experiment has been repeated by Crangle and Goodman (1971) from 4 to 1023° K. As well they have measured the absolute saturation and have found the above value for it.

In this section we report our measurement of the spontaneous magnetization of iron as a function of temperature from room temperature to the Curie point. By spontaneous magnetization $M_s(T)$ we mean the internal or domain magnetization in zero applied field. The units for magnetization which we use is magnetic moments per unit volume. Using the value of Gorton et al. (1965) for the lattice parameter of iron at 295° K, as well as Crangle and Goodman's value for the specific magnetization at the same temperature, we calculate the saturation magnetization to be $M_s(295^\circ\ K)$

= 1714 emu/cm^3.

Our technique is to measure the departure field H_d of a [100]-oriented iron whisker as a function of temperature. As described previously H_d is related to M_s by

$$H_d(T) = 4\pi D M_s(T) \qquad (62)$$

where D is the demagnetizing factor of the sample. The temperature dependence of D is not expected to change by more than 1% over the full temperature range for our size of sample(Bloomberg 1973). Bloomberg and Arrott (1975) show that 2.3% of the magnetic charge on an iron whisker is situated on the domain walls at room temperature. This expense in magnetostatic energy is compensated by a saving in anisotropy energy. With increased temperature, the charge on the walls goes to the surface of the whisker as the anisotropy decreases. We make a small correction for the temperature dependence of D according to their calculations. We also monitor the low field ac susceptibility of the sample as well, but this is not expected to be a good indicator of the temperature variation of D.

Finally we compare our data to those of Crangle and Goodman. We correct their data given as specific magnetization values in emu/g for the thermal expansion of iron. Our data being relative measurements are normalized to theirs. We curve fit both sets of data to the function

$$m(t) = \frac{(1-t)^{\beta}}{1-\beta t + A t^{3/2} - C t^{7/2}} \qquad (63)$$

where $t = T/T_c$ and $m(t) = M_s(T)/M_s(0)$. This fit to the data requires only the determination of the parameter C since β and A are previously well-determined experimental quantities. Our choice of the 7/2 power is based solely on us obtaining a better fit than if some other reasonable power had been used. For intensive studies of the deviation from the T to the 3/2 law at low temperatures, see the work by Argyle et al. (1963), Aldred and Froehle (1972), Riedi (1973), and Ododo (1977). As mentioned previously, the critical exponent β has been measured for many [100]-oriented whiskers by Heinrich and Arrott. The value $\beta = 0.371$ which we found for a [111]-oriented whisker, and have discussed above, is in good agreement as well.

The above calibration fit is used in the analysis of our anisotropy data as previously described. It can also be used as the calibration curve for an iron whisker magnetic thermometer. Such a thermometer has been designed by Arrott and Heinrich (1980) and is presently being used as an experimental tool.

2. The Experiment

The experiment is conducted in exactly the same way as for the [111] whisker which has been described above. The [100] whisker studied is 9.675 mm long and 0.150 mm on a side. Accurate measurements of the departure field H_d of the [100] whisker are made at each temperature using second harmonic detection with the phase sensitive lock-in amplifier. Our thermometry is described in the section "Discussion of the Measurements", above. A detailed measurement of H_d is made as the temperature of the sample is allowed to

slowly drift linearly in time from 3° K below T_c up to and through the Curie temperature. A fit to this data provides us with a value for the parameter C in eq. (63).

3. Results and Discussion

For a [100] whisker the ballistic demagnetizing factor, up to saturation, depends slightly on the anisotropy constant K_1. An approximate expression has been given by Bloomberg and Arrott (1975; see eq. 6.5 therein) for the relationship between M_s and departure field H_d.

$$H_d = 16\pi\left(\frac{d}{\ell}\right)^2\left[\ln\left(\frac{2\ell}{d}\right) - 1.792 - \frac{K_1}{6M_s^2}\right]M_s \qquad (64)$$

where d and ℓ are the thickness and length of the whisker, respectively. While this expression for the ballistic demagnetizing factor is accurate only to about 2% for predictions of the numerical relation between H_d and M_s, it should be quite adequate to correct the measured values of H_d determined at a temperature for which M_s is known. The correction for the whisker used to obtain the temperature dependence of M_s is 0.8% at room temperature and less than 0.1% above 750° K.

Our data is normalized to those of Crangle and Goodman, after correcting the latter for the thermal expansion of iron (see Gorton 1965 for thermal expansion study of iron). Both sets of data fit well to the function in eq. (63). The parameters of this equation are determined by the asymptotic

behaviour at low temperatures as measured by Argyle et al. (1963) and at high temperatures from our own work. Using

$\beta = 0.368$

$A = 0.1098$

$C = 0.129$

we obtain the values shown in table (6) and the fit curve in fig. (31).

As expected we do not find that the measured low field susceptibility follows the dc susceptibility at the lower temperatures. The measured ac signal increases by 6% from room temperature to about 550^{o} C. It does not vary by more then 1% above this temperature.

In fig. (31) we show a plot of our data interpreting our departure fields as relative measurements of the spontaneous magnetization. As stated above these have been corrected for the temperature dependence of the ballistic demagnetizing factor. As well we plot the data of Crangle and Goodman for iron. Since their data are relative measurements of the specific magnetization they must be corrected for the thermal expansion of iron in order to be compared with our data. To do this we use the x-ray measurements of the lattice parameter of iron made by Gorton et al. (1965). The agreement between the two sets of data is good except for our room temperature point which is about 0.3% higher than the data of Crangle and Goodman. This point is not the result of some error of measurement, although it is measured before and after heating to high temperatures and found to be smaller by 0.5% after this annealing treatment. A larger than expected departure field results if the internal susceptibility is lower for some reason. This can be caused by an interaction between the domain structure and imperfections of the crystal which will diminish with increased

temperature. A probable cause of the lower susceptibility in our samples is an interaction of the domain walls with an absorbed interstitial gas of carbon. As temperature is increased, the hopping frequency of the carbon atoms from site to site increases. The preference of carbon atoms for certain sites due to the local direction of the internal magnetization is reduced.

In summary equation (63) fits the combined sets of data well. This fit is used in our analysis to extract H_k values from our measured values as described in the previous section.

VII. SUMMARY

We have reported our study of the magnetic behaviour of the iron whisker which grows with its axis along the [111] crystallographic direction. We have compared this behaviour with the same for the [100] and [110]-oriented iron whiskers in terms of their response to applied ac and dc fields. A simple domain structure for the [111] whisker is proposed and is shown to be consistent with the observed ac behaviour and with the hexagonal cross section of such whiskers.

A detailed description of the growth of iron whiskers has been given. This is discussed further in terms of the proposed mechanisms of whisker growth. Both the screw dislocation mechanism and the VLS mechanism have been given special attention. The important role of impurities in whisker growth has been discussed and a summary of our methods and others of the detection of minute amounts of carbon in iron has been made.

A detailed measurement of the approach to saturation of the [111] whisker has been reported. This has been studied by ac susceptibility measurements as the whisker is magnetized in its [111] axial direction, the "hard" direction for magnetization. Measurements along the length of the whisker allowed a self-consistent determination of the distribution of magnetic charge along the whisker's length. This in turn was used to make corrections to the data for the effects of the demagnetizing field. Special interest was directed towards the nature of the transition to saturation at the whisker's centre. No first order jump to saturation was observed despite it being predicted by mean field anisotropy theory. A review of the experimental and theoretical work on the 3-state Potts model is given.

It has been suggested by others that cubic ferromagnets with three easy axes of magnetization could be physical realizations of this model. Experimental measurements on these physical realizations could reveal the nature of the Potts transition in 3 dimensions. However, even though we do not see a first order transition in iron, it could be "nearly second order". Conversely mean field anisotropy theory may not be appropriate for describing the nature of the transition.

A measurement of the anisotropy field $H_k \sim K_1/M_s$ as a function of temperature and magnetization has been made. This field has been extracted from measurements of the critical applied field which just saturates the centre of a [111] whisker. Corrections for the demagnetizing field are made. The agreement with similar data from torque curve measurements and FMR studies is good. Our technique has the advantage of being sensitive to very small anisotropy fields and thus allows the extraction of H_K versus M_s and versus T up to 0.5^o K below the Curie temperature T_c. We have found that K_1 follows the 4th power of M_s, but only for 1^o below T_c. The power law exponent quickly increases with further decrease in temperature. This is the first measurement of this power law in a cubic ferromagnet just below the Curie point. The power law is determined by the cubic symmetry of the ferromagnet and not by the detailed interactions. Two techniques for the correction for demagnetizing field effects have been made. At high temperatures a technique of integrating the measured ac response versus field is used. At lower temperatures, a calculation is made to model the distribution of magnetic charge on the surface of the whisker as the sources of the demagnetizing field.

Finally we have measured the temperature dependence of the spontaneous

magnetization of iron as a function of temperature. These data were obtained from our measurements of the departure field of a [100]-oriented iron whisker. Small corrections for the demagnetizing field effects were made. Comparison with the data of others obtained by a force technique has been made and the agreement is good. These results have been used to aid us in our analysis for the anisotropy field H_k versus temperature. A fit has been made to the magnetization data using a function of the form of a Padé approximate. All of the parameters of this fit have been experimentally determined from magnetization measurements in the low and high temperature asymptotic limit. This fit can be used as the calibration curve for an iron whisker magnetic thermometer.

Table 1. Steps in a VLS mechanism of whisker growth and suggested steps for iron.

Footnote: Information on the phase diagram of Fe and Cl is very sketchy. An extensive search of the literature found no binary alloys of Fe and Cl. $FeCl_2$ and $FeCl_3$ are stable compounds. Mellor (1961) reports that $FeCl_2$ melts in the temperature range 670-674°C, although sublimation is possible with a partial decomposition to $FeCl_3$ in the reaction $3FeCl_2 = 2FeCl_3 + Fe$. Apparently the decomposition is supressed if the sublimation takes place in an HCl atmosphere.

TABLE (1)

Step	Description	Iron Whisker
1	Diffusion of molecules in the vapour phase to the droplet.	Diffusion of sublimed $FeCl_2$ vapour & H_2 molecules to the droplet.
2	Vapour deposition at the droplet. Frequently involving a chemical reaction to produce whisker growth material.	$FeCl_2$ reacting with H_2 to produce Fe in solution of HCl. Carbon &/or water may play a role in droplet formation.
3	Diffusion of reaction by-products away from the droplet.	Diffusion of HCl and other by-products away from the droplet.
4	Transport of vapour molecules or new phase (whisker growth material) through droplet to S-L interface.	Diffusion of Fe through the droplet to the tip of the whisker.
5	Precipitation to form a whisker.	Precipitation of Fe to form next whisker growth layer.

Table 2. A summary of our present understanding of the nature of the transition for the d-dimensional q-state Potts model.

TABLE (2)

d \ q	2	3	4	5 ...
1	no transition	no transition		
2	higher order (Baxter)	higher order (Baxter)	higher order (Baxter)	first order (Baxter) →
3	second order	nearly second order		
4	first order	first order		
⋮	↓	↓		

Table 3. A comparison of three [111]-oriented iron whiskers at room temperature. The calculated H_D value depends on the measured ρ value. Agreement among the extracted H_K values can be seen.

TABLE (3)

Sample No.	$\rho \times 10^2$ (measured)	H_c(oe) (measured)	H_D(oe) (calc.)	H_k(oe) (calc.)
1	2.145	429.7	6.9	422.8
2	1.667	417.0	3.8	413.2
3	7.971	583.1	157.7	425.4

Table 4. A summary of experimental results from room temperature to 18°K below T_c for a [111] iron whisker.

TABLE (4)

T/T_c [±0.1%]	H_c [oe] [±0.1%]	H_D [oe] [±3.3%]	H_k [oe]	M_s [emu/cm^3] [±0.1%]
0.2828	417.0	-3.98	413.0(5)	1714.
0.5375	216.05	-4.49	211.6(4)	1612.
0.7256	88.18	-6.26	81.9(3)	1479.
0.8050	52.36	-7.83	44.5 "	1384.
0.8706	31.68	-9.28	22.4 "	1262.
0.8879	27.39	-9.59	17.8 "	1218.
0.9046	23.53	-9.82	13.7 "	1168.
0.9226	19.69	-9.97	9.7 "	1102.
0.9425	15.88	-9.85	6.0 "	1011.
0.9524	14.07	-9.64	4.4 "	954.6
0.9629	12.17	-9.25	2.9 "	882.6
0.9721	10.49	-8.69	1.8 "	804.0
0.9825	8.60	-7.60	1.0 "	686.8

Table 5. A summary of experimental results from 11°K below T_c to 0.5°K below T_c for the [111] iron whisker.

TABLE (5)

T_c-T [degK]	T/T_c	H_c [oe]	H_D [oe]	H_k [oe]	M_s [emu/cm^3]
10.10(8)	.99032(9)	6.72(2)	-6.23(7)	0.486	558.
5.88(6)	.99436(6)	5.41	-5.16(5)	0.254	460.
4.56(5)	.99563(5)	4.89	-4.71(4)	0.181	420.
4.35(5)	.99583(5)	4.80	-4.62 "	0.182	412.
1.93(3)	.99815(3)	3.50	-3.43(3)	0.066	307.
1.91 "	.99817 "	3.49	-3.43 "	0.064	306.
1.90 "	.99818 "	3.48	-3.42 "	0.064	305.
1.68 "	.99839 "	3.33	-3.27 "	0.057	292.
1.12(2)	.99893(2)	2.85	-2.82(2)	0.034	251.
0.947(19)	.99969 "	2.68	-2.65 "	0.030	236.
0.924 "	.99911 "	2.65	-2.62 "	0.029	234.
0.903 "	.99913 "	2.63	-2.60 "	0.027	232.
0.816(18)	.99922 "	2.53	-2.51 "	0.025	224.
0.789(17)	.99924 "	2.50	-2.48 "	0.025	221.
0.582(14)	.99944(1)	2.22	-2.20 "	0.016	198.
0.538(14)	.99948 "	2.16	-2.15 "	0.014	192.

Table 6. Measurements of the departure field of [100] whisker versus temperature. Correction for D(T), our values for $M_s(T)/M_s(R.T.)$, and values from the fit are also shown.

TABLE (6)

T/T_c	H_d(oe)	$D(T)/D(T_c)$	$M_s(T)/M_s$(R.T.)	$M_s(T)/M_s$(R.T.) (fit)
0.2823	20.40	1.009	1.000	1.000
0.5563	18.78	1.005	0.924	0.926
0.7223	17.01	1.002	0.841	0.844
0.7922	15.89	1.001	0.786	0.791
0.8053	15.64	1.001	0.774	0.779
0.8698	14.18	1.000	0.702	0.703
0.8858	13.89	1.000	0.687	0.678
0.9025	13.05	1.000	0.646	0.649
0.9199	12.37	1.000	0.611	0.612
0.9401	11.38	1.000	0.563	0.560
0.9501	10.76	1.000	0.532	0.528
0.9604	10.03	1.000	0.496	0.490
0.9699	9.25	1.000	0.457	0.447
0.9796	8.14	1.000	0.402	0.391
0.9882	6.85	1.000	0.339	0.323
0.9925	6.01	1.000	0.297	0.274
0.9956	4.61	1.000	0.228	0.226
0.9967	4.10	1.000	0.203	0.204
0.9977	3.43	1.000	0.169	0.178
0.9988	2.73	1.000	0.135	0.141

Fig. 1. Magnetization curve of iron single crystal measured by applying the magnetic field parallel to each of the three principal crystallographic directions (after Honda and Kaya, 1926).

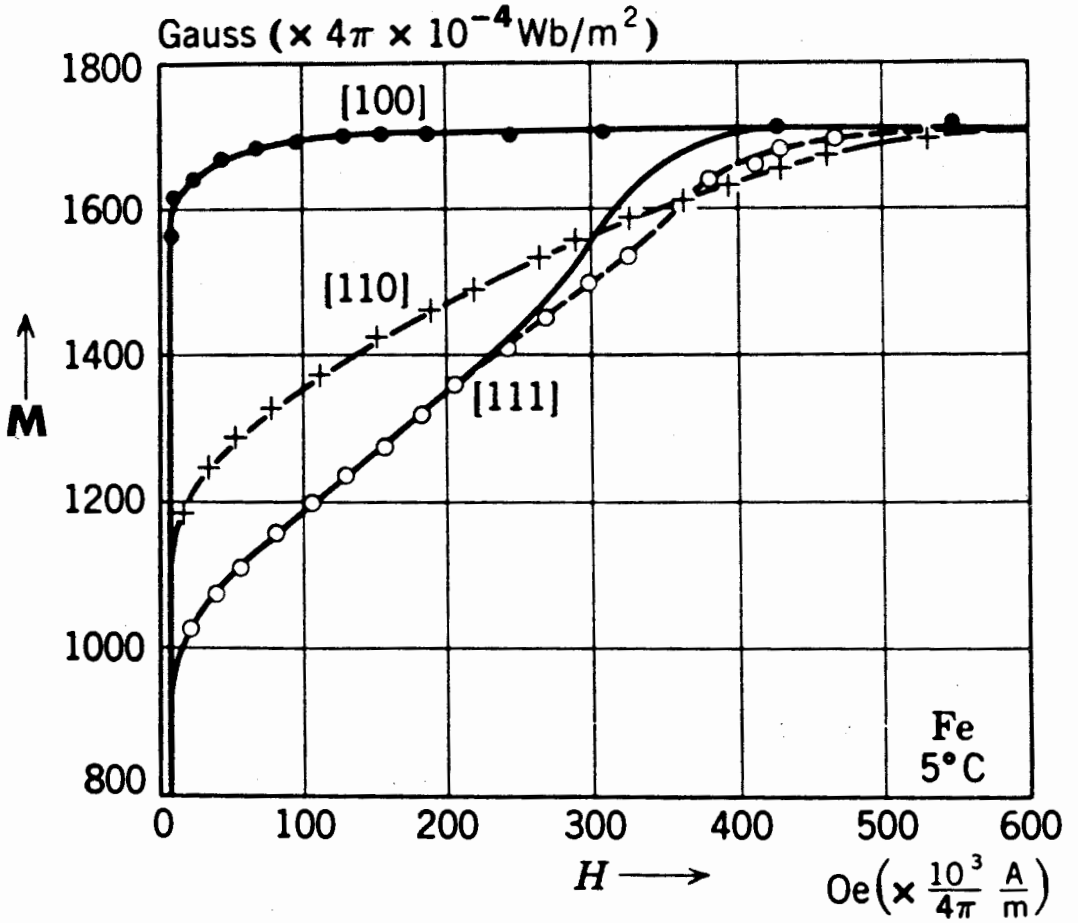
Gauss (× 4π × 10⁻⁴ Wb/m²)
1800
1600
1400
1200
1000
800
M
[100]
[110]
[111]
Fe
5°C
0
100
200
300
400
500
600
H ⟶
Oe (× 10³/4π A/m)

Fig. 2. The Landau Structure for a [100] oriented bar of iron in zero field. It is characterized by 4 domains, 2 major domains running the length of the bar and separated by a 180 degree wall, and 2 closure domains at the ends bounded by 90 degree walls. The domain walls are Bloch walls which become Neel-like at the side surfaces. This results in two essential singularities, one on each of the side surfaces.

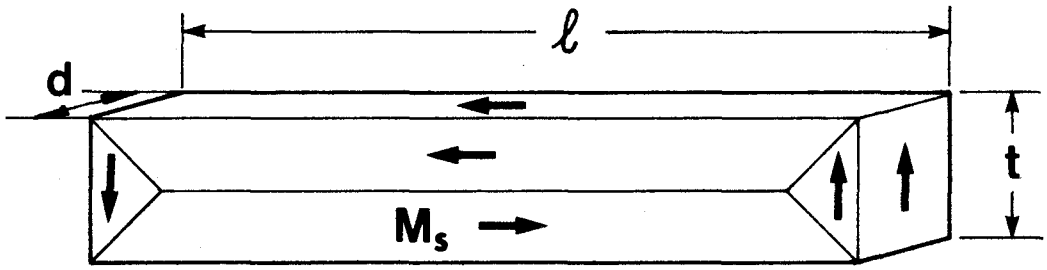
ℓ
d
t
M_s

Fig. 3. The whisker growth apparatus.

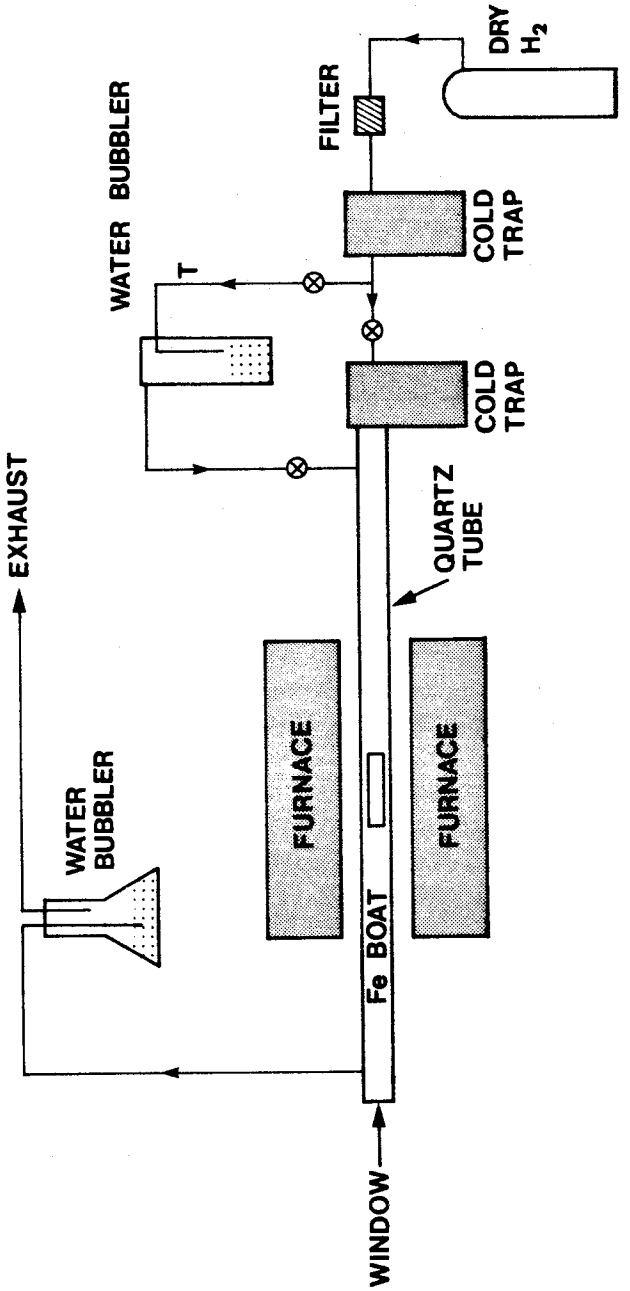
DRY
H_2
FILTER
COLD
TRAP
WATER BUBBLER
T
COLD
TRAP
EXHAUST
QUARTZ
TUBE
FURNACE
FURNACE
WATER
BUBBLER
Fe BOAT
WINDOW

Fig. 4. A single turn pick-up coil at position z detects 3 contributions to the ac flux: applied field, magnetization of sample, and the demagnetizing field. The total flux through surface B equals that through surface A. The distribution of magnetic charge along the length of the sample determines the distribution of effective susceptibility and of the demagnetizing field along the length. Surface A is the flat plane of the coil. Surface B is the cylindrical surface with the diameter of the coil plus the flat surface at position z. Thus A and B together form a completely closed surface with the shape of a can.

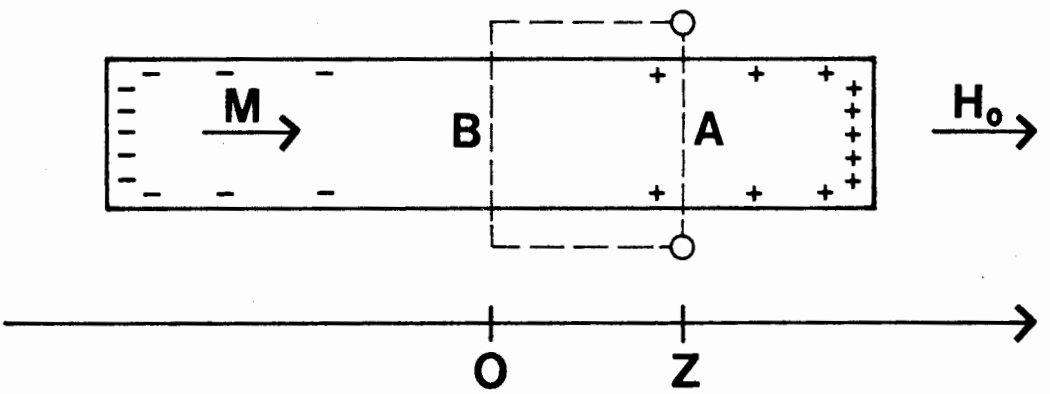
M
B
A
H_o
O
Z

Fig. 5. Continuously measured ac signal detected with a very short tightly-wound 2-turn pick-up coil as it is slid along the whisker. Curve A is for $H_o < H_d$, while curves B, C, and D are for successively larger fields which are greater than H_d. For each curve, the coil has been moved from position 1 to position 3 as shown in diagram. All measured signals are in phase with the driving field.

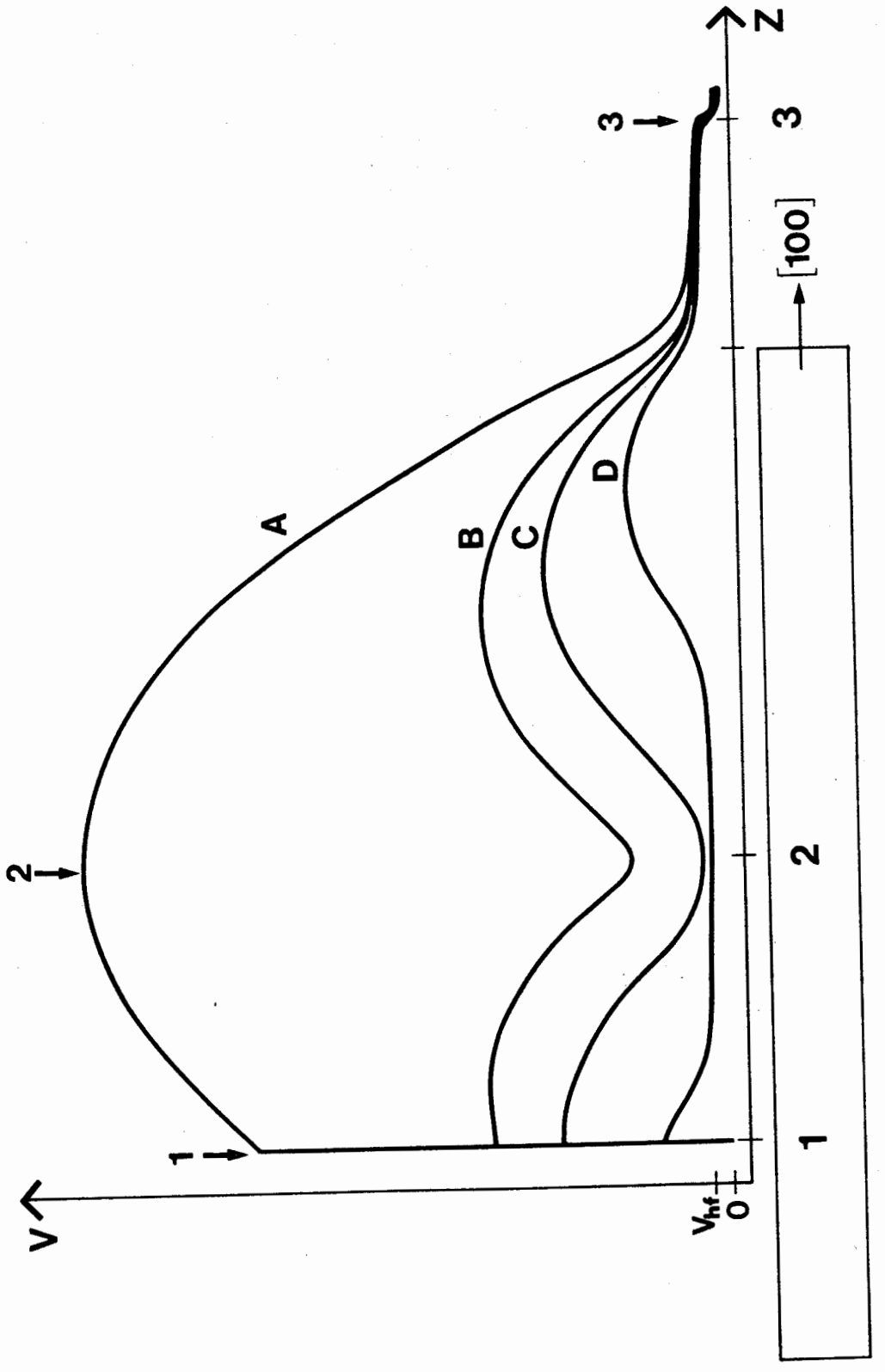
Z
V
A
B
C
D
1
2
3
[100]
V_{hf}
0

Fig. 6. Schematic drawings of possible domain structures for [100]-oriented iron whiskers and bars based on observed Bitter patterns. (a) a diamond, (b) multiple Landau walls and closure domains, (c) a whisker in an applied field near departure.

a)

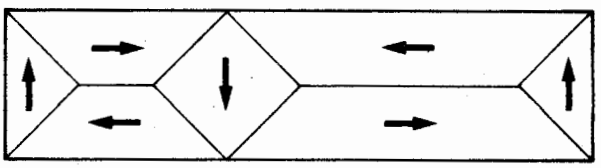

b)

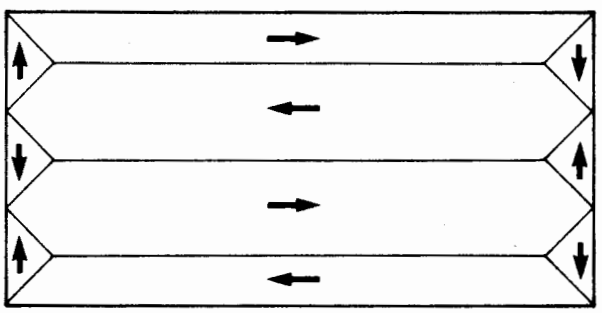

c)

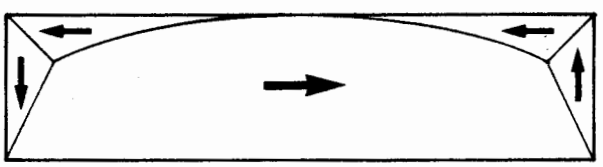

Fig. 7. Signals measured with lock-in amplifier for a [100] whisker driven at approximately 1 kHz. A long pick-up coil is used. (a) out-phase signal, and (b) in-phase signal vs. field. Various regions of behaviour are referred to in text. The ratio of in-phase to out-phase signal is much larger than is indicated (approx. 10 at 1 kHz).

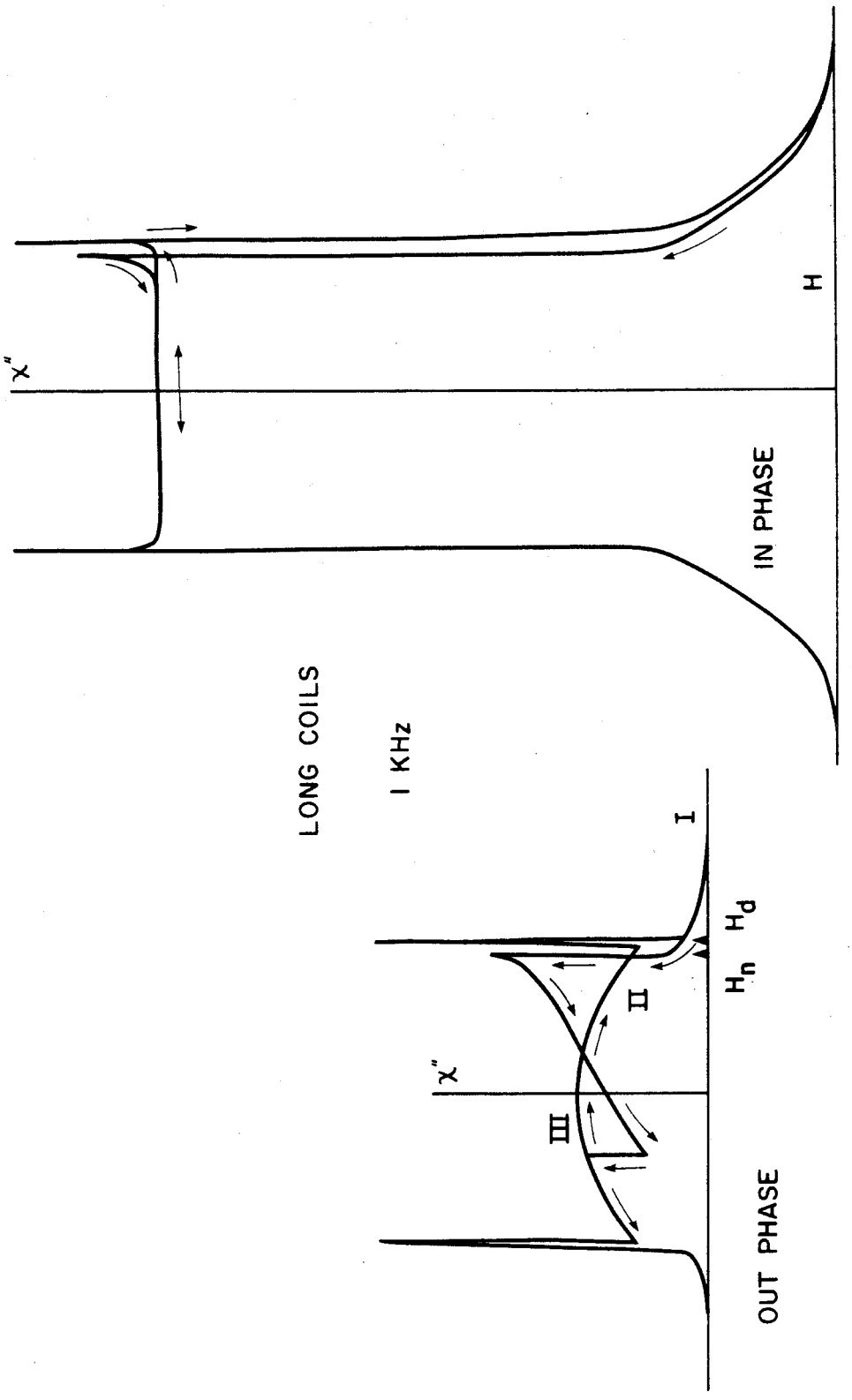
χ"
H
IN PHASE
LONG COILS
1 KHz
I
II
III
H_n H_d
χ"
OUT PHASE

Fig. 8. The growth tip of a [111]-oriented iron whisker. The whisker has an hexagonal cross section consisting of 6 (110)-type surfaces. The whisker often terminates in a tip consisting of three mutually perpendicular (100)-type surfaces. (a) top view, (b) perspective.

a)

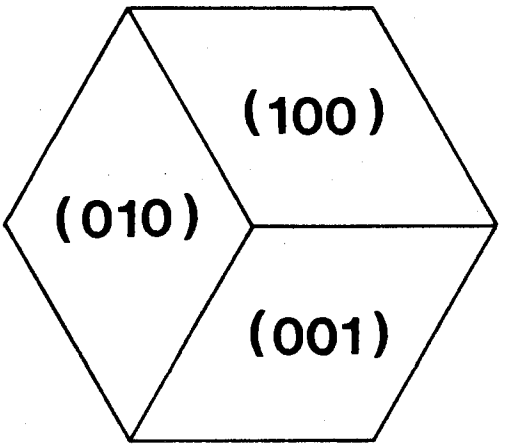

b)

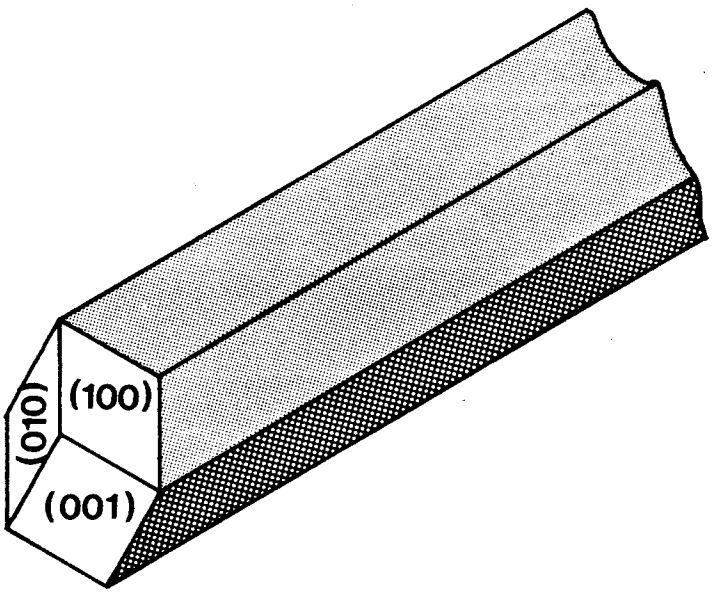

Fig. 9. The domain structure of a triangular prism. The [111] direction is perpendicular to the page. The [100], [010], and [001] directions are out of the page at angles of ~55 degrees from the perpendicular.

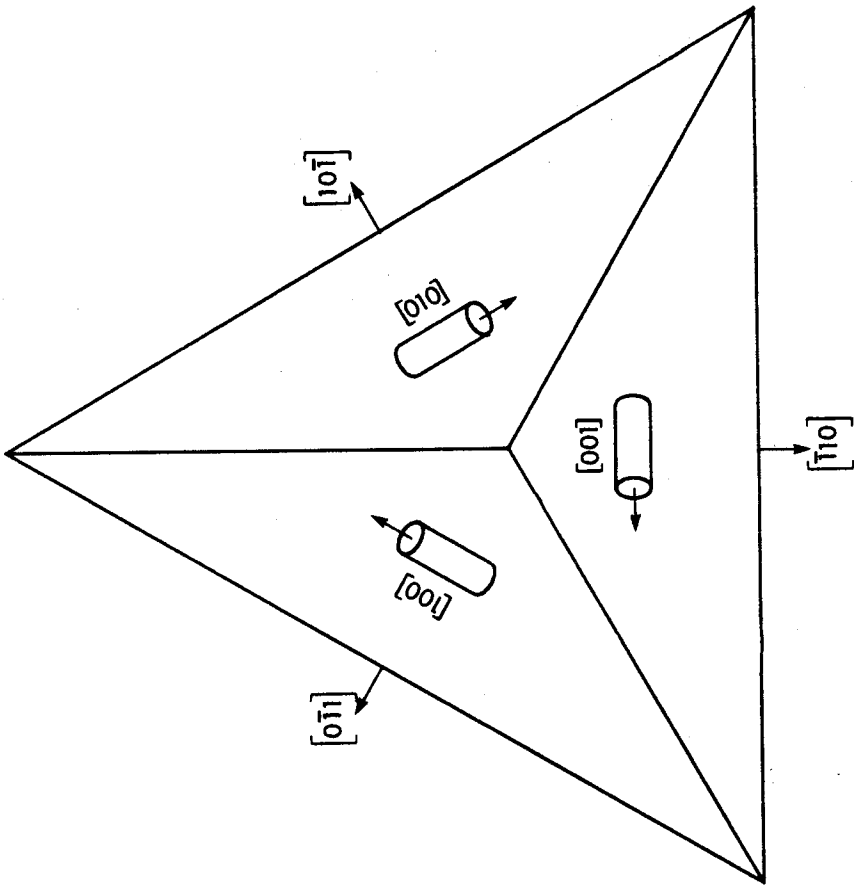
[10$\bar{1}$]
[010]
[001]
[$\bar{1}$10]
[001]
[01$\bar{1}$]

Fig. 10. Domain structure of a hexagonal prism. The result of nucleating one trio of 180 degree walls is shown at one of the six possible sites. All vectors are pointing in easy directions, which are ~55 degrees to the axis of the prism which is the [111] direction.

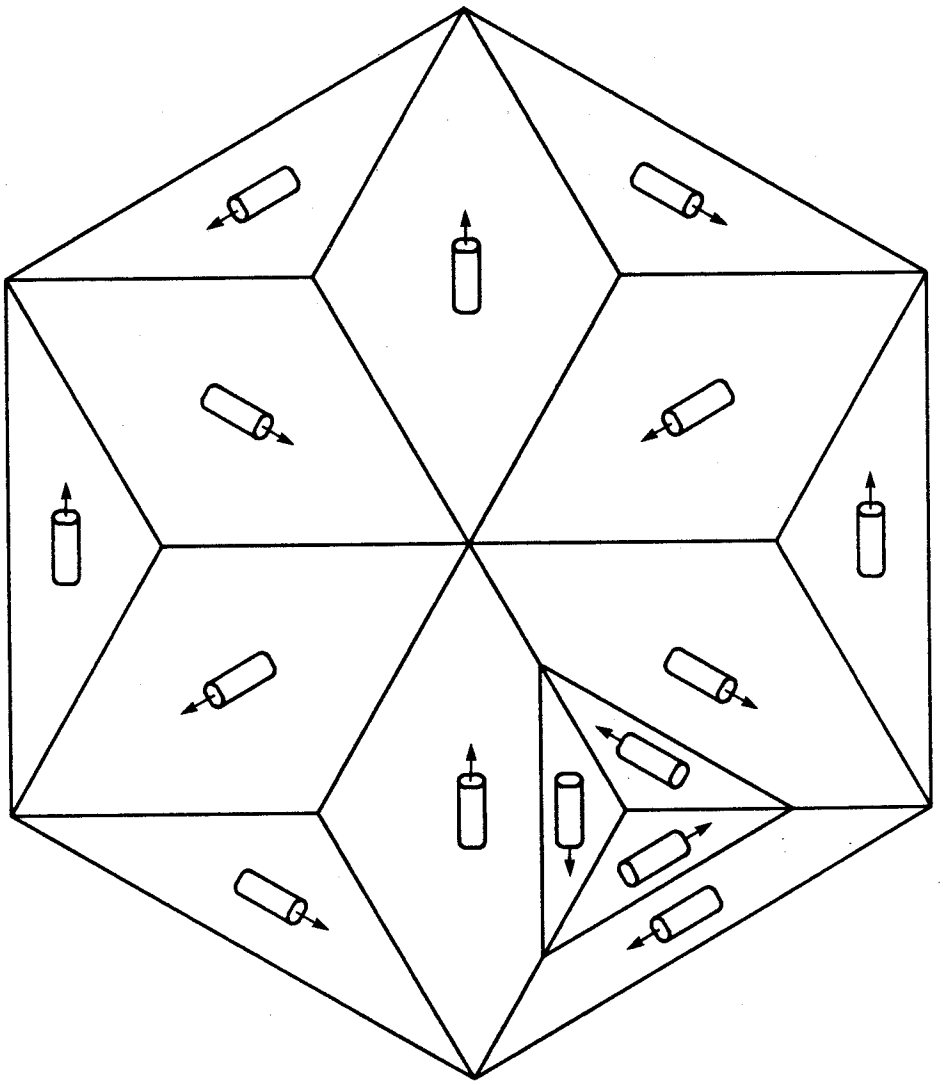

Fig. 11. Low field ac in-phase response for a [111] whisker vs. field. Note the six peaks which support the suggested domain structure of fig. (10). Each peak in signal corresponds to the nucleation of a trio of mobile 180 degree walls. $M_z < M_s/\sqrt{3}$ here.

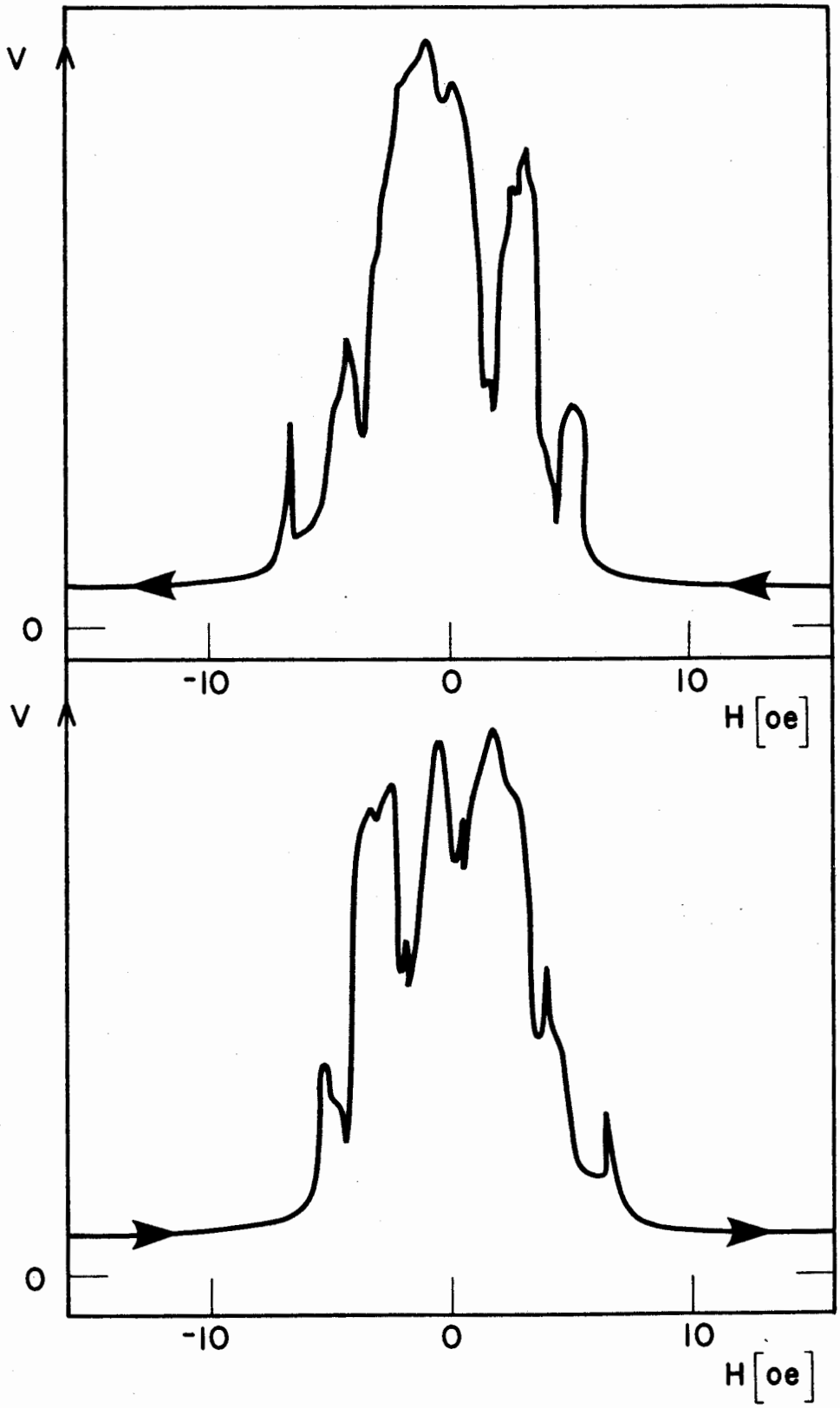
V
0
-10
0
10
H [oe]
V
0
-10
0
10
H [oe]

Fig. 12. In-phase signal vs. field for [111] whisker at 500 Hz. Sweep in field sufficient to saturate the centre of whisker at H_c in both directions. Note low field region of high susceptibility due to mobile domain walls. At higher fields, the susceptibility is much lower as moments are rotated against the anisotropy. A spike in susceptibility occurs as the centre of the whisker saturates.

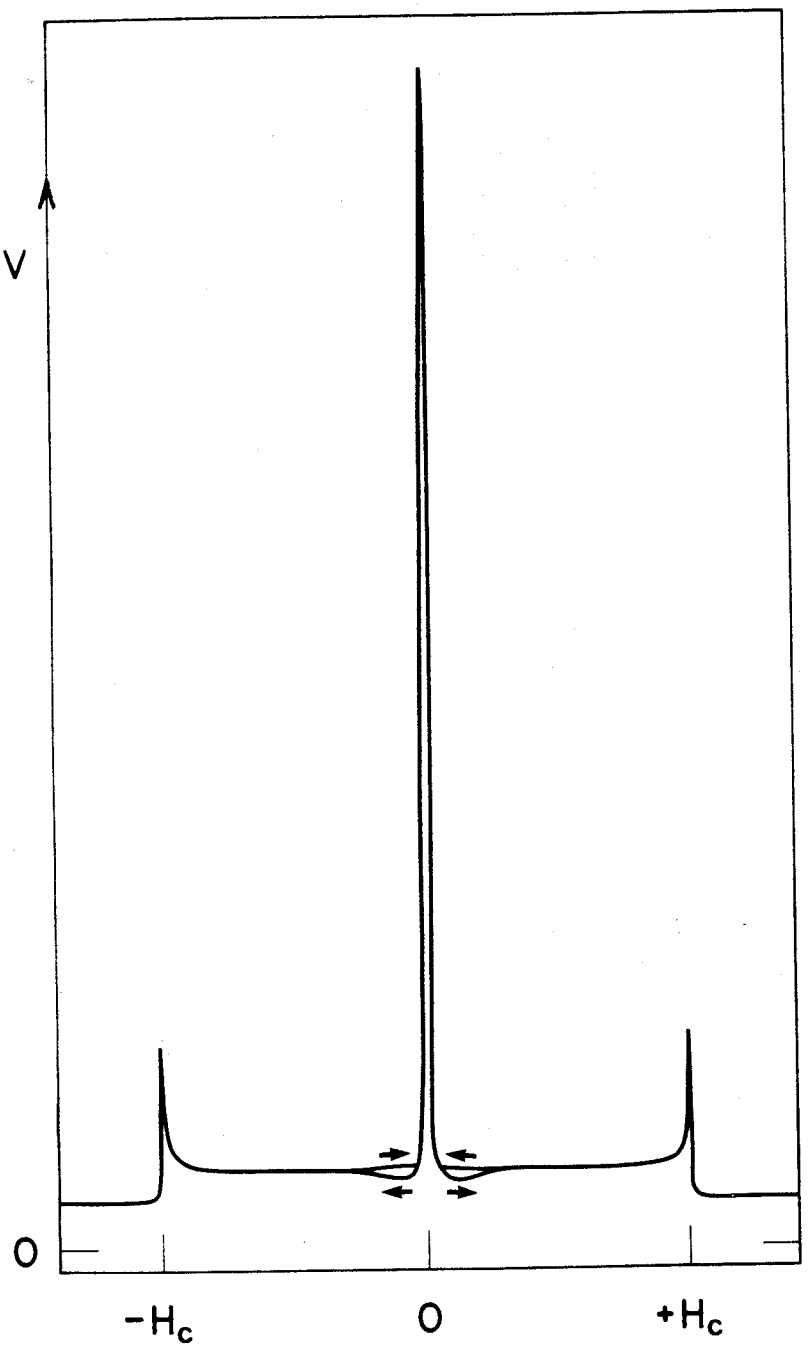
V
0
-Hc
0
+Hc

Fig. 13. A simple demagnetized state for the hexagonal prism using only 90 degree walls.

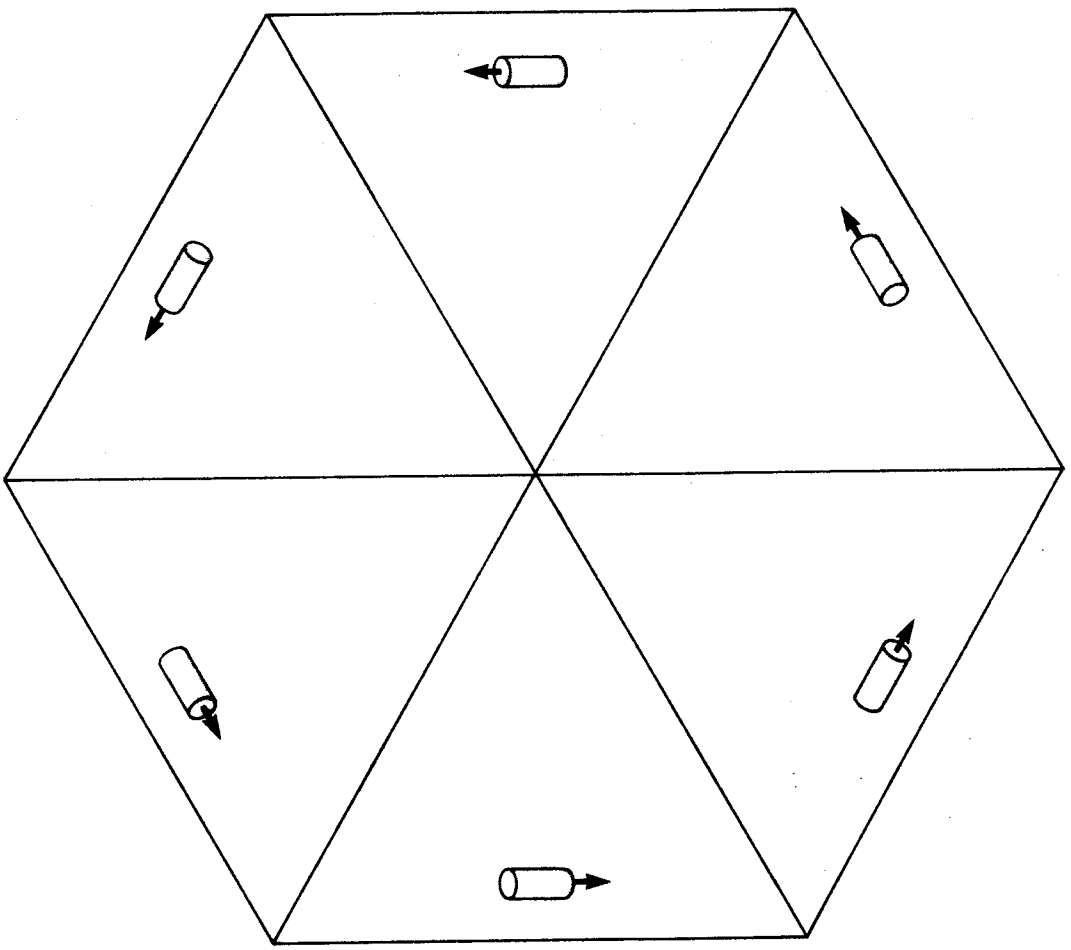

Fig. 14. A candy-stripe domain pattern observed on the side surface of a [111] whisker in zero field using the Bitter technique. The ratio s/w appears to be equal to $1/2\sqrt{2}$.

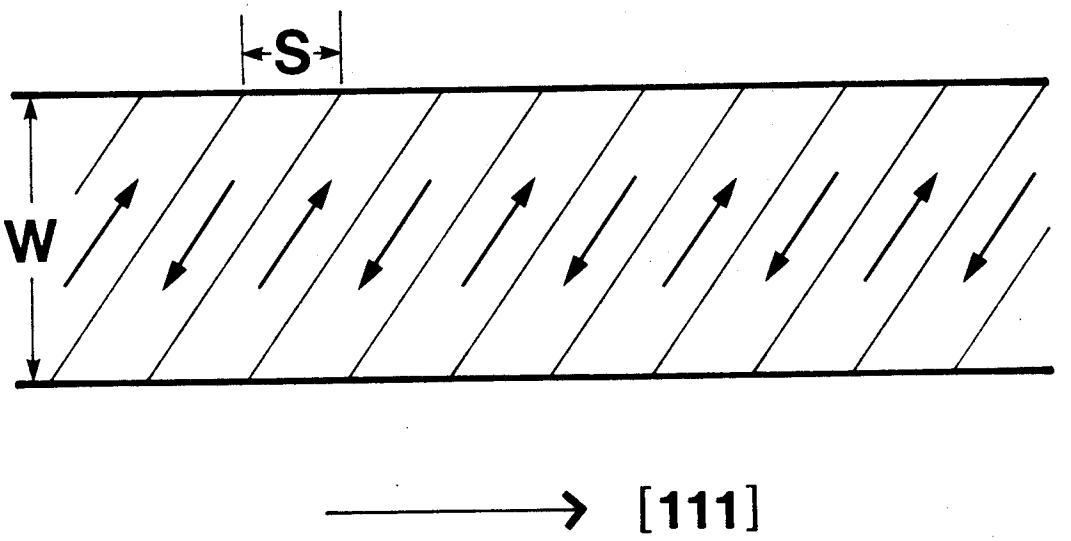
S
W
[111]

Fig. 15. A cross section of a [110]-oriented iron whisker showing the geometry of surfaces.

Fig. 16. Bitter pattern on the broad (100) face of the [110] whisker. 90 degree walls extend across the face and are evenly spaced.

Fig. 17. Bitter pattern on the broad (100)- face of the [110] whisker. Both 180 and 90 degree walls are observed. This is consistent only with a (100)-face. Thus the domain structure helps in orienting the crystal.

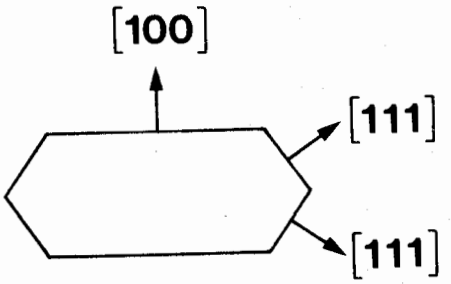

Fig. 15

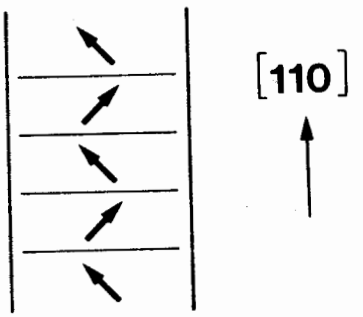

Fig. 16

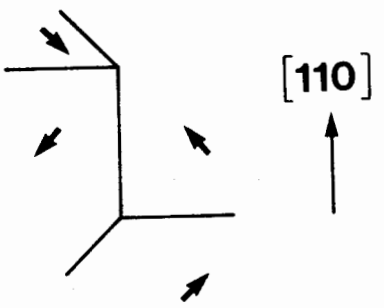

Fig. 17

Fig. 18. In-phase response vs. applied field for [110] whisker at low frequency. In the wall motion region ($-H_1 < H < H_1$), $M_z < M_s/\sqrt{2}$ and the susceptibility is high. At higher fields, the susceptibility is low as moments are rotated against the anisotropy. Ultimately, the whisker saturates at its centre with no peak in susceptibility at a field H_c.

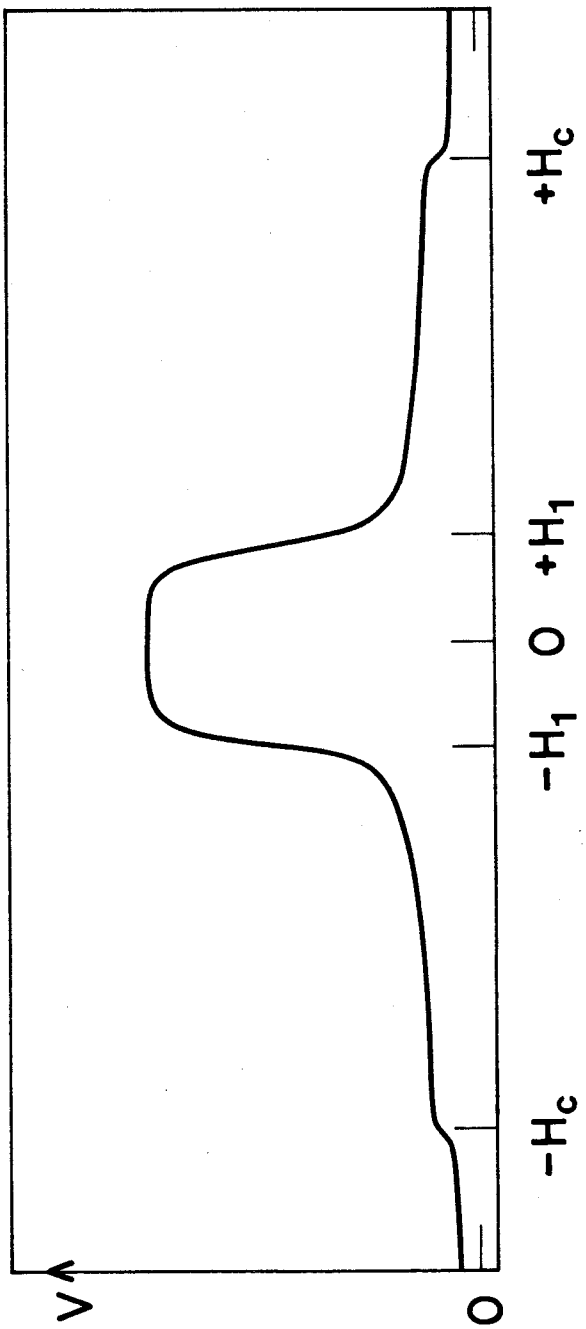
V
O
$-H_c$
$-H_1$ O $+H_1$
$+H_c$

Fig. 19. $H_D(0)$ vs. H_o for the centre of the [111] whisker. The fit to the data represents the function of eq. (29) which is necessary for the analysis. Note that H_D is not a monotonic function of H_o.

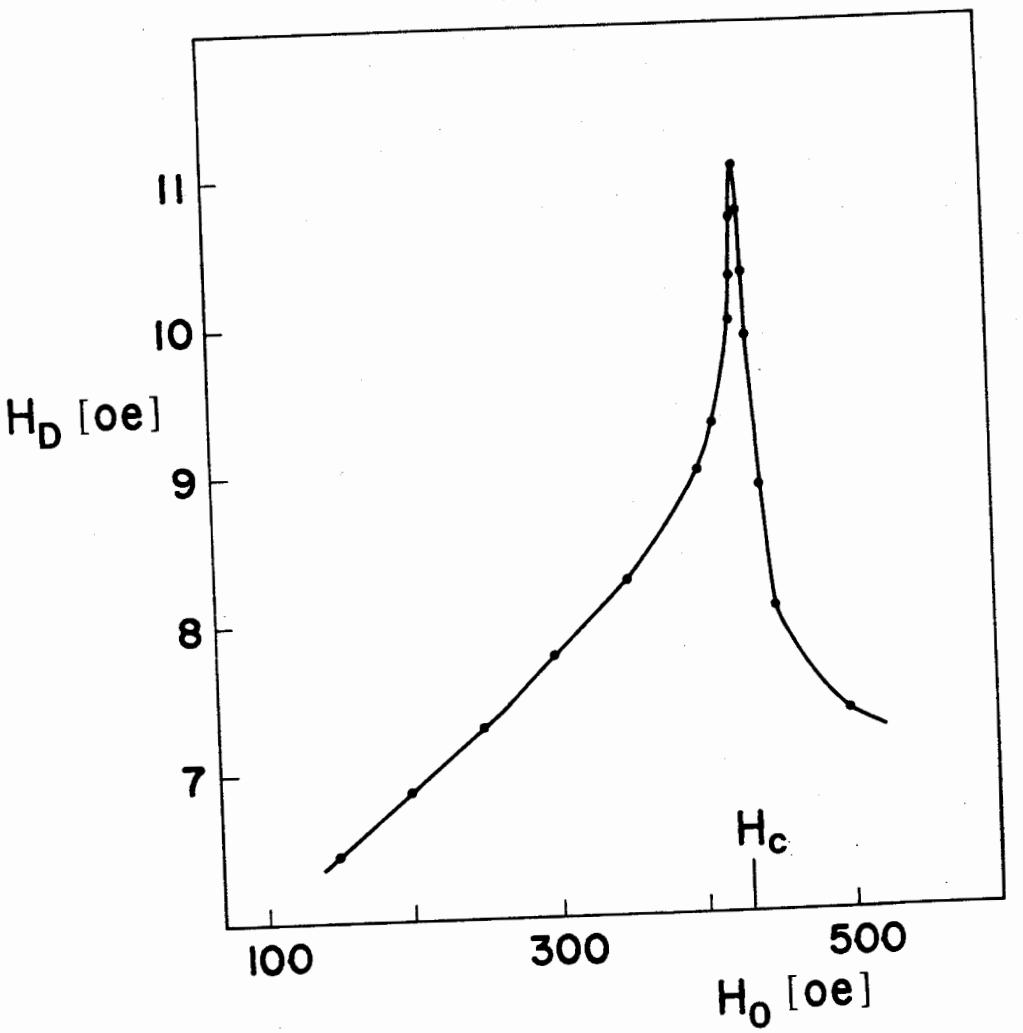
11
10
9
8
7
H_D [oe]
H_c
100
300
500
H_0 [oe]

Fig. 20. Experimental results for the intrinsic susceptibility χ_i as a function of internal field for [111] direction. The low field data are not fully corrected for the demagnetizing field contribution to the magnetic flux changes. Calculated susceptibility using mean field theory also shown.

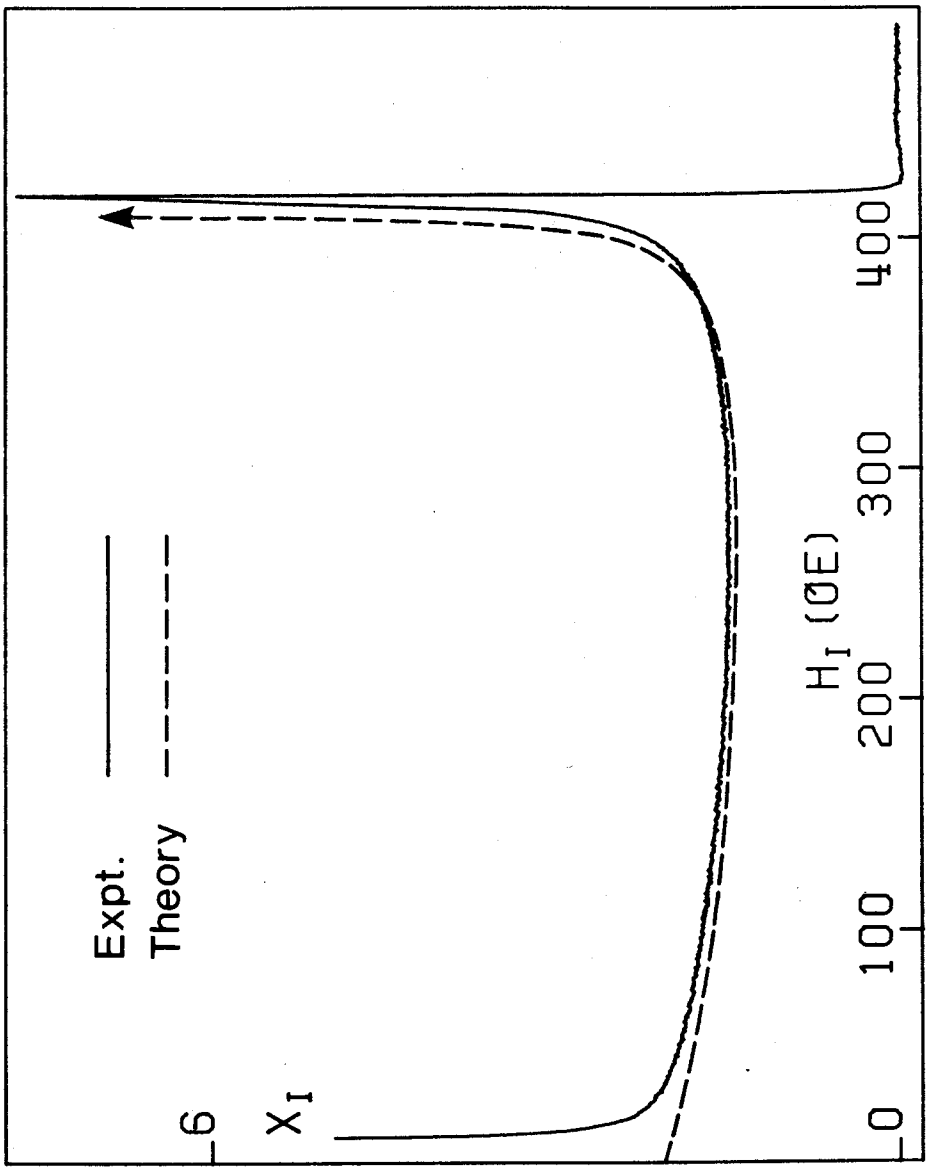
Expt.
Theory
6
X_I
0
100
200
300
400
H_I (ØE)

Fig. 21. Experimental results for M_z as a function of internal field for [111] direction. Mean field calculation of the dependence of magnetization on internal field for Fe also shown. At Hc_1, Mc_1, the magnetization jumps up spontaneously. At $H_{F.O.}$ the states with $M_z = M_s$ and $M_z = M_{F.O.}$ coexist thermodynamically. At Hc_2 the magnetization jumps down to Mc_2 spontaneously.

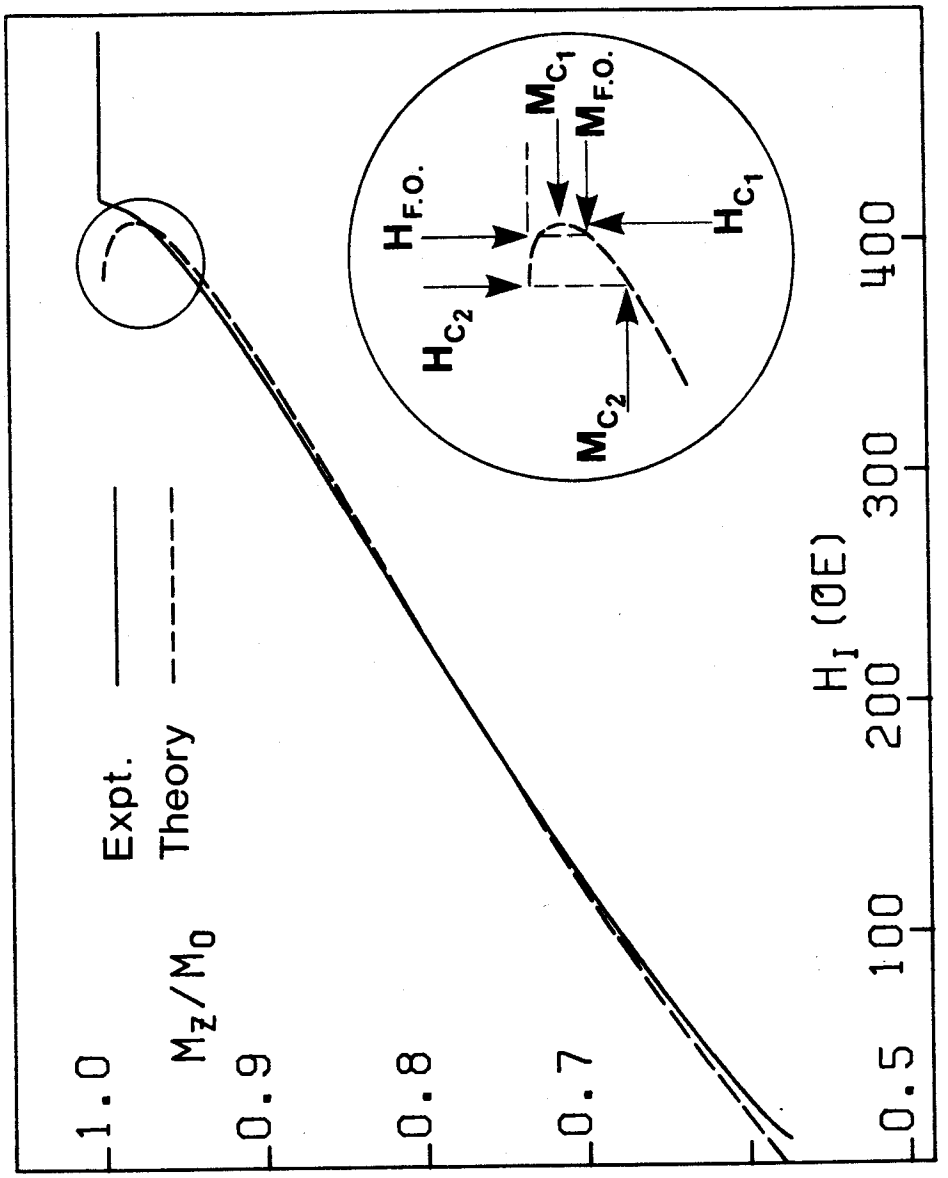
Expt.
Theory
M_z/M_0
1.0
0.9
0.8
0.7
0.5
100
200
300
400
H_I (ØE)
$H_{F.O.}$
H_{C_2}
M_{C_1}
$M_{F.O.}$
H_{C_1}
M_{C_2}

Fig. 22. Inverse susceptibility as a function of the fractional magnetization: (a) from experiment, (b) from mean field anisotropy theory. The expected first order phase change for coexistence of two phases should start at $M_z/M_o = 0.964$.

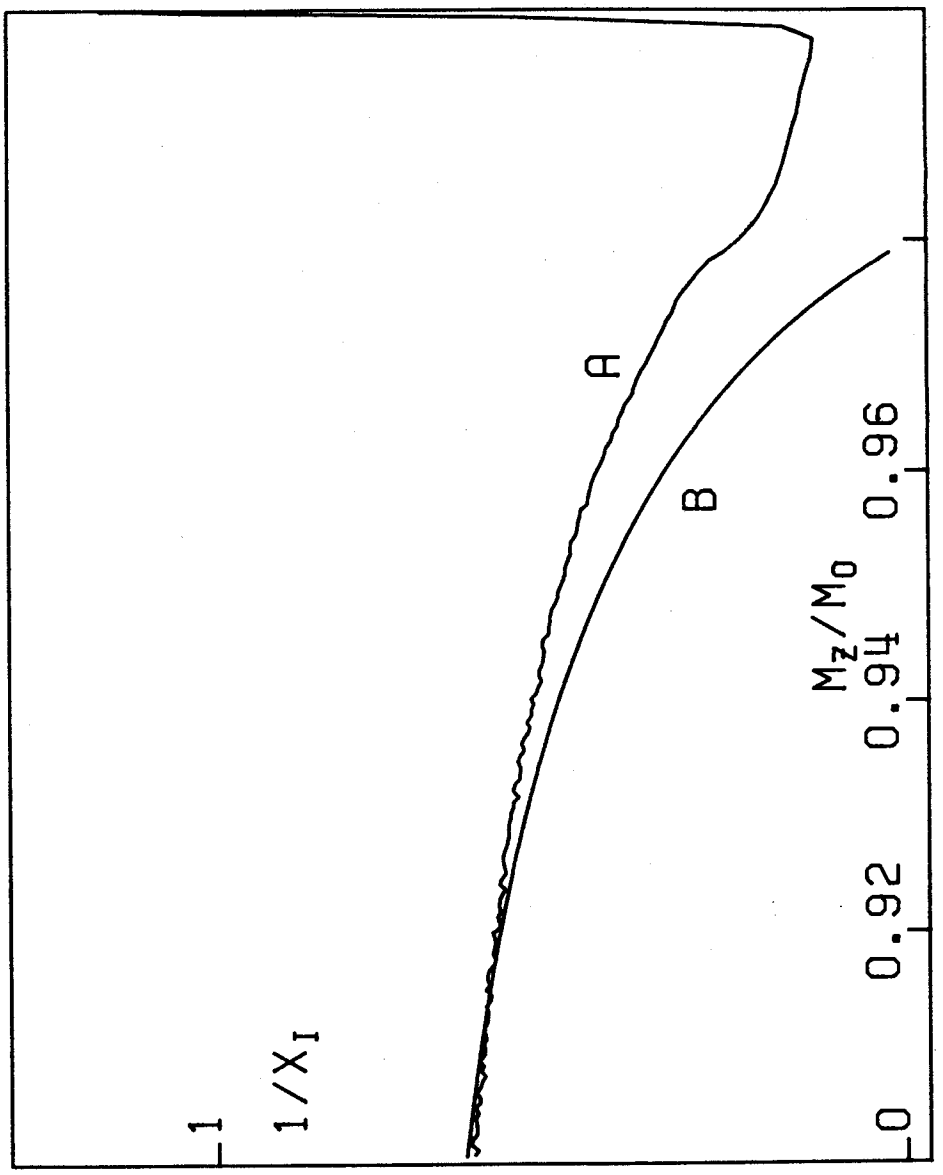
1
1/X_I
A
B
0
0.92
0.94
0.96
M_z/M_0

Fig. 23. Measured in-phase signal vs applied field normalized at each temperature (in the range 630° C to 760° C) to the field H_c. The temperatures are 632, 650, 666, 685, 705, 715, 726, 735, 745, 754 and 759° C.

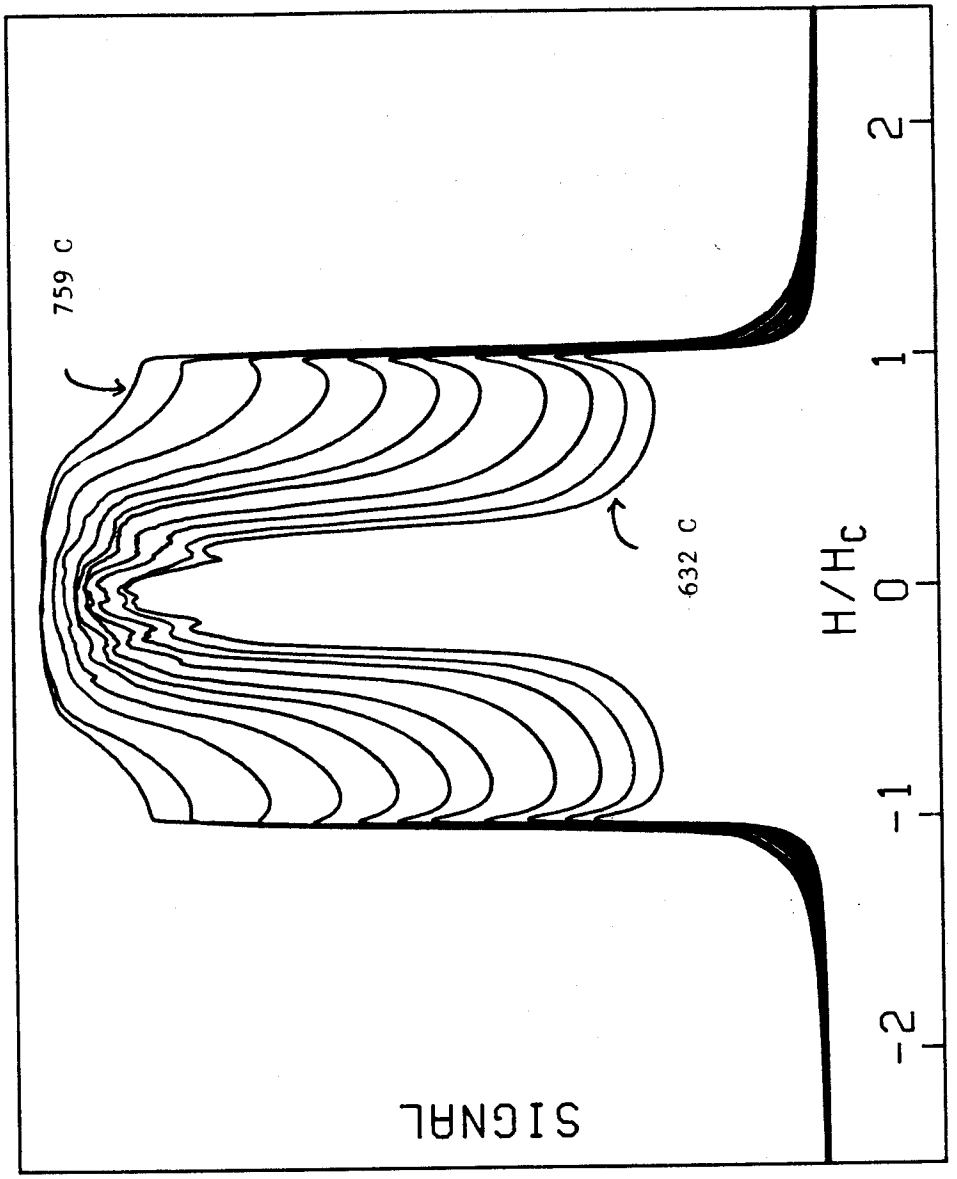
759 C
632 C
SIGNAL
H/Hc
-2
-1
0
1
2

Fig. 24. H_c vs. temperaure from room temperature to $T_c - T \sim 0.5^o$ K. At room temperature, $4\pi DM_s/\sqrt{3} \sim 11.0$ oe.

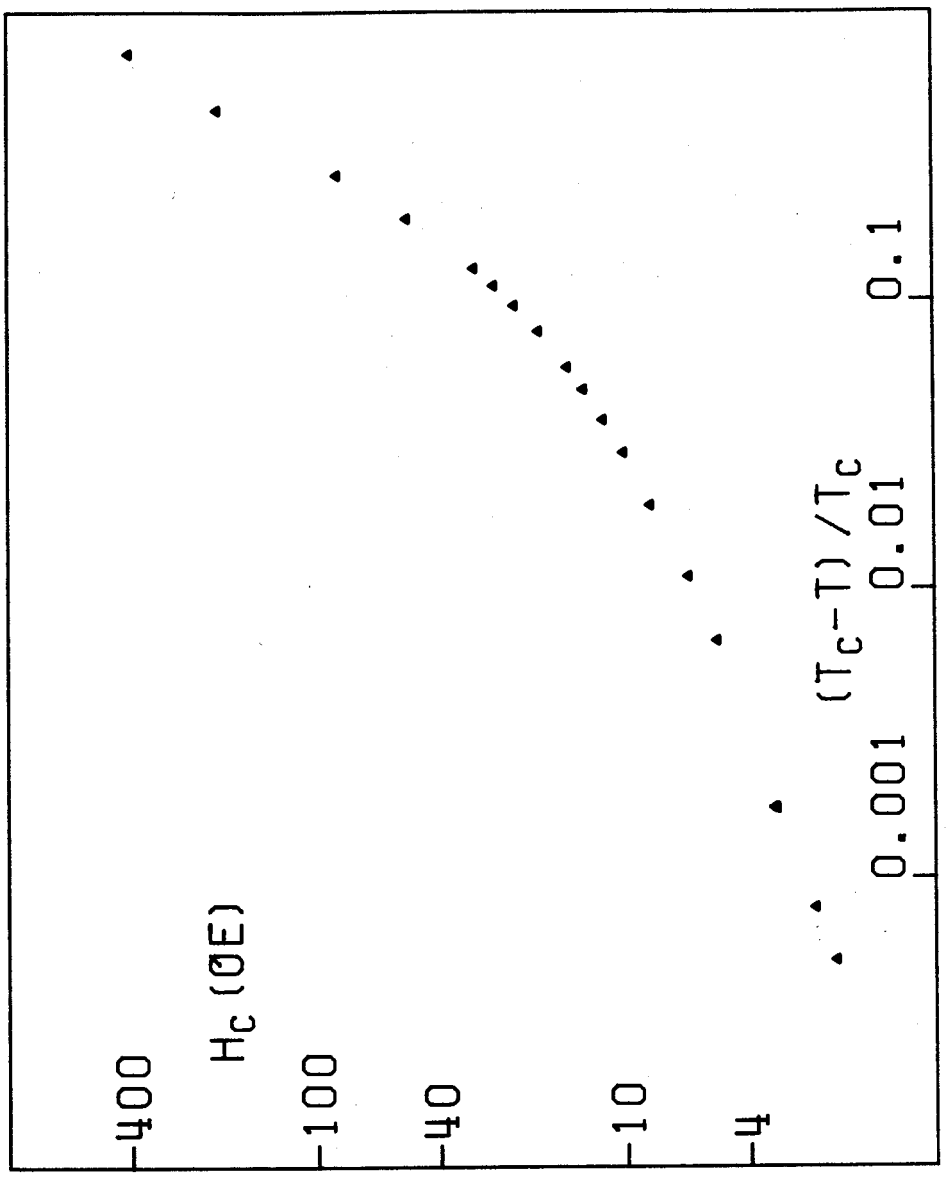
400
100
40
10
4
H_c (ØE)
0.001
0.01
0.1
$(T_c-T)/T_c$

Fig. 25. H_c and H_K vs. temperature just below the Curie point. The fits were made with $\beta = 0.371$ and $n = 3.11$. The H_c data is the calibration curve for the magnetic [111] iron whisker thermometer.

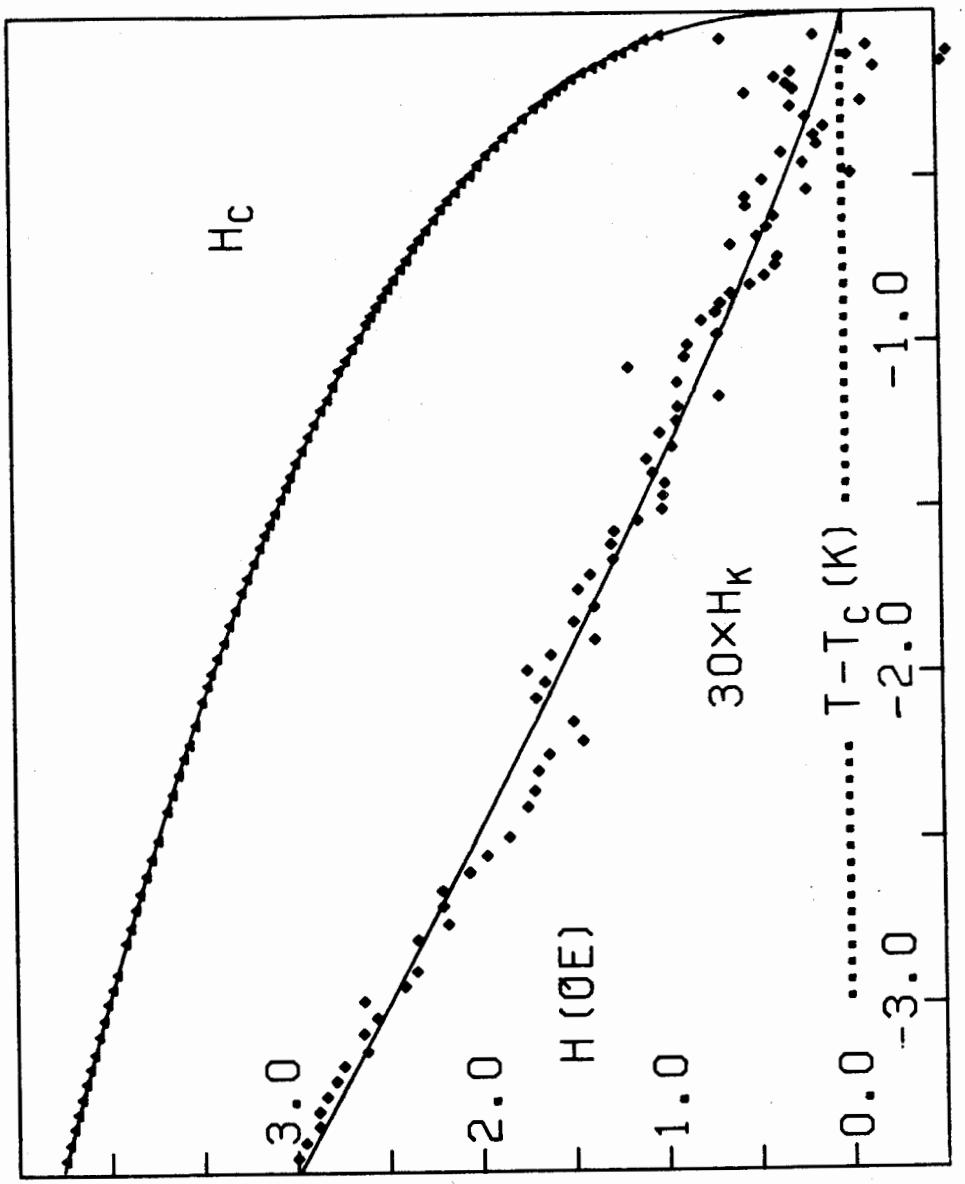
H_c
$30 \times H_K$
H (ØE)
3.0
2.0
1.0
0.0
-3.0
-2.0
-1.0
T-Tc (K)

Fig. 26. H_K vs. $(4\pi DM_s)^3$ in the temperature range $0.0005 < (T_c - T)/T_c < 0.002$. Solid curve shows fit with n = 3.11 (on these axes, the exponent is 3.11/3.00). Dashed curve is a fit to the 8 higher temperature points with n = 3.00.

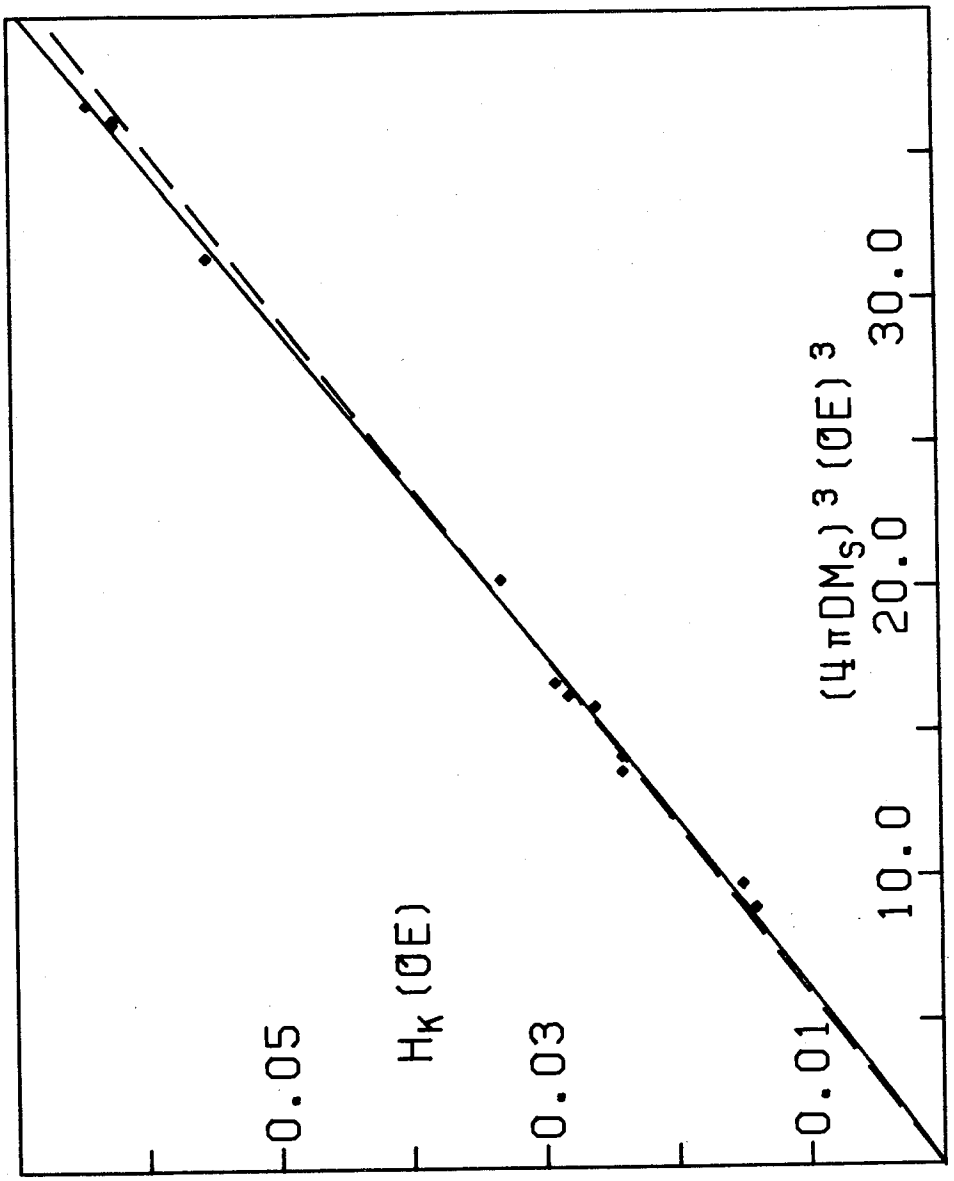
0.05
0.03
0.01
H_K (ØE)
10.0
20.0
30.0
$(4\pi DM_S)^3$ (ØE)^3

Fig. 27. $4\pi DM_s$ and H_K vs. temperature from the integral analysis. Fit curves assume n = 3.11, β = 0.371. The increase in n with decreasing temperature can be seen.

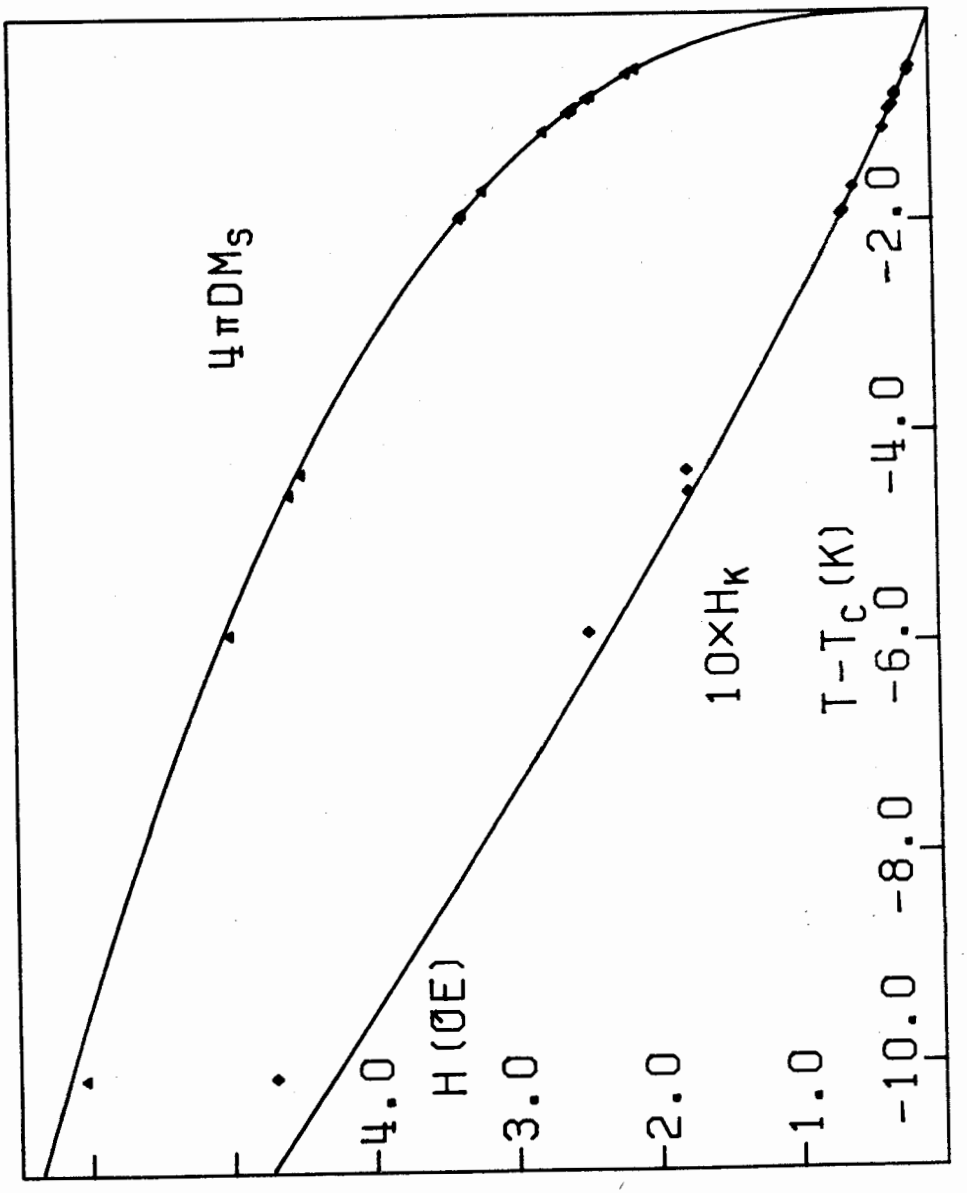
4πDMs
10×Hk
H (ØE)
4.0
3.0
2.0
1.0
T-Tc (K)
-2.0
-4.0
-6.0
-8.0
-10.0

Fig. 28. Log-log plot of $H_K(T)/H_K(0)$ vs. $M_s(T)/M_s(0)$. The (*) data are from our low temperature analysis and (+) data are from our high temperature analysis. T/T_c values are indicated for each point. The dashed curves indicate the power laws near room temperature (n = 11) and near T_c (n = 3.1). The solid curve is from the single anisotropy theory of Callen and Callen.

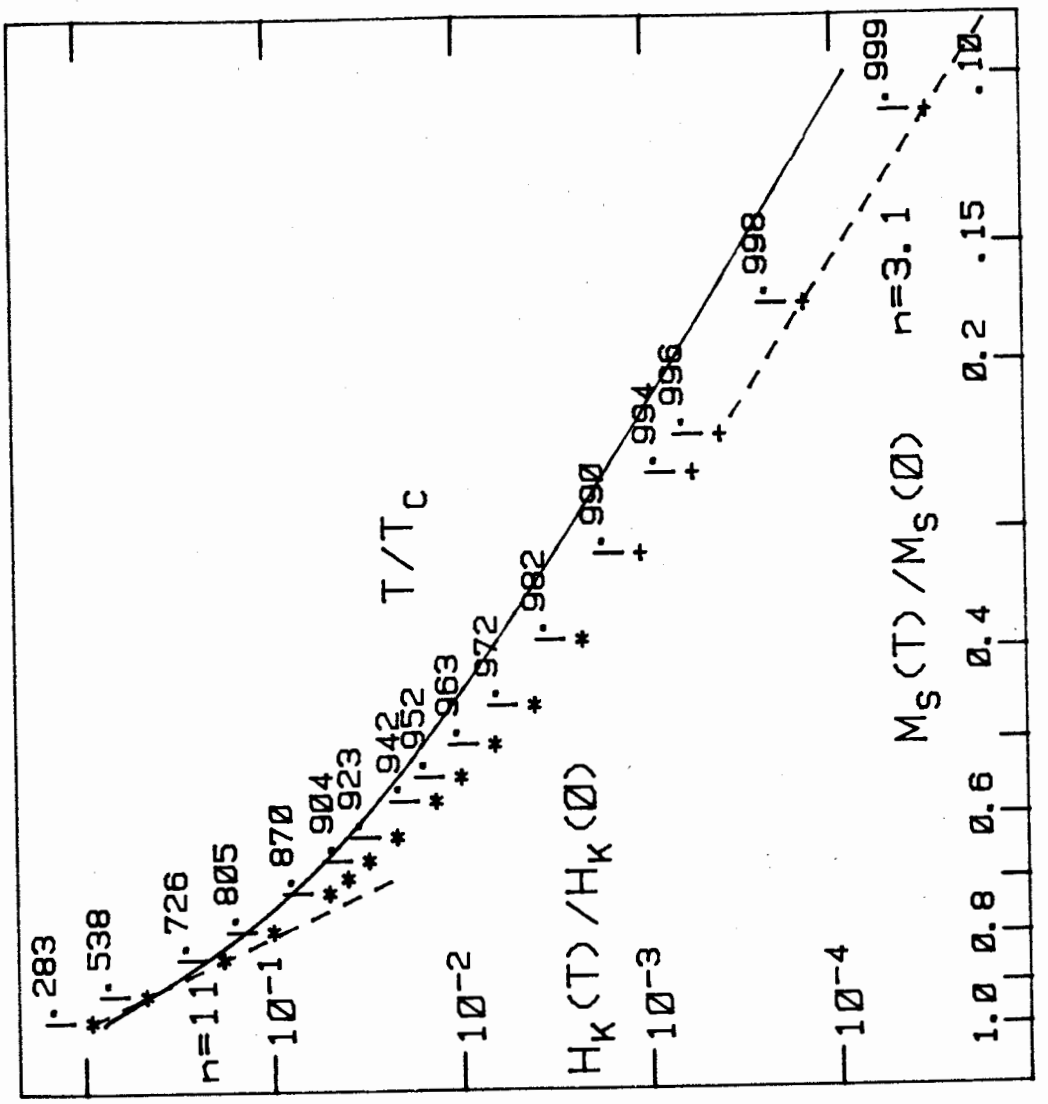
.283
.538
.726
.805
.870
.904
.923
.942
.952
.963
.972
.982
.990
.994
.996
.998
.999
n=1.1
n=3.1
10^{-1}
10^{-2}
10^{-3}
10^{-4}
$H_K(T)/H_K(0)$
$M_S(T)/M_S(0)$
T/T_C
1.0 0.8 0.6 0.4 0.2 .15 .10

Fig. 29. H_K vs. T/T_c from the experimental work of Gengnagel and Hofmann (torque curves), of Bhagat and Rothstein (FMR), and of ourselves (approach to saturation). Good agreement among the three sets of data can be seen. The resolution of the graph does not allow us to show our highest temperature data. The solid curves are from the single anisotropy theory of Callen and Callen where a different temperature dependence of M_s has been used for each. The M_s dependence on temperature shown in fig. (31) is used for the upper solid curve. The Langevin function is used for the lower solid curve.

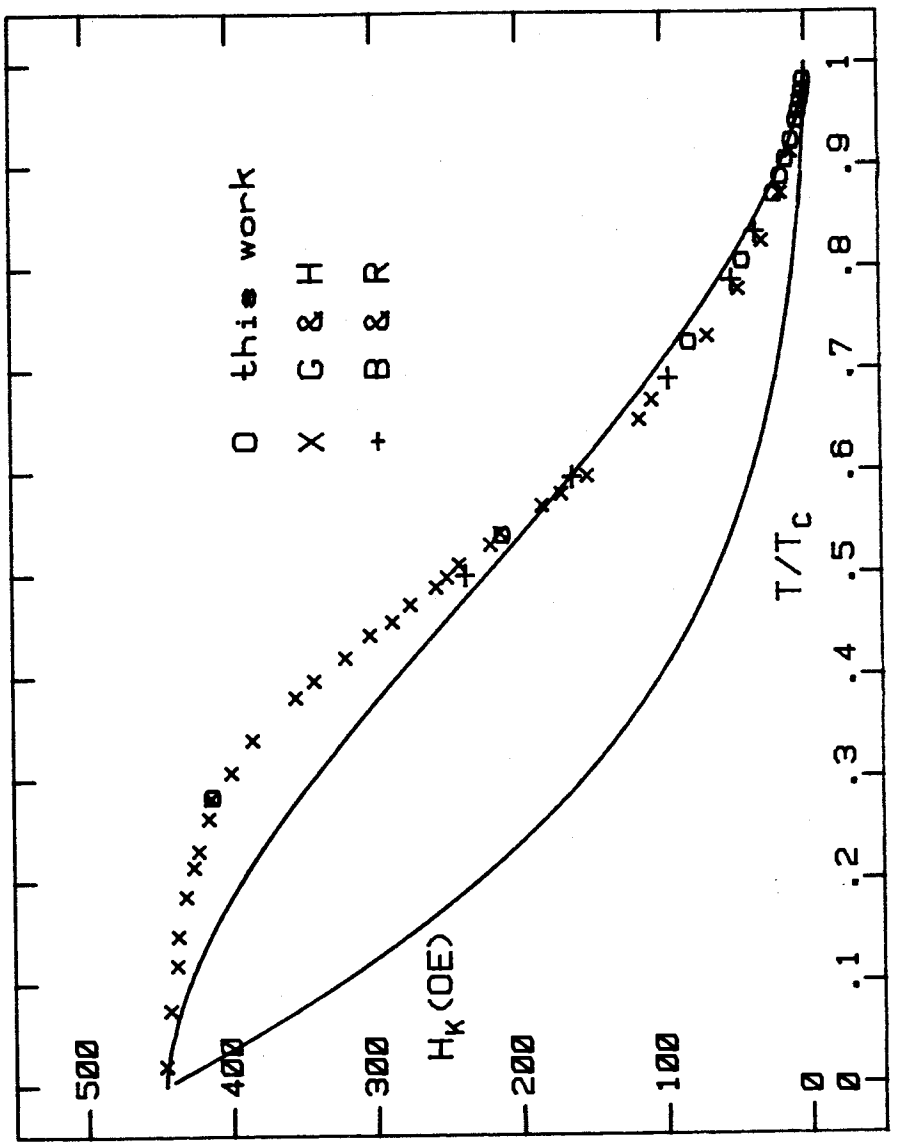
O this work
X G&H
+ B&R
H_K(OE)
T/T_c
500
400
300
200
100
0
0
.1
.2
.3
.4
.5
.6
.7
.8
.9
1

Fig. 30. H_K vs. T/T_c where the data of fig. (29) is shown as a composite plot. These are compared with the data of Bozorth, of Yang et al., and with the theory curve of Callen and Callen now normalized to Bozorth's lowest point. The agreement among these sets of data is poor.

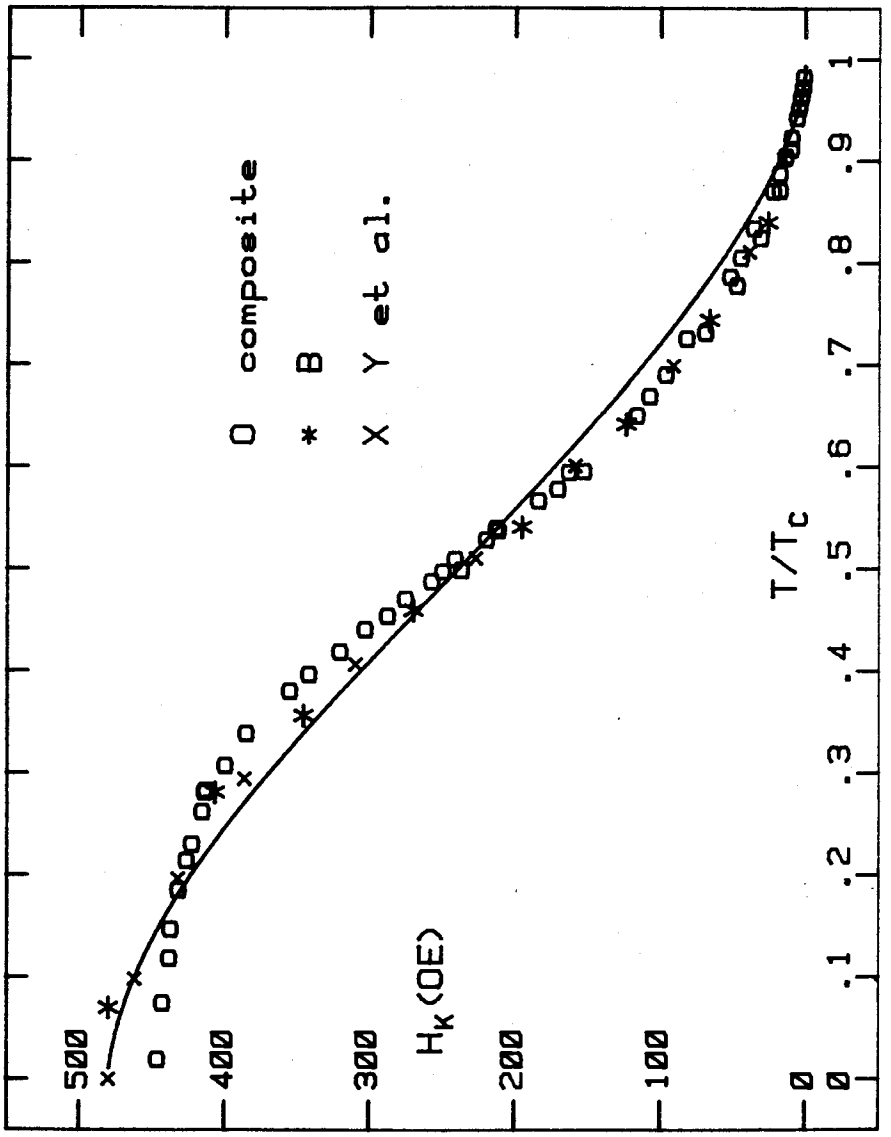
O composite
* B
X Y et al.
H_K(OE)
T/T_c
500
400
300
200
100
0
0
.1
.2
.3
.4
.5
.6
.7
.8
.9
1

Fig. 31. $M_s(T)/M_s(0)$ vs. T/T_c from the work of Crangle and Goodman (force technique) and from our work (saturation technique). The data of C & G are corrected for the thermal expansion of iron. Corrections are made to our data for demagnetizing field effects due to the temperature dependence of the anisotropy. The agreement between the two sets of data is good. The solid curve is a fit to both sets of data as expressed in eq. (63).

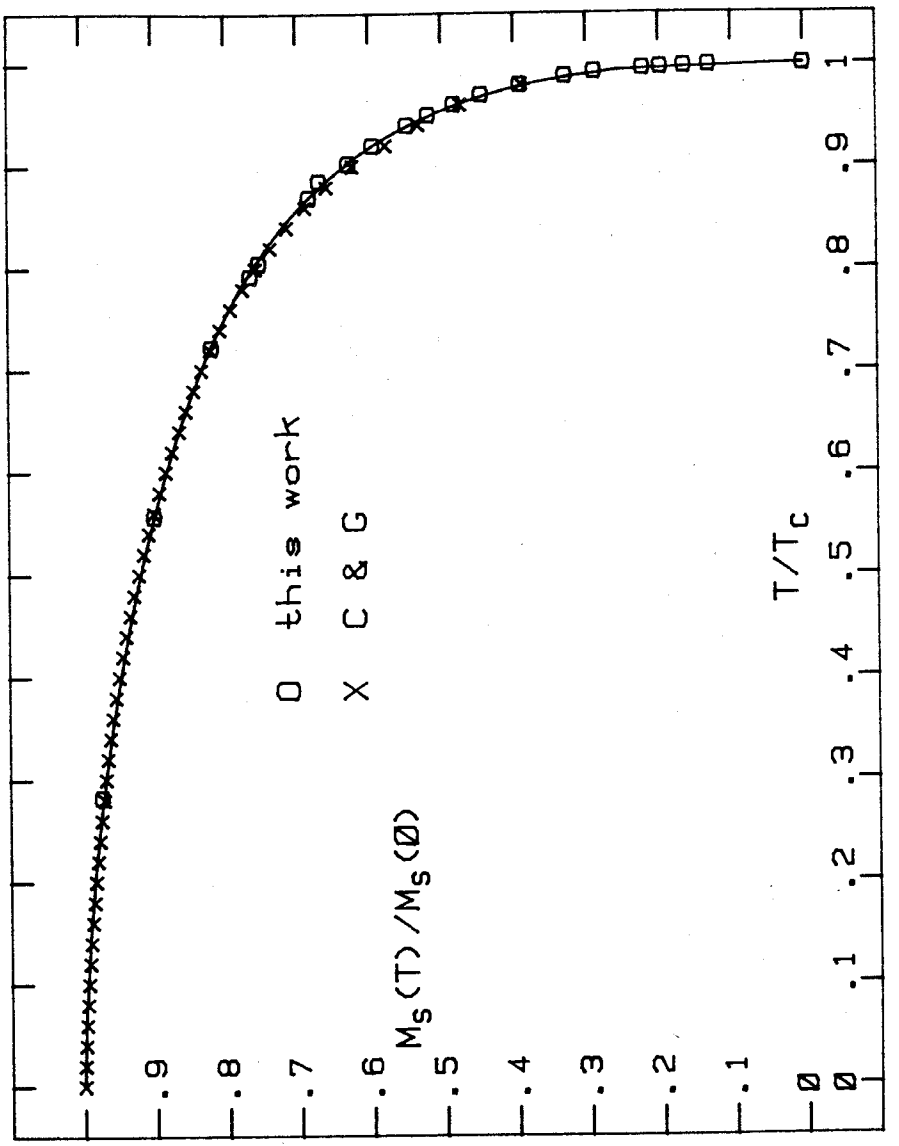
O this work
X C & G
$M_S(T)/M_S(0)$
T/T_c
0
.1
.2
.3
.4
.5
.6
.7
.8
.9
1

VIII. REFERENCES

Aharony, A., K.A. Muller, and W. Berlinger. 1977. Trigonal-to-tetragonal transition in stressed SrTiO3: a realization of the three-state Potts model. Phys. Rev. Lett. 38:33-36.

Akulov, N. 1936. Z. Phys. 100:197.

Aldred, A.T., and P.H. Froehle. 1972. Temperature and field dependence of the magnetization of iron. Intern. J. Magnetism 2:195-203.

Argyle, B.E., S.H. Charap, and E.W. Pugh. 1963. Deviation from $T^{3/2}$ law for magnetization of ferrometals: Ni, Fe, and Fe + 3% Si. Phys. Rev. 132:2051-2062.

Arrott, A.S., B. Heinrich, and D.S. Bloomberg. 1973. Domain configurations, Bloch walls, and magnetization processes in iron whiskers from D.C. to 200 kHz. Theory and experiment II. AIP Conf. Proc. 6:941-960.

Arrott, A.S., A. Aharoni, and B. Heinrich. 1979. Point singularities and magnetization reversal in ideally soft ferromagnetic cylinders. IEEE Trans. Magnetics. MAG-15: 1228-1235.

Arrott, A.S., and B. Heinrich. 1980. Application of magnetization measurements in iron to high temperature thermometry. Presentation GP-21 of 26th annual MMM conf. to be published in J. Appl. Phys. spring 1981.

Barbara, B., M.F. Rossignol, and P. Bak. 1978. First-order transitions and tricritical points in DyAl2: a realization of the three-state Potts model. J. Phys. C 11:L183-L186.

Baxter, R.J. 1973. Potts model at the critical temperature. J. Phys. C 6:L445-L448.

Beitchman, J.G., C.W. Trussel, and R.V. Coleman. 1970. Electron transport and Lorenz number in iron. Phys. Rev. Lett. 25:1291-1294.

Berger, L. 1978. Low-field magnetoresistance and domain drag in ferromagnets. J. Appl. Phys. 49:2156-2161.

Bhagat, S.M., and M.S. Rothstein. 1972. Ferromagnetic resonance in iron at high temperatures. Sol. State. Comm. 11:1535-1538.

Bloomberg, D.S. 1973. Magnetostatics and the micromagnetics of iron whiskers. Ph.D. thesis. Simon Fraser Univ. Canada.

Bloomberg, D.S., and A.S. Arrott. 1975. Micromagnetics and magnetostatics of an iron single crystal whisker. Can. J. Phys. 53:1454-1471.

Blote, H.W.J., and R.H. Swendsen. 1979a. First-order phase transitions and the three-state Potts model. Phys. Rev. Lett. 43:799-802.

Blote, H.W.J., and R.H. Swendsen. 1979b. First order phase transitions in three-state Potts models; their nature from the point of view of renormalization group theory. to be published.

Blote, H.W.J., and R.H. Swendsen. 1979c. First order phase transitions and the three-state Potts model. preprint presented at Joint Intermag-MMM Conference, New York. to be published in J. Appl. Phys.

Bozorth, R.M. 1936. Determination of ferromagnetic anisotropy in single crystals and in polycrystalline sheets. Phys. Rev. 50:1076-1081.

Bozorth, R.M., and H.J. Williams. 1941. Calculation of the torque on a ferromagnetic single crystal in a magnetic field. Phys. Rev. 59:827-833.

Bozorth, R.M. 1951. "Ferromagnetism". Van Nost. New York.

Brenner, S.S. 1956. The growth of whiskers by the reduction of metal salts. Acta Metall. 4:62-74.

Brenner, S.S. 1963. "The art and science of growing crystals". Wiley. New York. p.30.

Bretz, M. 1976. Ordered helium films on highly uniform graphite - finite size effects, critical parameters, and the three-state Potts model. Phys. Rev. Lett. 38:501-505.

Brown, Jr., W.F. 1969. Annals N.Y. Acad. Sci. 147:461(1969).

Bruce, A.D., and A. Aharony. 1975. Coupled order parameters, symmetry-breaking irrelevant scaling fields, and tetracritical points. Phys. Rev. B 11:478-499.

Callen, H.B., and E. Callen. 1966. The present status of the temperature dependence of magnetocrystalline anisotropy, and the $\ell(\ell+1)/2$ power law. J. Phys. Chem. Sol. 27:1271-1285.

Chikazumi, S. 1964. Physics of magnetism. Wiley. New York.

Coleman, R.V., and A. Isin. 1966. Magnetoresistance in iron single crystals. J. Appl. Phys. 37:1028-1029.

Coleman, R.V., and G.G. Scott. 1957. Magnetic domain patterns on single crystal iron whiskers. Phys. Rev. 107:1276. G.G. Scott and R.V. Coleman. 1957. Domain changes during longitudinal magnetization of iron whiskers. J. Appl. Phys. 28:1512. R.V. Coleman and G.G. Scott. 1958. Magnetic domain patterns on iron whiskers. J. Appl. Phys. 29:526.

Crangle, J., and G.M. Goodman. 1971. The magnetization of pure iron and nickel. Proc. Roy. Soc. Lond. A 321:477-491.

Danan, H., A. Herr, and A.J.P. Meyer. 1968. New determinations of the saturation magnetization of nickel and iron. J. Appl. Phys. 39:669-670.

Darby, M.I., and E.D. Issac. 1974. Magnetocrystalline anisotropy of ferro- and ferrimagnets. IEEE Trans. Mag. 10:259-304.

DeBlois, R.W., and C.D. Graham, Jr. 1958. Domain observations on iron whiskers. J. Appl. Phys. 29:528. R.W. DeBlois and C.D. Graham, Jr. 1958. Domain observations on iron whiskers. J. Appl. Phys. 29:931.

Du Plessi, P. DeV. 1971. On the magnetization dependence of the magnetocrystalline anisotropy of iron. J. Phys. Chem. Sol. 32:1691-1696.

Evans, C.C. 1972. "Whiskers". Mills & Boon. London.

Friedel, J. 1964. "Dislocations". Addison-Wesley. New York. ch. 7.

Gans, R., and E. Czerlinski. 1932. Schr. Konigsh. Gelehrt. Ges. Naturw. Kl. 9:1 (ref. from Stewart 1954).

Gengnagel H., and U. Hofmann. 1968. Temperature dependence of the magnetocrystalline energy constants K_1, K_2, and K_3 of iron. Phys. Stat. Sol. 29:91-97.

Givargizov, E.I. 1975. Fundamental aspects of VLS growth. J. Cryst. Growth 31:20-30.

Golner, G.R. 1973. Investigation of the Potts model using renormalization-group techniques. Phys. Rev. B 8:3419-3422.

Gorton, A.T., G. Bitsianes, and T.L. Joseph. 1965. Thermal expansion coefficients for iron and its oxides from x-ray diffraction measurements at elevated temperatures. Trans. Met. Soc. AIME 233:1519-1525.

Grabke, H.J., G. Tauber, and H. Viefhaus. 1975. Equilibrium surface segregation of carbon on iron (100) faces. Scripta Met. 9:1181-84.

Graham, Jr., C.D. 1958. Magnetocrystalline anisotropy constants of iron at room temperature and below. Phys. Rev. 112:1117-1120.

Graham, Jr., C.D. 1960. J. Appl. Phys. 31:150S.

Greiner, E.S., J.A. Gutowski, and W.C. Ellis. 1961. J. Appl. Phys. 32:2489.

Hanham, S.D., B. Heinrich, and A.S. Arrott. 1979. Domain structure and the approach to saturation in [111] oriented iron whiskers. J. Appl. Phys. 50: 2146-2148.

Hansen, M. 1958. "Constitution of binary alloys". second edition. McGraw-Hill. New York. p.353-360.

Heinrich, B., and A.S. Arrott. 1972. Domain configurations, Bloch walls, and magnetization processes in iron whiskers from D.C. to 200 kHz. Theory and experiment. I. Can. J. Phys. 50:710-720.

Heinrich, B., and A.S. Arrott. 1975. Magnetization processes in ideally soft materials. AIP Conf. Proc. 24:702-720.

Heinrich, B., and A.S. Arrott. 1976. Logarithmic frequency dependence of the phase in the ac susceptibility of iron whiskers within millidegrees of the critical temperature. A.I.P. Conf. Proc. 29:469-471.

Heinrich, B., A.S. Arrott, and J.E. Noakes. 1978. Size effects in critical phenomena in iron whiskers. J. Appl. Phys. 49:1395-1397.

Hejnal, T. 1977. On the magnetic relaxation due to carbon and nitrogen in bcc iron. Acta Phys. Polonica A51:379-391. 42 refs.

Honda, K., and S. Kaya. 1926. Sci. Rep. Tohoku Univ. 15:721.

Isin, A., and R.V. Coleman. 1965. Magnetoresistance of iron whiskers. Phys. Rev. 137:A1609-A1613.

Kanamori, J. 1963. Anisotropy and magnetostriction of ferromagnetic and antiferromagnetic materials. Chapt. 4 of "Magnetism" Vol. I, G.T. Rado and H. Suhl, edit. Acad. Press. New York.

Keffer, F. 1955. Temperature dependence of ferromagnetic anisotropy in cubic crystals. Phys. Rev. 100:1692-1698.

Kishi, K. and M. W. Roberts. 1975. Carbon monoxide adsorption on iron in the temperature range 85 to 350 K as revealed by x-ray and vacuum ultraviolet [He(II)] photoelectron spectroscopy. J.C.S. Faraday I 71:1715-20.

Kittel, C. 1949. Physical theory of ferromagnetic domains. Rev. Mod. Phys. 21:541.

Klein, H.P., and E. Kneller. 1966. Variation of magnetocrystalline anisotropy of iron with field and temperature. Phys. Rev. 144:372-374.

Lonzarich, G.G. 1973. Temperature dependence of the exchange splitting in ferromagnetic metals. Ph.D.thesis. Univ. British Columbia. Canada.

Lowrey, W.H. 1976. High-field galvanomagnetic properties of iron. Ph.D. thesis. Univ. Virginia. USA.

Mellor, J.W. 1961. "A comp. treatise on inorganic and theoretical chemistry". v.14. Fe(part 3). p.15.

Mori, N. 1969. Calculation of ferromagnetic anisotropy energies for Ni and Fe metals. J. Phys. Soc. Jap. 27:307-312.

Mori, N., Y. Fukuda, and T. Ukai. 1974. Ferromagnetic anisotropy energies of Ni and Fe metals - Band model. J. Phys. Soc. Jap. 37:1263-1271.

Mukamel, D., M.E. Fisher, and E. Domany. 1976. Magnetization of cubic ferromagnets and the three-component Potts model. Phys. Rev. Lett. 37:565-568.

Mukamel, D., E. Domany, and M.E. Fisher. 1977. Critical behaviour of cubic and tetragonal ferromagnets in a field. Physica B+C 86-88:572-574.

Néel, L. 1952. Theorie du traînage magnétique de diffusion. J. Phys. Radium 13:249-264.

Néel, L. 1959. Directional order and diffusion aftereffect. J. Appl. Phys. 30:3S-8S.

Neugebauer, Ed. 1959. "Growth and perfection of crystals". Wiley. New York.

Ododo, J.C. 1977. The temperature dependence of the spontaneous magnetization of nickel and iron. Sol. State. Comm. 22:585-588.

Potter, H.H. 1934. The magneto-caloric effect and other magnetic phenomena in iron. Proc. Roy. Soc. Lond. A 146:362-387.

Potts, R.B. 1952. Some generalized order-disorder transformations. Proc. Camb. Phil. Soc. 48:106-109.

Riedi, P.C. 1973. Temperature dependence of the hyperfine field and hyperfine coupling constant of iron. Phys. Rev. B 8:5243-5246.

Rudnick, J. 1975. ϵ expansion for the free energy of the continuous three-state Potts model: evidence for a first-order transition. J. Phys. A 8:1125-1129.

Sato, H., and B.S. Chandrasekhar. 1957. Determination of the magnetic anisotropy constant K_2 of cubic ferromagnetic substances. J. Phys. Chem. Sol. 1:228-233.

Shumate, Jr., P.W., R.V. Coleman, and R.C. Fivaz. 1970. Resistivity of iron as a function of magnetization and stress. Phys. Rev. B1:394-405.

Stewart, K.H. 1954. "Ferromagnetic Domains". Cambridge.

Straley, J.P., and M.E. Fisher. 1973. Three-state Potts model and anomalous tricritical points. J. Phys. A 6:1310-1326.

Straley, J.P. 1974. Three-dimensional Potts model. J. Phys. A 7:2173-2180.

Swartz, J.C., and L.J. Cuddy. 1971. Electrical resistivities of Fe(C) and Fe(n) solutions between 4 and 1300 K. J. Phys. Chem. Solids 32:685-695.

Tino, Y., and E. Mukoyama. 1969. On the initial stage of the reduction growth of iron whiskers. Jap. J. Appl. Phys. 8:314-319.

Trussell, Jr., C.W., J.E. Christopher, and R.V. Coleman. 1970. Resistivity of iron from 0.3 to 4.2 K. J. Appl. Phys. 41:1424-1426.

Van Vleck, J.H. 1937. On the anisotropy of cubic ferromagnetic crystals. Phys. Rev. 52:1178-1198.

Wagner, R.S. 1970. "VLS mechanism of crystal growth". in: Levitt, A.P. ed. "Whisker technology". Wiley. New York. p. 47-119.

Wagner, R.S., and W.C. Ellis. 1965. The VLS mechanism of whisker growth. Trans. Met. Soc. AIME 233:1054-1064.

Weiss, P., and R. Forrer. 1926. Magnetization of Ni and the magneto-caloric effect. Annls. Phys. 5:153-213.

Weiss, P., and R. Forrer. 1929. Absolute saturation of ferromagnetics and law of approach as a function of H and T. Annls. Phys. 12:279-374.

Westerstrand, B., P. Nordblad, and L. Nordborg. 1975. The magneto-crystalline anisotropy constants of iron and iron-silicon alloys. Physica Scripta. 11:383-386.

Williams, H.J., W. Schockley, and C. Kittel. 1950. Studies of the propagation velocity of a ferromagnetic domain wall. Phys. Rev. 80:1090-1094.

Wolf, W.P. 1957. Effect of crystalline electric fields on ferromagnetic anisotropy. Phys. Rev. 108:1152-1157.

Yang, T., J. Yang, and L.B. Robinson. 1973. Temperature dependence of ferromagnetic anisotropy energy in cubic crystals. Sol. State. Comm. 13:53-57.

Yosida, K. 1968. The status of the theories of magnetic anisotropy. J. Appl. Phys. 39:511-518.

Zener, C. 1954. Classical theory of the temperature dependence of magnetic anisotropy energy. Phys. Rev. 96:1335-1337.